11-4-2008

OWSS And MIMO-STC-OFDM: Signaling Systems for the Next Generation of High Speed Wireless LANs

Dinesh Divakaran
University of South Florida

OWSS And MIMO-STC-OFDM: Signaling Systems for the Next Generation of High Speed Wireless LANs

by

Dinesh Divakaran

A dissertation submitted in partial fulfillment
of the requirements for the degree of
Doctor of Philosophy
Department of Electrical Engineering
College of Engineering
University of South Florida

Co-Major Professor: Wilfrido A. Moreno, Ph.D.
Co-Major Professor: Paris H. Wiley, Ph.D.
Kenneth A. Buckle, Ph.D.
Nagarajan Ranganathan, Ph.D.
Fernando J. Falquez, Ph.D.

Date of Approval:
November 4, 2008

Keywords: wireless systems, wlans, wavelets, space time coding, multiplexing

DEDICATION

To my mother

ACKNOWLEDGEMENTS

The foremost, I would like to thank my advisors, Dr. Wilfrido Moreno and Dr. Paris Wiley for their guidance and encouragement during the course of this dissertation. Working with them has been a fruitful and enjoyable experience. This dissertation would not have been possible without their support.

I wish to thank Dr. Kenneth Buckle, Dr. Nagarajan Ranganathan and Dr. Fernando Falquez, for serving in my committee, for their support, valuable time, feedback and suggestions; and to Dr. Carlos Smith for chairing my defense. I owe a lot to Dr. Vijay Jain and the people of Conexant Systems Corp., especially Dr. Brent Myers and Dr. Dave Hedberg, who guided and partially supported my work for a duration of my PhD program. I would also like to thank the staff of the Electrical Engineering department, especially Gayla Montgomery, for helping out with various issues over the years.

My deepest gratitude goes to my parents, especially my mother to whom this dissertation is dedicated. I will forever be indebted to both of them of them for their sacrifices, encouragement and patience. They were always there to share my joys and disappointments, and to provide the support, hope and motivation when I needed it. I would also like to thank my brother Darshan, for his continued support and encouragement throughout the years. Last but by no means least, I would like to remember my dear departed grandparents, especially my Ammuma, who always encouraged me in my endeavors.

TABLE OF CONTENTS

LIST OF TABLES

LIST OF FIGURES

OWSS AND MIMO-STC-OFDM: SIGNALING SYSTEMS FOR THE NEXT GENERATION OF HIGH SPEED WLANS

DINESH DIVAKARAN

ABSTRACT

The current popularity of WLANs is a testament primarily to their convenience, cost efficiency and ease of integration. Even now the demand for high data rate wireless communications has increased fourfold as consumers demand better multimedia communications over the wireless medium. The next generation of high speed WLANs is expected to meet this increased demand for capacity coupled with high performance and spectral efficiency. The current generation of WLANs utilizes Orthogonal Frequency Division Multiplexing (OFDM) modulation. The next generation of WLAN standards can be made possible either by developing a different modulation technique or combining legacy OFDM with Multiple Input Multiple Output (MIMO) systems to create MIMO-OFDM systems. This dissertation presents two different basis technologies for the next generation of high speed WLANs: OWSS and MIMO-STC-OFDM.

OWSS, or Orthogonal Wavelet Division Multiplexed - Spread Spectrum is a new class of wavelet pulses and a corresponding signaling system which has significant advantages over current signaling schemes like OFDM. In this dissertation, CSMA/CA is proposed as the protocol for full data rate multiplexing at the MAC layer for OWSS. The excellent spectral characteristics of the OWSS signal is also studied and simulations show

that passband spectrum enjoys a 30-40% bandwidth advantage over OFDM. A novel pre-distortion scheme was developed to compensate for the passband PA non-linearity. Finally for OWSS, the fundamental limits of its system performance were also explored using a multi-level matrix formulation. Simulation results on a 108 Mbps OWSS WLAN system demonstrate the excellent effectiveness of this theory and prove that OWSS is capable of excellent performance and high spectral efficiency in multipath channels.

This dissertation also presents a novel MIMO-STC-OFDM system which targets data rates in excess of 100 Mbps and at the same time achieve both high spectral efficiency and high performance. Simulation results validate the superior performance of the new system over multipath channels. Finally as channel equalization is critical in MIMO systems, a highly efficient time domain channel estimation formulation for this new system is also presented.

In summary, both OWSS and MIMO-STC-OFDM appear to be excellent candidate technologies for next generation of high speed WLANs.

CHAPTER 1

INTRODUCTION

In recent years the demand for high data rate wireless communications [1] has increased steadily as consumers demand better multimedia communications over the wireless medium. A wireless LAN or WLAN [2], [3] is a wireless local area network which connects two or more computers or devices without using wires. Current state of the art WLAN systems like 802.11a/g [4],[5] utilize Orthogonal Frequency Division Multiplexing (OFDM) [6]-[8] modulation technology based on radio waves in the 5 and 2.4 GHz public spectrum bands, to enable communication between devices in a limited area, also known as the basic service set. This gives users the mobility to move around within a broad coverage area and still be connected to the network. The popularity of wireless LANs is a testament primarily to their convenience, cost efficiency, and ease of integration with other networks and network components. The majority of computers sold to consumers today come pre-equipped with all necessary WLAN technology.

The current WLAN systems are capable of a maximum data rate of 54 Mbps [2]-[5]. The next generation of WLAN standards is expected to touch bit rates of 108 Mbps and possible even 240 Mbps [2]. This can be made possible either by developing new standards based on a different modulation technique than OFDM or combining OFDM with state of the art Multiple Input Multiple Output (MIMO) [9]-[12] systems (systems

employing multiple transmit and receive antennas) to create MIMO-OFDM systems [12]-[16]. Current R&D efforts including the eagerly awaited 802.11n standard [17]-[18] are directed at MIMO-OFDM, however there is an urgent need to look at other signaling schemes which can overcome the inherent disadvantages of OFDM without the use of MIMO. OWSS, or Orthogonal Wavelet Division Multiplexed - Spread Spectrum [19]-[22] is a new class of wavelet [23] pulses and a corresponding signaling system which can be a candidate technology for the next generation high speed WLANs. These pulses are generated through a combination of Orthogonal Wavelet Division Multiplexing (OWDM) [24] and Spread Spectrum (SS) [25] concepts. The OWSS system has significant advantages over current signaling schemes like OFDM, TDMA [1] and even OWDM. Some of these unique advantages are: wide time and frequency support [19], multiple user capability [28], [32] [19], effective multipath channel equalization [27], [29],-[31], continuously pipelined operation (in contrast to OFDM), high bandwidth efficiency [26], [31] and robustness against deep fading frequency selective channels unlike OFDM [19],[21].

OWSS is a new modulation scheme for high speed WLANs, however as mentioned earlier current research trends based on combining the current modulation scheme OFDM with MIMO. Towards this end, a new MIMO-STC-OFDM system [33]-[35] was developed which targets next generation data rates (108 Mbps), and at the same time achieve both high spectral efficiency and high performance (high data rate with low BER) over frequency selective channels. This new system is accomplished by a combination, or layering [36] of MIMO OFDM [12]-[16], group transmit signals and

antennas [37], space time coding [38], [39], array processing [37] at the receiver and a new Least Squares (LS) decoding scheme [33]. The current system is a 4×4 system (4 transmit and 4 receive antennas) but can easily be extended to larger MIMO systems that achieve data rates in excess of 108 Mbps.

In this dissertation, two different basis technologies for the next generation of high speed WLANs are presented: OWSS and the new MIMO-STC-OFDM. The dissertation is organized as follows. Following the introduction the outline of this dissertation consists of five parts

(1) Background on OWSS system, OFDM, MIMO Systems and STC (Chapter 2)

(2) Medium Access Control in OWSS WLANs and Spectral Characteristics of OWSS. (Chapter 3 and 4)

(3) Performance limits of OWSS based on a theoretical multi-level matrix formulation. (Chapter 5)

(4) The new MIMO-STC-OFDM system with high spectral efficiency and high performance (Chapter 6).

(5) Multipath Channel Modeling and Estimation for the new MIMO-STC-OFDM system. (Chapter 7).

The first part given above provides detailed information about OWSS system and a background on OFDM, MIMO systems and STC. The last four parts contain the main contribution of the dissertation and include original research results.

Specific novel contributions of this dissertation in different chapters are listed below:

(1) OWSS and MIMO-STC-OFDM are both presented as viable candidates for the next generation of high speed WLANs. OWSS is a new modulation technique capable of high data rates without using multiple antennas at the transmitter and receiver. MIMO-STC-OFDM on the other hand, achieves next generation data rates by combining transmit and receive diversity techniques with legacy OFDM systems.

(2) A CSMA/CA based MAC protocol is proposed for OWSS to access the medium [28]. The frame format for OWSS data packets and MAC attributes of OWSS are also proposed. Performance of OWSS at the MAC layer in terms of saturation throughput and average delay is analyzed using a simple theoretical model.

(3) The spectrum efficiency of OWSS is analyzed vis-a-vis OFDM. The OWSS passband spectrum is found to have 30-40% bandwidth advantage over OFDM for 54 Mbps operation [26]. OWSS also readily extends to higher bit rates, such as 108 Mbps, in a bandwidth efficient manner.

(4) A novel pre-distortion scheme [70] was developed to compensate for the passband spectral regrowth due to PA non-linearity. At 6 dB backoff in 108 Mbps OWSS, this scheme yields an improvement of 10 dB in spectral regrowth distortion levels.

(5) A Forward Equalizer - Decision Feedback Equalizer (FE-DFE) structure was originally proposed for the OWSS receiver. Towards this end, a novel multi-level matrix formulation [27] has been conceptualized to model the entire OWSS transreceiver and establish its fundamental theoretical performance (BER) in random multipath fading channels. This formulation can also be used for channel estimation, i.e. to estimate the optimum channel equalizer (weights of the FE and DFE) for these channels.

(6) A new MIMO-STC-OFDM system [33] has been developed that achieves both high spectral efficiency and high performance over frequency selective channels. This new system was achieved combining MIMO-OFDM, group coding antennas using STC, array processing at the receiver (for interference suppression) and new LS decoding technique. (7) A highly effective channel equalization technique [34] in the time domain has also been developed for the new MIMO-STC-OFDM system. The multipath channel model for the system is also conceptualized.

The dissertation is organized in detail as follows. It starts by providing a detailed background for both OWSS and MIMO-STC-OFDM in Chapter 2. OWDM and its combination with Spread Spectrum (SS) concepts to synthesize OWSS pulses is studied. The inherent advantages and special nature of the OWSS pulses is discussed. The corresponding OWSS signaling system is presented and a powerful adaptive equalizer structure in the OWSS receiver [27], [29] which combats multipath fading is described. In the second part of the chapter 2, a review of OFDM, MIMO systems and STC, key concepts that serve as a basis for the new MIMO-STC-OFDM system is provided.

Chapter 3 looks at the Medium Access Control (MAC) layer in OWSS WLAN system. OWSS will use a Carrier Sense Multiple Access with Collision Avoidance (CSMA/CA) [40] based MAC protocol similar to the IEEE 802.11a [4] standard to access the medium. A frame format for OWSS data packets in the MAC layer and MAC attributes of OWSS in terms of DCF parameters are proposed. Using a simple theoretical model called Bianchi's Model [41], [42], an analysis of the performance of OWSS in the

MAC layer in terms of two key parameters, system throughput and average packet delay is carried out.

Chapter 4 analyzes the excellent spectral characteristics of the OWSS signal and studies its bandwidth efficiency as compared to OFDM. It is shown that the theoretical baseband spectrum of OWSS is perfectly flat, and the passband spectrum offers a 30-40% bandwidth advantage [26], [31] over 802.11a OFDM for 54 Mbps operation. OWSS also readily extends to higher bit rates, such as 108 Mbps, in a bandwidth efficient manner. The effect of spectral regrowth in the OWSS passband spectrum was analyzed using the Rapp Model. This spectral regrowth can be compensated to a large extent using a novel pre-distortion scheme. At 6 dB backoff in 108 Mbps OWSS, this scheme yields an improvement of 10 dB in the spectral regrowth distortion levels.

Chapter 5 explores the fundamental limits to OWSS performance. Towards this purpose, a multi-level matrix formulation [27] is employed to model the signal processing system. The total minimum mean-square error (TMSE) for the Forward Equalizer – Decision Feedback Equalizer (FE–DFE) structure [27], [29], [30] is derived in a closed form, and thereupon minimized rigorously to provide the optimum equalizer weights and corresponding theoretical BER performance of the OWSS system. Simulation results on a 108 Mbps system demonstrate the effectiveness of this theory and prove that OWSS is capable of excellent performance and high spectral efficiency in multipath fading channels.

Chapter 6 introduces the new MIMO-STC-OFDM system [33]-[35] that achieves both high spectral efficiency and high performance over frequency selective channels. This is accomplished by a combination, or layering [36] of MIMO OFDM [12]-[16], group transmit signals and antennas [37], space time coding [38], [39], array processing [37] at the receiver and a new Least Squares (LS) decoding scheme [33]. The new system is compared with other MIMO OFDM systems and simulation results validate the superior performance of the new system.

Chapter 7 presents an efficient new time domain channel estimation [34], [35] formulation for the new high performance MIMO STC-OFDM system, which uses high power QPSK symbols. Four matrix-vector multiplications and a single data frame enables high accuracy estimation of all sixteen MIMO channels in the 4×4 system.

Chapter 8 provides a list of novel contributions of this dissertation, concluding remarks and suggestions for future research in OWSS and MIMO-STC-OFDM.

CHAPTER 2

BACKGROUND

2.1 Background on OWSS Systems

OWSS, or Orthogonal Wavelet Division Multiplexed - Spread Spectrum [19]-[22] is a new class of pulses and a corresponding signaling system for next generation high speed WLANs and targets bit rates upwards of 108 Mbps. These pulses are generated through a combination of Orthogonal Wavelet Division Multiplexing (OWDM) [24] and Spread Spectrum (SS) concepts [25]. The OWSS system has significant advantages over current signaling schemes like OFDM [6]-[8], TDMA [1] and even OWDM. Some of these unique advantages are : (1) single or multiple user capability at the PHY or MAC layer (2) effective multipath channel equalization due to wide time and frequency support (3) continuously pipelined operation (in contrast to OFDM) (4) high bandwidth efficiency, which is about twice for DS-CDMA [43] (assuming rectangular chips for DS-CDMA). As mentioned earlier, OWSS pulses are derived from OWDM pulses by spreading them in the wavelet domain [23], using a suitable family of PN codes [25]. Therefore, let us begin with a discussion on OWDM pulses.

2.1.1. Orthogonal Wavelet Division Multiplexing (OWDM)

OWDM is based on the concepts of orthogonal multipulse signaling [44]. Consider that the pulses $\varphi_m(t)$, $m = 0, 1, \ldots, M-1$, form an orthonormal set over a

certain period of time and that each pulse is orthogonal to itself shifted by non-zero integer multiples of a certain interval T [44]. Each basis pulse $\varphi_m(t)$, can then serve to create a 'virtual' channel over which the symbol a_m is carried. The vector of symbols $A = [a_0, a_1, \ldots, a_{M-1}]^T$ is called a supersymbol, and the interval $T = MT_s$ as the supersymbol/block interval, where T_s is the basic symbol interval . Then the base band transmitted signal becomes

$$s(t) = \sum_{i=-\infty}^{\infty} \sum_{m=0}^{M-1} a_{i,m}\, \varphi_m(t - iT) = \sum_{i=-\infty}^{\infty} \underline{A}_i^T \; \underline{\varphi}(t - iT) \tag{2.1}$$

At the receiver, symbol and block timing extraction is performed, and the received signal is correlated with $\varphi(t - iT)$ to detect the nth supersymbol at time iT (actually at time $iT + \tau$, where τ denotes the optimum timing phase [44]). Since CMOS VLSI implementation of signal processing techniques is often less complicated and economical in the discrete time domain, discrete time formulation of orthogonal multipulse signaling will be used from now on. The discrete time orthogonal multipulse's are $\varphi_m(n)$, $m = 0, 1, \ldots, M-1$, and the corresponding transmitted orthogonal multipulse signal becomes

$$s(n) = \sum_{i=-\infty}^{\infty} \sum_{m=0}^{M-1} a_{i,m}\, \varphi_m(n - iM) = \sum_{i=-\infty}^{\infty} \underline{A}_i^T \; \underline{\varphi}(n - iM) \tag{2.2}$$

However for convenience and simplicity, the variable t will be used to denote both the continuous time variable as well as the discrete time sample index. Also, M and T will be used interchangeably to denote the block length.

Orthogonal multipulse signaling has the following distinct advantages: (1) potentially less sensitive to multipath fading (2) potential to reach channel capacity and countering selective fading (3) potential for multiplexing at the physical layer. For a more detailed review of OWDM pulses, refer to [24]. The OWDM system uses wavelet pulses as the basis pulses in orthogonal multipulse signaling.

2.1.2 OWDM Pulses from Full Tree Wavelet Filters

The use of basis functions in the analysis of signals modulated by transforms is a time proven concept. For example, in the Discrete Fourier transform (DFT) [45] the basis set consists of all complex sinusoids of the form $e^{j\omega n}$ where ω can take on any real value. In recent years attention has been focused on basis sets generated from wavelets [23]. The OWDM basis sets are generated through the process of scaling or *shifts* from a single parent function, called the *mother wavelet* $\phi(t)$. Appropriately, then, the basis pulses are indexed by two indices x and y, signifying scale and shift respectively. Thus, the basis pulses are of the form

$$\phi_{x,y} = 2^{-x/2} \quad \phi\left(2^{-x}t - y\right) \tag{2.3}$$

A three stage ($M = 2^3 = 8$ input nodes) synthesis tree for generating the wavelet pulses $\varphi_i(t)$, which serve as the basis pulses, is shown in Figure 2.1. More generally, for an s-stage tree there would be $M = 2^s$ input nodes. The impulse response from the i-th input node to the output node is denoted as $\varphi_i(t)$, where $i = 0, 1, \ldots, M-1$. The prototype type filter G_0 can be a Haar wavelet [23], a Daubechies filter [23], or other [45] – [48].

As an example, consider the well-known *Haar wavelet* $\psi = [1 \quad -1]/\sqrt{2}$ and its *scaling function* $\phi = [1 \quad 1]/\sqrt{2}$. Either of them or both can be used to create the OWDM basis set. In terms of implementation this is frequently done through the tree structure [8]. To illustrate, let us define the high pass and low pass filters as g_0 = [1 1] and g_1 = [1 –1]. Both are identical to the mother wavelet and its scaling function, except they are not normalized. In the Figure 2.1, several different sampling frequencies are observed. The input sampling frequency F_s will be doubled in each stage to become an output sampling frequency of $8F_s$. The z-transforms $G_0(z)$ and $G_1(z)$ are shown as the filter transfer functions.

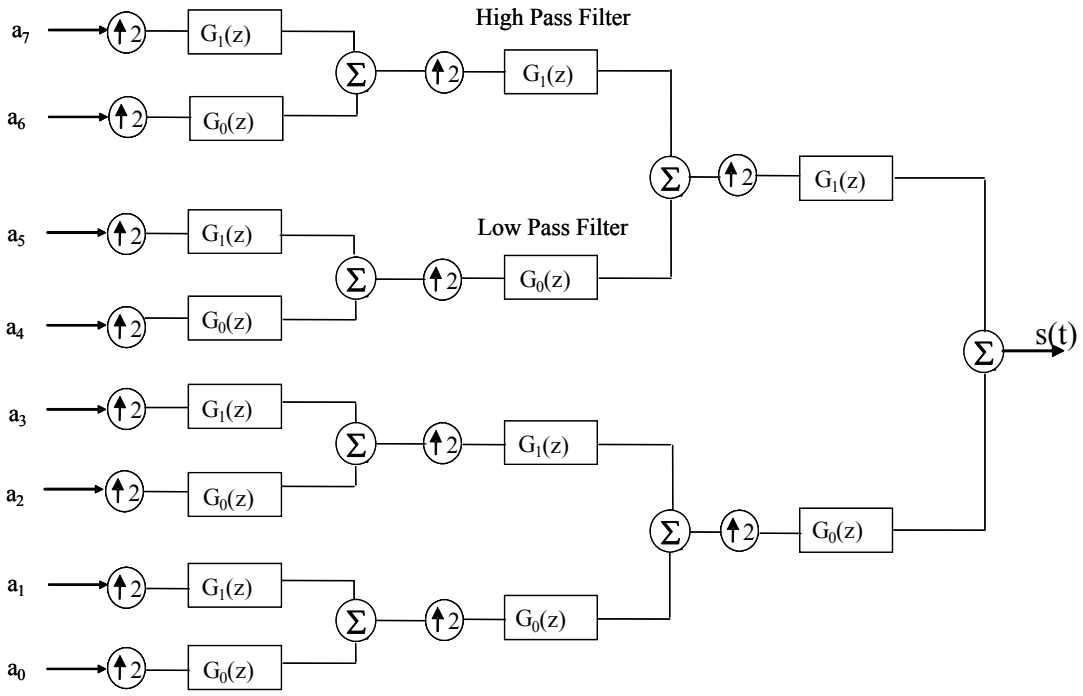

Figure 2.1 OWDM Synthesis Tree

In the figure, a member of the OWDM basis set can be generated by applying a unit pulse at only one input node while all other nodes receive a zero input. Thus, for example if input node 5 is driven by a unit pulse, and all other input nodes are held at zero, the output turns out to be $\varphi_5 = [1\ -1\ 1\ -1\ -1\ 1\ -1\ 1]$. Here is a general formula: consider an arbitrary leaf node, say node $n = [i\ j\ k]$ (binary address). Then the transfer function from this node to the output node is $P_{i,j,k} = P_i(z)P_j(z^2)P_k(z^4)$, where for node 5, $P_i(z) = G_1(z)$, $P_j(z) = G_0(z)$, and $P_k(z) = G_1(z)$. The tree of Figure 2.1 can be represented by a equivalent tree as shown in Figure 2.2. It can be shown that the pulses generated in this set are orthogonal, and in fact if the normalization factor $1/\sqrt{2}$ was not ignored, these pulses would be orthonormal. Hereafter the normalization factor is included so that the set of wavelet pulses $\{\varphi_0, \varphi_1, \ldots, \varphi_{M-1}\}$ will be doubly orthonormal, i.e. the pulses satisfy the generalized Nyquist criterion [23].

$$\langle \varphi_i(t), \varphi_k(t - nT) \rangle = \delta_{i-k}\delta_n \quad \text{for } i, k=0,1,..,\ M\text{-}1 \text{ and all } n. \tag{2.4}$$

Also, it can be shown that these pulses are power complementary, i.e.,

$$\frac{1}{M}\sum_{m=1}^{M} |\Phi_m(f)|^2 = 1 \tag{2.5}$$

The structure shown in Figure 2.1 and 2.2., can be used for other wavelets as well. Thus, the synthesis tree can generate eight Daubechies wavelet pulses $\varphi_i(t)$, $i = 0, \ldots, 7$ if the Daubechies scaling function [23] and the corresponding mother wavelet [23] are used as the filters g_0 and g_1.

In this dissertation, the OWDM pulses generated by through a Daubechies filter as the prototype $G_0(z)$ are used. An example family, generated from a 4-tap Daubechies

filter $G_0(z)$ = [0.3415, 0.5915, 0.1585,−0.0915] and a 2-stage tree, is given in Table 2.1. Note that each pulse is normalized to unit energy. Actually as shown originally in Figure 2.1 , the tree structure shown can be used to synthesize the transmitted OWDM signal $s(t)$ of (2.2) and (2.3). By applying the ith supersymbol $A_i = [a_{0,i}, a_{1,i}, \ldots, a_{M-1,i}]^T$at instant iM, and of course repeating this process for all i, it is easily seen using superposition that the output signal from the synthesis tree is (2.1). The synthesis tree is a multi-rate multiple input single output (MISO) [38] linear filter. The corresponding analysis trees at the receiver will also be multi rate linear filter, but of the single input multiple output (SIMO) type [38].

2.1.3 OWSS Pulses

While the OWDM pulses do satisfy the generalized Nyquist criterion, they are not broadband and are just as susceptible to deep fades, as are the OFDM pulses. Overcoming this deficiency, the OWSS pulses are derived from OWDM pulses $\varphi_m(t)$ by spreading them in the wavelet domain through a suitable family of PN codes. The OWSS transmit signal synthesizer and receiver signal analyzer is illustrated in Figure 2.2 and 2.3. The new broadband OWSS pulse is given by

$$\psi^{(i)}(t) = \sum_{m=0}^{M-1} c_m^{(i)} \varphi_m(t) = \underline{c}^{(i)T} \underline{\phi}(t) \tag{2.6}$$

Here $c(i)$, $i = 0, \ldots, M-1$, are the code vectors which perform the spreading in wavelet domain. The superscript connotes the ith pulse, which is assigned to the ith user. In this dissertation, Hadamard codes [25] will be used. Using Hadamard codes, it can readily be shown that the OWSS pulses, $\psi^{(i)}(t)$, $i = 0, \ldots, M-1$, are also doubly-orthogonal.

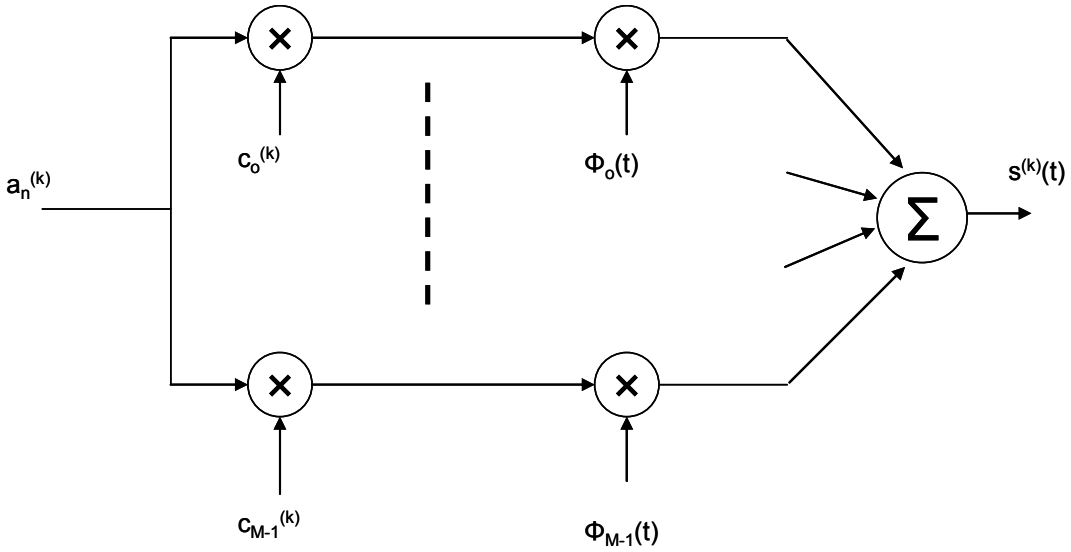

Figure 2.2 Block Diagram of OWSS Transmitter (For *k*-th User)

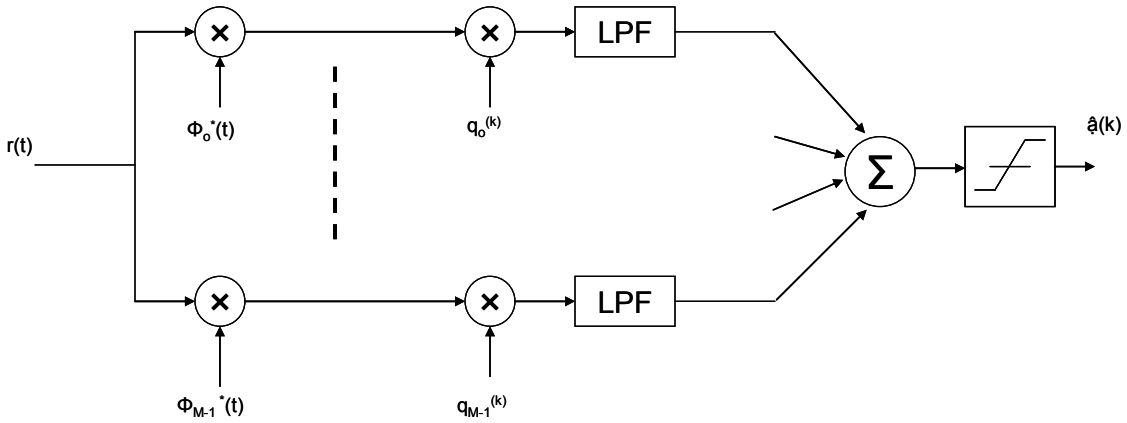

Figure 2.3 Block Diagram of Correlator Bank and Summer at OWSS Receiver

(For k-th User)

That is, they (like OWDM pulses) satisfy the generalized Nyquist criterion.

$$\langle \psi_i(t), \psi_k(t - nT) \rangle = \delta_{i-k}\delta_n \quad \text{for } i, k=0,1,.., M-1 \text{ and all } n. \tag{2.7}$$

Thus, these pulses provide a means for creating M virtual channels. Also, it can be shown

that these pulses are power complementary, i.e.,

$$\frac{1}{M}\sum_{m=1}^{M}\left|\Psi_m(f)\right|^2 = 1 \tag{2.8}$$

Most importantly, they are broadband. That is, each pulse in the family of M pulses broadband [1]. For $M = 4$ and $M = 8$, the corresponding Hadamard code matrices are given by

$$H_4 = \frac{1}{2}\begin{bmatrix} 1 & 1 & 1 & 1 \\ 1 & -1 & 1 & -1 \\ 1 & 1 & -1 & -1 \\ 1 & -1 & -1 & 1 \end{bmatrix}$$

$$H_8 = \frac{1}{\sqrt{8}}\begin{bmatrix} 1 & 1 & 1 & 1 & 1 & 1 & 1 & 1 \\ 1 & -1 & 1 & -1 & 1 & -1 & 1 & -1 \\ 1 & 1 & -1 & -1 & 1 & 1 & -1 & -1 \\ 1 & -1 & -1 & 1 & 1 & -1 & -1 & 1 \\ 1 & 1 & 1 & 1 & -1 & -1 & -1 & -1 \\ 1 & -1 & 1 & -1 & -1 & 1 & -1 & 1 \\ 1 & 1 & -1 & -1 & -1 & -1 & 1 & 1 \\ 1 & -1 & -1 & 1 & -1 & 1 & 1 & -1 \end{bmatrix} \tag{2.9}$$

For the OWDM pulses of Table 2.1 and code H_4 of (2.9) , the OWSS pulses are listed in Table 2.2. It is important to remark that these pulses need not be generated on-line; they can be computed off-line and conveniently stored in a ROM.

Table 2.1 OWDM Pulses Derived from 2-stage Tree with 4-tap Daubechies Filter

	Tap Weights									
Tap	0	1	2	3	4	5	6	7	8	9
Pulse 0	0.2333	-0.4040	-0.2958	0.7623	-0.0792	-0.2958	0.1127	-0.0792	0.0290	0.0167
Pulse 1	0.0625	-0.0183	-0.0792	0.2042	-0.4542	0.6708	-0.4208	0.2958	-0.1083	-0.0625
Pulse 2	0.0625	-0.1083	-0.5123	-0.0458	0.7288	0.3538	-0.1708	-0.1373	-0.1083	-0.0625
Pulse 3	0.0167	-0.0290	-0.1373	-0.0123	0.0792	0.2958	0.6373	0.5123	0.4040	0.2333

Table 2.2 OWSS Pulses Derived from 2-stage Tree with 4-tap Daubechies Filter

	Tap Weights									
Tap	0	1	2	3	4	5	6	7	8	9
Pulse 0	0.1845	-0.3248	-0.5123	0.4542	0.1373	0.5123	0.0792	0.2958	0.1083	0.0625
Pulse 1	0.1083	-0.1875	-0.2958	0.2623	0.5123	-0.4542	-0.1373	-0.5123	-0.1875	-0.1083
Pulse 2	0.1083	-0.1875	0.1373	0.5123	-0.6708	-0.1373	-0.3873	-0.0792	-0.1875	-0.1083
Pulse 3	0.0625	-0.1083	0.0792	0.2958	-0.1373	-0.5123	0.6708	0.1373	0.3248	0.1875

Pulse 0 and its magnitude spectrum is shown in Figure 2.4. In the interest of space, the other three pulses are not displayed, but they generally have similar time and spectral behavior. The blockwise autocorrelation for Pulse 0 is shown in Figure 2.5**,** using a rectangular sample-transmit pulse. The cross-correlation map of all 4 member pulses is shown in Figure 2.6 on a logarithmic scale. The actual matrix of cross-correlations is a 4 x 4 identity matrix. To summarize, OWSS has the following properties : (1) the pulses are broadband as seen from their spectrum, (2) the pulses are broad-time, since their time-support is long, (3) each pulse has an excellent autocorrelation behavior, and (4) the pulses are mutually orthogonal, so as to support multi-user operation. This excellent behavior holds up even in the presence of deep channel fades. For a detailed discussion on the beneficial properties of OWSS pulses, refer to [19]-[22]. The set of 16 pulses synthesized by a four stage OWSS synthesizer is illustrated in Figure 2.7.

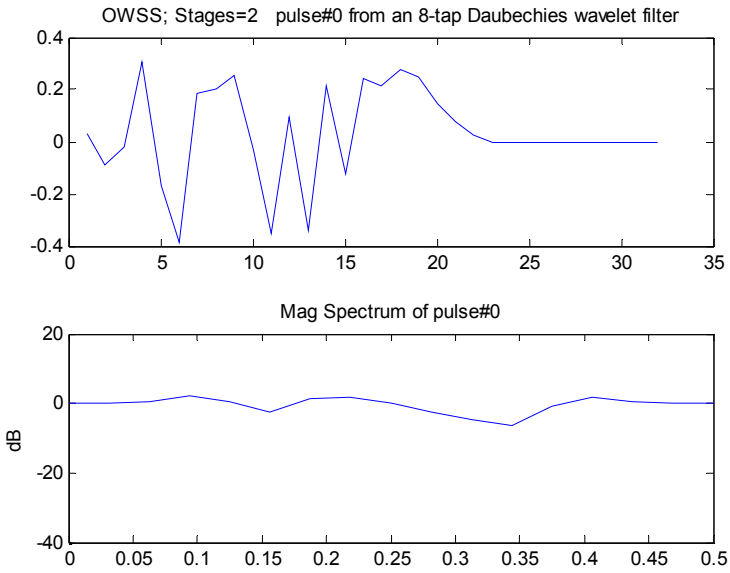

Figure 2.4 A Typical OWSS Pulse and its Magnitude Spectrum

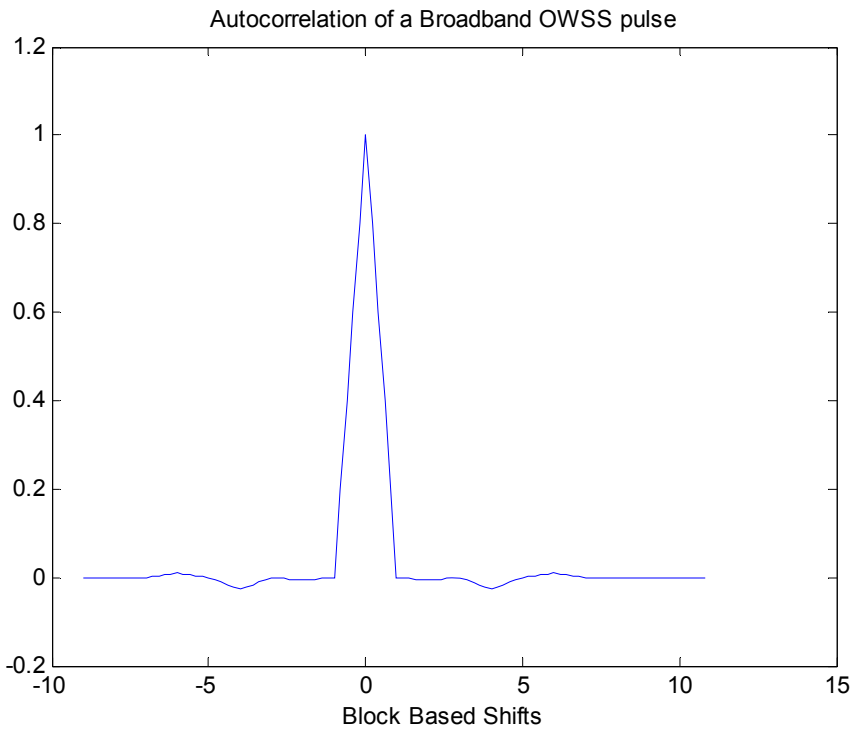

Figure 2.5 Autocorrelation of OWSS Pulse 0

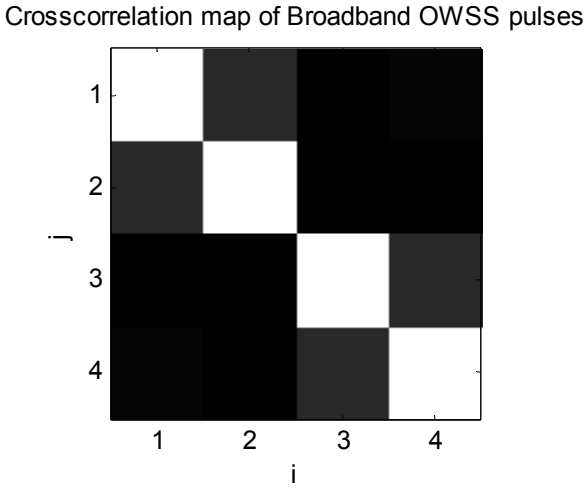

Figure 2.6 Cross Correlation Map of 4 OWSS Pulses

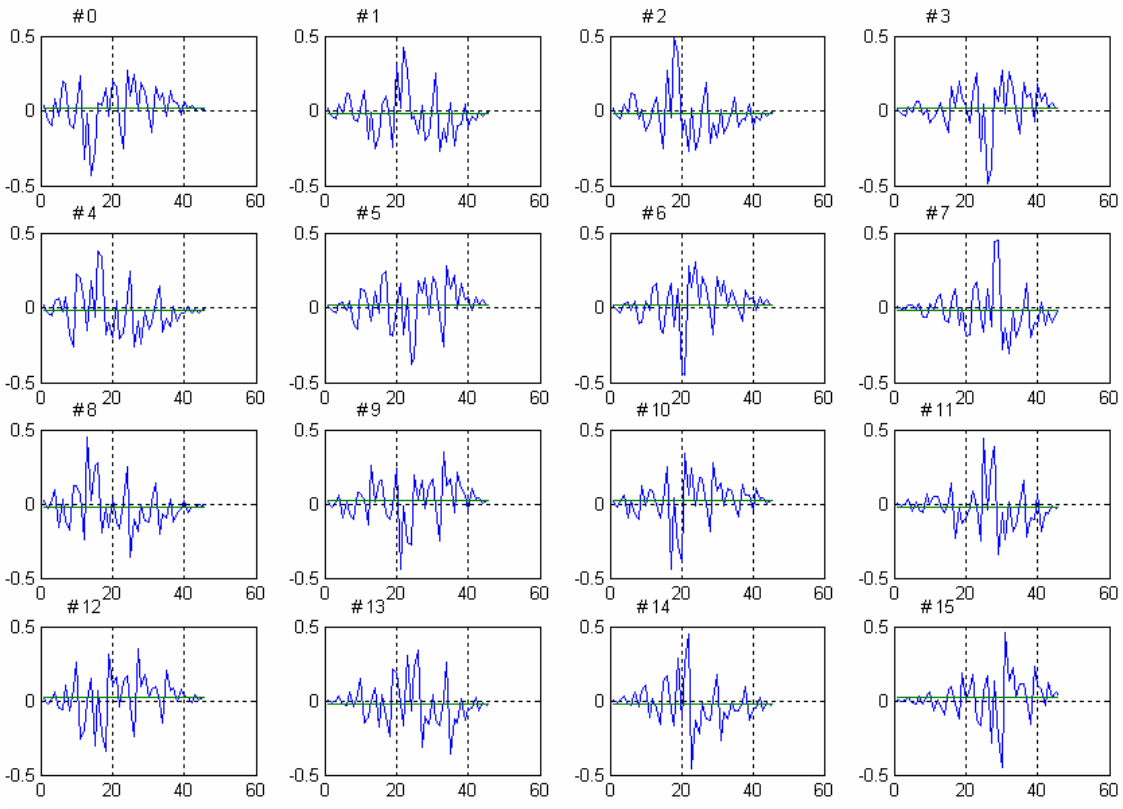

Figure 2.7 OWSS Pulses M=16 from a 4 stage OWSS Filter Tree

2.1.4 OWSS Signaling System

An overview of OWDM Spread-Spectrum (OWSS) transreceiver is illustrated in Figure 2.8 and a simplified ROM based system is shown in Figure 2.9. The training phase is not shown, during which a set of known samples *s(t),* previously stored at the receiver and produced by a set of known transmitted symbols, is used for training the channel equalizer [44]. The details of the transmitter block and the 'correlator and summer' block at the receiver were given in Figure 2.2 and 2.3. Here $\psi(t)$ is the set of the OWSS pulses, assembled in the form of a vector.

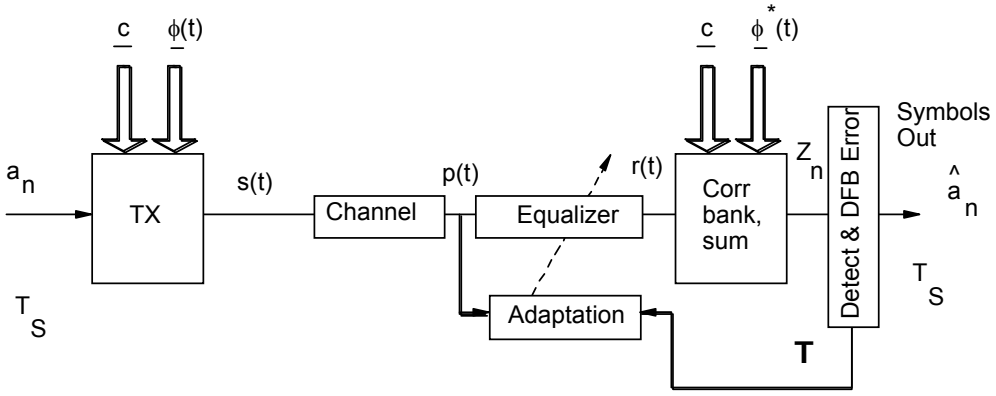

Figure 2.8 OWSS Signaling System

Referring to Figure 2.3 and Figure 2.8, the transmitted signal for the i-th user is

$$s^{(i)}(t) = \sum_n a_n^{(i)} \sum_{m=0}^{M-1} c_n^{(i)} \varphi_m(t - nT) = \sum_n a_n^{(i)} \psi^{(i)}(t - nT) \tag{2.10}$$

where $\psi^{(i)}(t)$ is the new OWSS broadband pulse for the *i*-th user. The received signal equals the sum of the signals received from all transmitters. For this discussion, assume ideal channel conditions without channel attenuation and multipath effects [1],[50]. Thus, at *k*-th receiver the received signal is

$$r(t) = \sum_{i=1}^{U} r^{(i)}(t) = \sum_{i=1}^{U} \sum_n a_n^{(i)} \psi^{(i)}(t - nT - \tau_i) \tag{2.11}$$

Assuming perfect timing, the output of the *k*-th correlator in the OWSS receiver is

$$\begin{aligned} z_n^{(k)} &= \left\langle r(t), \psi^{(i)}(t - nT - \tau_k) \right\rangle \\ &= a_n^{(k)} \left\langle \psi^{(i)}(t - nT - \tau_k), \psi^{(i)}(t - nT - \tau_k) \right\rangle \\ &\quad + \underbrace{\sum_{l \neq n} a_n^{(k)} \left\langle \psi^{(i)}(t - lT - \tau_k), \psi^{(i)}(t - nT - \tau_k) \right\rangle}_{ISI} \\ &\quad + \underbrace{\sum_{i \neq k} \sum_l a_l^{(k)} \left\langle \psi^{(i)}(t - lT - \tau_i), \psi^{(i)}(t - nT - \tau_k) \right\rangle}_{ICI} + \underbrace{N^{(k)}}_{AWGN} \\ &= a_n^{(k)} + ISI_n^{(k)} + ICI_n^{(k)} + +N^{(k)} \end{aligned} \tag{2.12}$$

The inter symbol interference term (*ISI)* [1] is zero due to the impulsive nature of the autocorrelation of the OWSS pulses. Also for the down-link case, all τ_i, are equal, so that the inter channel interference term (*ICI)* [1] is also zero. Thus the output of the *k*-th OWSS receiver correlator is

$$z_n^{(k)} = a_n^{(k)} + N^{(k)} \tag{2.13}$$

This means that except for the addition of Adaptive White Gaussian Noise (AWGN) [1], [44], the input to the decision device is the *n*-th symbol of the *k*-th user. Thus, the probability of symbol error would be the same as in the single user AWGN case for QAM symbols [1], [44].

Figure 2.2, 2.3 and 2.8 have provided a detailed structural realization of the OWSS transreceiver, however simpler realization is possible as illustrated in Figure 2.9. This is a ROM based design, where the S/P and P/S conversions have been omitted for simplicity. Here the PN code has already been imbibed in the transmit pulse $\psi^{(i)}(t)$ for the *i*-th transmitter-receiver pair.. Also, Decision Feedback Equalizer (DFE) [44] has been added, which will be discussed in the next sub-section. Also note that the wavelet pulse set $\{\psi^{(i)}(t)\}$ is common to all users. It is only the PN codes that are different for each user pair, as signified by the superscript *i* in equation (2.10).

2.1.5 Equalization in the OWSS Receiver

To surmount the ISI introduced by a time varying multipath channel [1], [44], a powerful adaptive equalizer [44] structure has been developed for the OWSS system. The

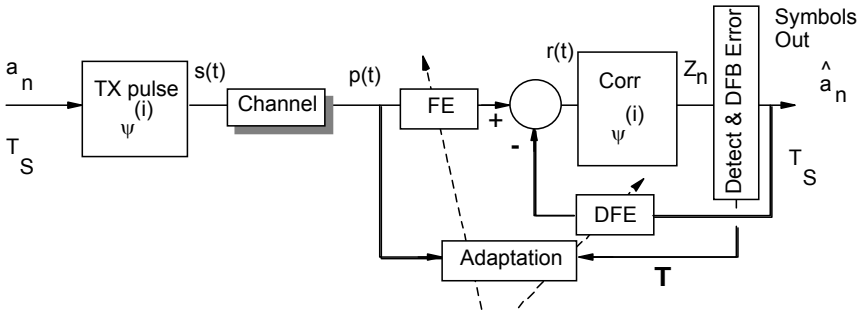

Figure 2.9 Simplified ROM Based OWSS Signaling System

baseband part of an OWSS receiver is shown in Figure 2.10. It deploys an adaptive Forward Equalizer (FE) and a Decision Feedback Equalizer (DFE), both of finite impulse response (FIR) form [45]. Not shown is the adaptation mechanism, which will not be discussed here but can be found in [29], [30]. The receiver also uses a correlator, a decision device, and an upsampler. Indeed, the output of the equalizer is correlated with an OWSS pulse, which is specific to the user, thus despreading it for detection. Note also that the correlator generates its output every *M*th sample. Therefore, the decision device [1] and error computations operate at a lower rate than does the equalizer. Thus the OWSS receiver is a multi rate system [51]. Since the DFE operates at the same speed as the FE, an upsampler [45] is needed, as shown in the figure. Initially, the coefficients of the FE and DFE are obtained through a training phase (using a prestored sequence of symbols and the LMS [44] algorithm for update). Subsequently, the receiver goes into maintenance mode. Of course, the equalizer coefficients are updated in this mode as well. The training phase begins with an arbitrary set of equalizer weights. These weights tend to converge to minimize the Mean Square Error (MSE) [44]. The final weights obtained at the end of the training are then used to initialize the maintenance phase. As stated will

earlier, the theory of the adaptive equalizer, in particular the adaptation mechanism, will not be discussed here. Readers can refer to [26], [39] and [30] for further details.

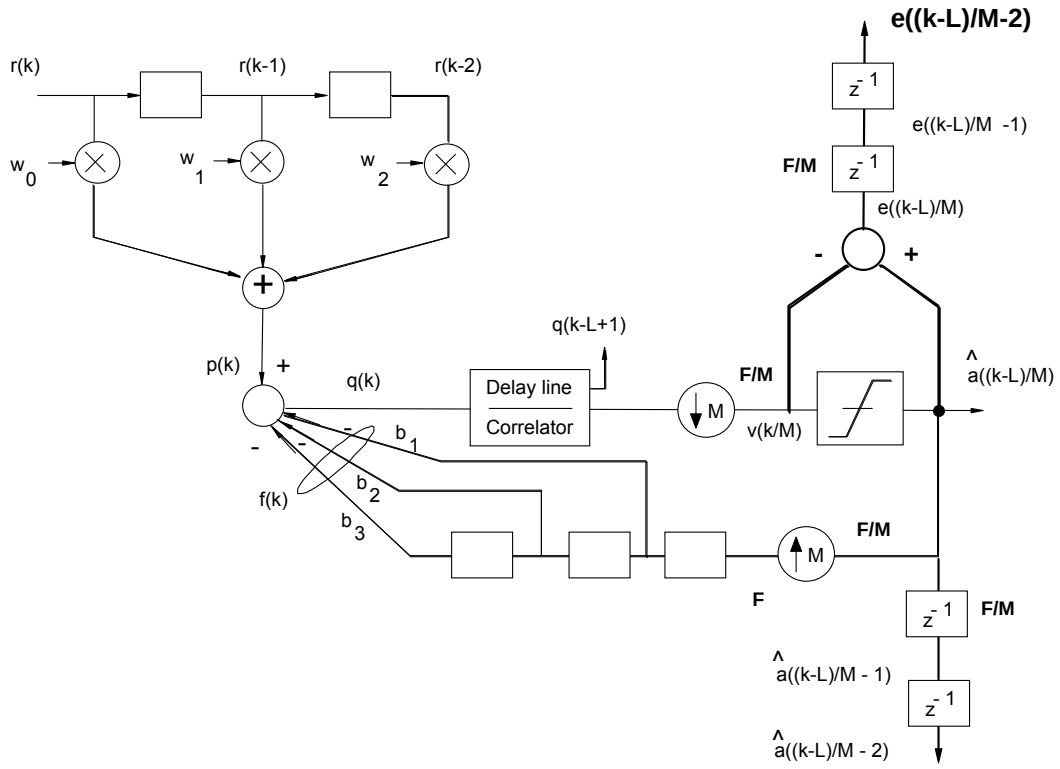

Figure 2.10 Details of the Baseband Portion of the OWSS Receiver

2.1.6 Bandwidth Estimate and Multiple Access Capability of OWSS

The transmission bandwidth of the 108 Mbps OWSS System will now be discussed. Let us assume a 108 Mbps gross bit rate, of which 8 Mbps is to be set aside for overhead. A 64QAM modulation [44] is assumed, so that the symbol rate becomes R_s = $108/\log_2 16 = 108/6 = 18$ Msps. For M wavelet channels the symbol rate on each channel becomes $R_{sc} = 18/M$ Msps with a corresponding super-symbol interval $T = M/18$. Then the bandwidth of each of the underlying M wavelets is $\Delta f = 18/M$ MHz. Correspondingly,

the baseband bandwidth becomes $BW_{BB} = (M)(\ 18/M)$ MHz. Finally, the transmission bandwidth is given by $B_T = (18)((M+1)/M)$. Due to the overlap between the spectra of the wavelet pulses, the bandwidth expansion takes place only for the boundary wavelets, giving rise to the factor $(M+1)/M$. Thus For M=4, T=3.5555 μs and B_T = 18.28125 MHz. For M=8, T=0.44444 μs and B_T = 20.25 MHz.

As mentioned earlier the OWSS scheme can be used for multiple access, from a high single-user data rate to various shades of multi-user and correspondingly reduced data rates. Denote the overall system bit rate R. Then any of the combinations, $U = 1$, $U = 2$, $U = 4$, …, $U = M$ can be incorporated. For example, if the number of users is $U = 8$, the bit rate for each would be $R/8$ and the number of codes allocated to each $M/8$; needless to say, M should be chosen to be greater than or equal to 8 (e.g., 16). It is useful to remark that in the single user case, random access sharing of the channel could well be done using CSMA/CA [40] at the MAC layer. Thus, the term *single user* must be interpreted carefully. It simply means that only a single user can access the bandwidth at a time (whereas with $U = 8$, up to eight users can access the channel simultaneously).

2.2 Background on MIMO-STC-OFDM

The prevailing 54Mbps WLAN standards, 802.11a/g [4], [5] are based on OFDM [6]-[8]. Next generation WLAN standards are also expected to be based on OFDM and the Industry is specifically interested in Multiple Input Multiple Output (MIMO) systems [9] – [16] which are compatible with OFDM, namely current legacy systems. This would allow reuse of functionality and existing standard protocols. A high data rate extension 802.11 n targeting bit rates of over 100 Mbps is due in 2009 and will probably combine concepts of OFDM with Multiple Input Multiple Output (MIMO) algorithms. A novel MIMO-STC-OFDM system [33] – [35] has been developed which is capable of targeting bit rates upwards of 108 Mbps. This system combines basically combines OFDM technology with Space Time Block Coding (STBC) [38], [39], [52], [53] in a MIMO environment. We begin with an analysis of OFDM.

2.2.1 Background on OFDM

In early systems high data rates of the time were obtained by achieving parallel transmissions of data the frequency domain. This was achieved by dividing the total signal frequency band into non-overlapping frequency subchannels or subcarriers, a technique called Frequency Division Multiplexing (FDM) [44]. FDM however was spectrally inefficient due to the use of guard spaces to eliminate ICI. A more efficient use of the spectrum can be achieved if the subchannels in FDM are able to overlap. This would however require the subchannels to be mutually orthogonal and this was the basic concept behind OFDM. OFDM is a multi carrier (MC) technique [44], that operates with

specific orthogonality constraints between the subcarriers. Due to this, OFDM achieves high spectral efficiency.

In OFDM the subcarrier pulse is chosen to be rectangular and number of subcarriers is selected to be a power of 2. This has the advantage that the pulse shaping and modulation can be done by a simple inverse discrete fourrier transform (IFFT) [5]-[8], resulting in remarkable reduction of hardware complexity. A simple baseband OFDM transreceiver is illustrated below in Figure 2.11.

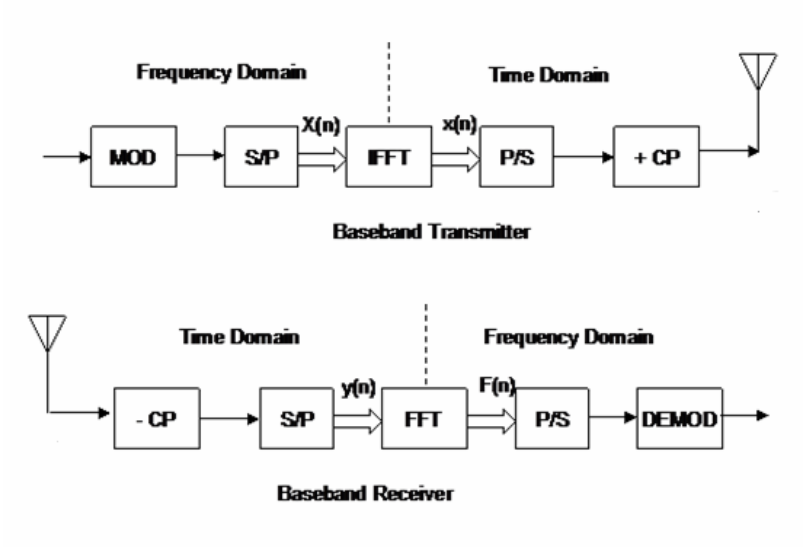

Figure 2.11 Simple Baseband OFDM Transreceiver

OFDM converts serial data stream $\underline{X(n)}$ into parallel blocks of size K (where K is the number of subcarriers), and uses IFFT to obtain time-domain signal $\underline{x(n)}$. Before transmission, the inverse FFT (IFFT) described by matrix F^H to applied to the QAM symbols, to obtain

$$\underline{x}(n) = F^H \underline{X}(n) \tag{2.14}$$

where F is a $K \times K$ FFT matrix.

Let $h(l)$, $l=0,\ldots,L$ be the chip rate sample discrete-time baseband equivalent L^{th} order FIR channel between the transmit and receive antenna. Knowledge of the channel is not required, except for the upper bound L on its maximum channel order. In order to eliminate the inter-block interference (IBI) caused by the FIR channel, the cyclic prefix (CP) of length L is inserted at the beginning of $\underline{x}(n)$ which is discarded at the receiver.

Time domain OFDM signal is cyclically extended to mitigate the effect of time dispersion [5]-[8]. The length of cyclic prefix (CP) [5] has to exceed the maximum excess delay of the channel in order to avoid IBI. Basic idea of cyclic extension is to replicate part of the OFDM time-domain symbol from back to the front to create a guard period. As long as maximum excess delay is smaller than the length of the cyclic extension, the signal distortion stays within the guard interval, which is removed later at the receiver. Hence, ISI is prevented at the expense of a spectral efficiency loss.

The CP insertion can be described by $P = [I_P^T \; I_K^T]$, where I_P is formed by the last rows of the $K\times K$ identity matrix I. The operation of discarding the first L receiver symbols in the receiver can be described by the matrix $Q = [0_{K\times L} \; I_K]$. The FIR channel is described by the $(K+L)\times(K+L)$ Toeplitz matrix H_i with the (k,l) entry $h(k-l)$.Let $G=PHQ$ denote the equivalent channel matrix in the receiver after eliminating the IBI. The $K\times 1$ IBI-free received symbol block $\underline{y}(n)$ is given by

$$\underline{y}(n) = GF^H \underline{X}(n) + Q\underline{w}(n) \tag{2.15}$$

is the received symbol block from the transmit antenna. $\underline{w}(n)$ is the AWGN vector.

Given $\underline{y}(n)$, the FFT described by the matrix F is performed on $y(n)$ to obtain

$$\underline{Y}(n) = F\,\underline{y}(n) = D\underline{X}(n) + FQw(n) = D\underline{X}(n) + \underline{W}(n) \tag{2.16}$$

where D is the diagonalized equivalent channel matrix by pre- and post-multiplication of the circulant matrix G with F and F^H. The diagonalized channel matrix can now be equalized by the Zero Forcing (ZF) [44] approach and fed to symbol decision device like a slicer to recover the QAM symbols at the receiver.

In the OFDM transmitter, the sub-carriers at the ends of the spectrum are usually set to zero in order to simplify the spectrum shaping requirements at the transmitter, *e.g.* IEEE 802.11a [4]. These subcarriers are used as frequency guard bands and are referred as *virtual carriers* or *null subcarriers* in literature [4]. To avoid difficulties in D/A and A/D converter offsets, and to avoid DC offset, the center subcarrier falling at DC is not used as well. The power spectrum for a 54 Mbps 802.11a OFDM spectrum is shown in Figure 2.12. The system has 64 sub-carriers, uses 64QAM modulation and number of sub-carriers that are set to zero at the sides of the spectrum is 11. In the figure the 802.11a OFDM spectrum has been simulated, the associated spectrum mask and spectrums provided by the 802.11a standard and Richard Van Nee. For a more detailed review of the OFDM and the 802.11a standard, refer to [4],[8].

2.2.2 Background on MIMO and STC

Physical limitations on wireless channels present a fundamental challenge to the reliability of wireless communications. Factors such as bandwidth limitations, propagation loss, time variance, noise, interference, offsets and multipath channel fading limit the capacity of the wireless channel making it a narrow pipe that has limited ability

accommodate the flow of data. Further challenges come from power limitation as well as size, shape and speed of devices in wireless portables. In order to achieve very high data

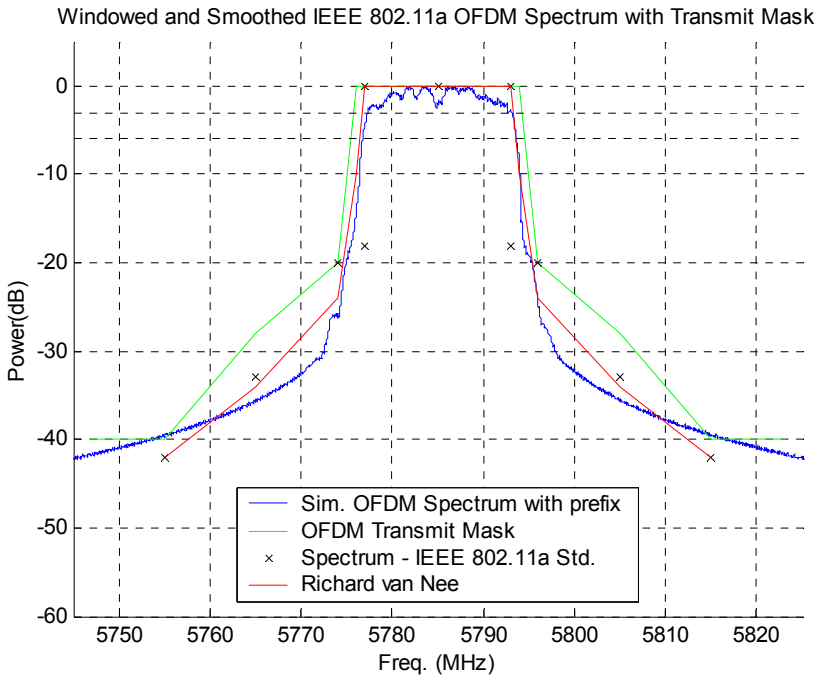

Figure 2.12 802.11a OFDM Passband Spectrum and Spectrum Mask

rates on narrowband wireless channels, many antennas at both transmitter and receiver will be needed. Deploying multiple antennas at both the base and remote stations, i.e. Multiple Input Multiple Output (MIMO) [9], [10] systems, increases the capacity [11], [12] of wireless channels and information theory provides measures of this increase. MIMO technology has attracted significant attention in wireless communications, since it offers significant increases in data throughput and link range without additional bandwidth or transmit power. It achieves this by higher spectral efficiency (more bits per second per hertz of bandwidth) and link reliability or diversity (reduced fading). Because of these properties, MIMO is the current theme of international wireless research.

2.2.2.2 Basic Mathematical Model of MIMO Systems

Consider a wireless communication systems with *n* transmit and *m* receive antennas where the channel between each transmit and receive antenna is quasi-static Rayleigh [1], flat and mutually independent. This is illustrated in Figure 2.13. If *n* is fixed, then the capacity increases only logarithmically with *m*. If *m* is fixed, the mathematics of outage capacity proves that there comes a point when adding more transmit antennas will not make much difference.

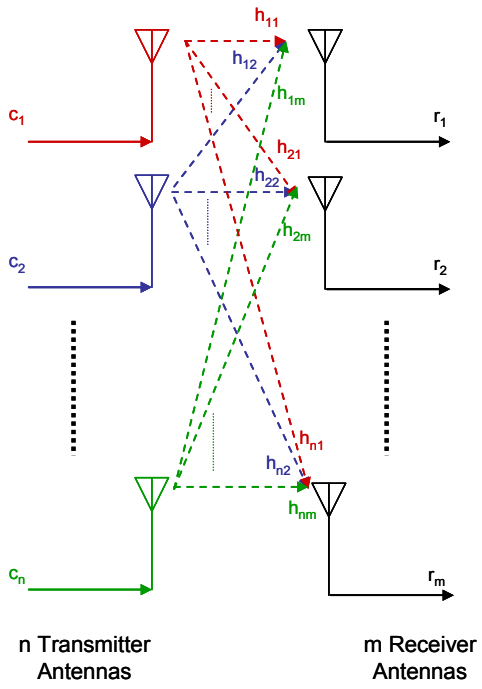

Figure 2.13 Basic MIMO System

For instance, if there is one transmit antenna i.e. $n = 1$, then Foschini et al. [11] prove that the capacity of the system is a random variable of the form $log_2(1 + (x_{2m}^2/2m)\ SNR)$, where x_{2m}^2 is a random variable formed by summing the squares of $2m$ independent Gaussian random variables with mean zero and variance one. This means

that by the strong law of large number in distribution, in the limit $(x_{2m}^2/2m)$ tends to 1. Practically speaking, for $m = 4$, $(x_{2m}^2/2m) \approx 1$, and the capacity is the familiar Gaussian capacity $log_2(1 + SNR)$ per complex dimension. Thus in the presence of one receive antenna, little can be gained in terms of outage capacity by using more than four transmit antennas. A similar argument shows that if there are two receive antennas, almost all the capacity increase can be obtained using transmit antennas

If m increases and $n \geq m$, then information theory [11], [12] shows that the capacity of the system increases at least linearly as a function of m. Therefore by using multiple transmitter and receiver antennas to create multiple-input multiple-output (MIMO) systems to obtain higher capacities. The number of degrees of freedom is given by the product $n \times m$.

Consider the wireless communication system with n antennas at the base station and m antennas at the remote. At each time slot t, signals are transmitted simultaneously from n transmit antennas.

$$c_t^i, i = 1, 2, ..., n \tag{2.17}$$

n signals are transmitted simultaneously each from a different antenna and all these signals have the same transmission period T. The channel is assumed to be flat fading [1], and the path gain from transmit antenna i to receiver antenna j is defined to be $h_{i,j}$. η_j^t is the noise for channel between transmit antennas and receive antenna j at time t.
The path gains are modeled as samples of independent complex Gaussian random

variables with variance 0.5 per real dimension. The wireless channel is assumed to be quasi-static so that path gains are constant over a frame of length *l* and vary from one frame to another. The noise samples are independent samples of a zero mean complex Gaussian random variable with variance *n/(2 SNR)* per complex dimension.

At time *t, t=1,2,3,..,l* the signals received at antenna *j, j=1,2,3,...,m* is given by

$$r_j^t = \sum_{i=1}^{n} h_{i,j} c_i^t + \eta_j^t \tag{2.18}$$

Using matrices and vectors, the above relation can be expressed as

$$\underline{r}_t = H\underline{c}_t + \underline{\eta}_t \tag{2.19}$$

where the received signal vector, transmitted signal vector, channel matrix and noise vector are expressed as

$$r_t = (r_t^1, r_t^2, ..., r_t^m)^T;\ c_t = (c_t^1, c_t^2, ..., c_t^n)^T;\ \eta_t = (\eta_t^1, \eta_t^2, ..., \eta_t^l)^T \tag{2.20}$$

$$H = \begin{pmatrix} h_{1,1} & h_{2,1} & \dots & \dots & h_{n,1} \\ h_{1,2} & h_{2,2} & \dots & \dots & h_{n,2} \\ \vdots & \vdots & \vdots & & \vdots \\ \vdots & \vdots & & \vdots & \vdots \\ h_{1,m} & h_{2,m} & \dots & \dots & h_{n,m} \end{pmatrix} \tag{2.22}$$

Mathematically MIMO transmissions can be seen as a set of *m* equations (received signals) with a number of *n* unknowns (transmitted signals). To solve a problem of *m* equations and *n* unknowns, *m* should be at least equal to *n*. If $m = n$, there exists a unique solution to the problem and if $m > n$, a solution can be found by performing a

projection using a least squares method, also known as the *Zero Forcing* (ZF) method. If $m = n$, ZF gives the unique solution.

For (2.19), you can recover the transmitted signals by ZF and using a decision device (slicer). In this case assume $m = n$ and H is invertible, the ZF equalization [44] of the channel matrix can be carried out by multiplying both sides of (2.19) by the hermitian transpose H^H.

$$\begin{aligned} \hat{c} &= H^H r = H^H Hc + H^H \eta = Ic + H^H \eta \\ \hat{c} &= c + H^H \eta \end{aligned} \tag{2.23}$$

The output of the ZF equalizer is fed to the slicer to recover the original QAM symbols. Minimum Mean Squared Error (MMSE) equalization [44] can also be used for better performance.

2.2.2.2 MIMO Technologies

MIMO technologies can be sub-divided into three main categories: (1) Precoding, (2) Spatial Multiplexing (SM) and (3) Diversity Coding.

Precoding can be interpreted as multi-layer beamforming in a narrow sense. Beamforming is a signal processing technique used in sensor arrays for directional signal transmission or reception. In (single-layer) beamforming, the same signal is emitted from each of the transmit antennas with appropriate phase weighting (sometimes with gain) such that the signal power is maximized at the receiver input. The benefits of beamforming are to increase the signal gain from constructive combining and to reduce the multipath fading effect. The improvement compared with an omnidirectional

reception/transmission is known as the receive/transmit gain (or loss). In a wide sense precoding means that all spatial processing is done at the transmitter. When the receiver has multiple antennas, the transmit beamforming cannot simultaneously maximize the signal level at all of the receive antenna and precoding is used. Note that precoding requires knowledge of the channel state information (CSI) at the transmitter.

Spatial multiplexing (SM) requires actual MIMO antenna configuration, i.e. multiple antennas at the transmitter and receiver. In SM, a high rate signal is split into multiple lower rate streams and each stream is transmitted from a different transmit antenna in the same frequency channel. If these signals arrive at the receiver antenna array with sufficiently different spatial signatures, the receiver can separate these streams, creating parallel channels for free. Spatial multiplexing algorithms like BLAST [56]-[58] are a very powerful technique for increasing channel capacity at higher Signal to Noise Ratio (SNR). The maximum number of spatial streams is limited by the lesser in the number of antennas at the transmitter or receiver. Spatial multiplexing can be used with or without transmit channel knowledge.

Diversity coding techniques are used when there is no channel knowledge at the transmitter. In diversity methods a single stream (unlike multiple streams in SM) is transmitted, but the signal is coded using techniques called space-time coding [52], [53]. The signal is emitted from each of the transmit antennas using certain principles of full or near orthogonal coding. Diversity exploits the independent fading in the multiple antenna

links to enhance signal diversity. Because there is no channel knowledge, there is no beamforming or array gain from diversity coding.

Combinations of the three different technologies are possible. Spatial multiplexing can also be combined with precoding when the channel is known at the transmitter or combined with diversity coding when decoding reliability is in trade-off. In this dissertation new MIMO-STC-OFDM system [33]-[35] is being presented combining concepts of MIMO systems, OFDM and STC. Hence the concepts of STC, especially Space Time Block Coding (STBC) will now be reviewed.

2.2.2.3 Space Time Coding (STC)

Space Time Codes [52], [53] are basically of two types : (1) Space Time Trellis Codes (STTC) (2) Space Time Block Codes (STBC). In this dissertation STBC has been used and as such the terms STC and STBC are interchangeable. However from now on STC will be used to denote space time block codes.

Space–time block coding is a coding technique used in wireless communications to transmit multiple copies of a data stream (generally QAM symbols) across a number of antennas and to exploit the various received versions of the data to improve the reliability of the communication. The transmitted signal traverses a difficult environment with fading, scattering, reflection, refraction and is further corrupted by thermal noise (AWGN) in the receiver, which means that some of the received copies of the data will be 'better' or ‘less corrupted’ than others. This redundancy results in a higher chance of

being able to use one or more of the received copies to correctly decode the received signal. In fact, space–time coding combines all the copies of the received signal in an optimal way to extract as much information from each of them as possible. Originally proposed by Tarokh et al., these space–time block codes (STCs) achieve significant error rate improvements over single-antenna (SISO) systems. Their original scheme was based on trellis codes (STTC) but the simpler block codes were first utilized by Alamouti [39], and later by Tarokh et al. [38] to develop space–time block-codes (STBCs). STC nowadays primarily refers to STBC. STC involves the transmission of multiple redundant copies of data to compensate for channel fading and AWGN in the hope that some of them may arrive at the receiver less corrupted than others. In the case of STBC in particular, the data stream to be transmitted is encoded in blocks, which are distributed across space (transmit antennas) and time (time instant slots). While it is necessary to have multiple transmit antennas, it is not necessary to have multiple receive antennas, although to do so improves performance. This process of receiving diverse copies of the data is known as diversity reception.

A STC is usually represented by a matrix. Each row represents a transmission from an antenna over time and each column represents a time slot as shown below in (2.24).

$$\begin{array}{c} \\ 1 \\ 2 \\ \downarrow \\ n \end{array} \begin{array}{c} \begin{array}{cccc} 1 & 2 & \rightarrow & T \end{array} \\ \begin{bmatrix} s_{11} & s_{12} & \cdots & s_{1T} \\ s_{21} & s_{22} & \cdots & s_{2T} \\ \vdots & \vdots & \ddots & \ddots \\ s_{n1} & s_{n2} & \cdots & s_{nT} \end{bmatrix} \end{array} \tag{2.24}$$

Here, s_{ij} is the modulated symbol to be transmitted in time slot j from antenna i. There are to be T time slots and n transmit antennas as well as m receive antennas. This block is usually considered to be of 'length' T.

The code rate of an STC measures how many symbols per time slot it transmits on average over the course of one block . If a block encodes k symbols, the code-rate is

$$r = \frac{k}{T} \tag{2.25}$$

STCs as originally introduced, and generally studied as orthogonal. This means that the STC is designed such that the vectors representing any pair of rows taken from the coding matrix are orthogonal. This results in simple, linear, optimal decoding at the receiver. Its most serious disadvantage is that all but one of the codes that satisfy this criterion must sacrifice some proportion of their data rate. The design of STC is well documented in literature and readers can refer to [52][53], for further details.

Alamouti [39] invented the simplest of all the STC. It was designed for a two-transmit antenna system and has the coding matrix:

$$C_2 = \begin{bmatrix} s_1 & -s_2^* \\ s_2 & s_1^* \end{bmatrix}$$

where * denotes complex conjugate.This is a rate-1 code and it takes two time-slots to transmit two symbols. Using the optimal decoding scheme discussed below, the bit-error rate (BER) of this STC is equivalent to 2m-branch (2 receiver antennas) maximal ratio

combining (MRC). This is a result of the perfect orthogonality between the symbols after processing at the receiver there are two copies of each symbol transmitted and *m* copies received.

Alamouti's STC is a very special STC. It is the only orthogonal STBC that achieves rate-1. That is to say that it is the only STC that can achieve its full diversity gain without needing to sacrifice its data rate. Strictly, this is only true for complex modulation symbols. Since almost all constellation diagrams rely on complex numbers (QAM symbols) however, this property usually gives Alamouti's code a significant advantage over the higher-order STBCs even though they achieve a better error-rate performance. The significance of Alamouti's proposal is that it was the first demonstration of a method of encoding which enables full diversity with *linear* processing at the receiver. Furthermore, it was the first open-loop transmit diversity technique which had this capability. Subsequent generalizations of Alamouti's concept have led to a tremendous impact on the wireless communications industry.

Higher STC for more than 2 transmit antennas have been designed. However none of them are full rate codes. For example, the maximum rate for 3 transmit antennas is ¾. One particularly attractive feature of orthogonal STCs is that maximum likelihood decoding can be achieved at the receiver with only linear processing. For further details on higher order STCs and decoding of STCs, refer to [38], [52], [53].

2.3 Conclusion

In this chapter, a background on the OWSS, MIMO systems, OFDM and STC has been provided. OWSS is a promising technology for the next generation of high speed WLANs due to the unique advantages it enjoys over current WLAN signaling schemes like OFDM. Another promising technology for the next generation of high speed WLANs is the combination of MIMO systems and OFDM. MIMO algorithms are generally narrowband and the combination of OFDM with MIMO can deal with the wideband frequency selective fading channels of the future.

CHAPTER 3

MEDIUM ACCESS CONTROL IN OWSS WLANs

3.1 Medium Access Control in WLANs

The Medium Access Control (MAC) [59] protocol sub-layer, is the lower sub-layer of the Data Link Layer (DLL) [59], specified as the second layer above the PHY layer in the seven layer OSI model [59]. In WLANs, the MAC Layer manages and maintains communications between the wireless stations (radio network cards and access points) by controlling and coordinating access to the shared radio channel and utilizing protocols that enhance the transfer of data packets over the wireless medium. The 802.11a [4] standard specifies a common MAC Layer, which provides a variety of functions to support the operation of different 802.11 PHY layer specifications, such as 802.11a/g [4], [5] and the eagerly awaited 802.11n standard [17], [18], [60].

The channel access control mechanisms provided by the MAC layer are generally known as a multiple access protocols. The multiple access protocols are broadly classified into circuit mode [59] (like FDMA, TDMA, CDMA etc.) or packet mode methods [59] (like CSMA/CA, Slotted ALOHA). Hybrids of these techniques are also frequently used. In wireless networks, especially 802.11 WLANs, the packet mode method called Carrier Sense Multiple Access with Collision Avoidance (CSMA/CA) [40] is the basic channel access protocol in the MAC layer.

OWSS offers multiplexing capability either at the PHY layer or at the MAC layer. The primary advantage of using the MAC layer approach is that users can transmit and receive data packets at the full system bit rate, which is this paper, is 108 Mbps. Thus efficient resource sharing can occur for bursty users. Towards this end, OWSS will use a MAC protocol similar to that of the 802.11 WLAN Standard. Called the distributed co-ordination function (DCF) [4], it is a carrier sense multiple access with collision avoidance (CSMA/CA) scheme with binary slotted exponential backoff.

3.2 CSMA/CA: The Basic Access Method

The IEEE 802.11 standard [4], [5] uses CSMA/CA MAC protocol with *binary exponential backoff* algorithm to access the medium, called Distributed Coordination Function (DCF). DCF defines two methods, two way handshaking basic access (for broadcast frames) illustrated in Figure 3.1 and optional four way handshaking technique known as request-to-send and clear-to-send (RTS-CTS) technique, illustrated in Figure 3.2. A summary of the two DCF access methods is given here.

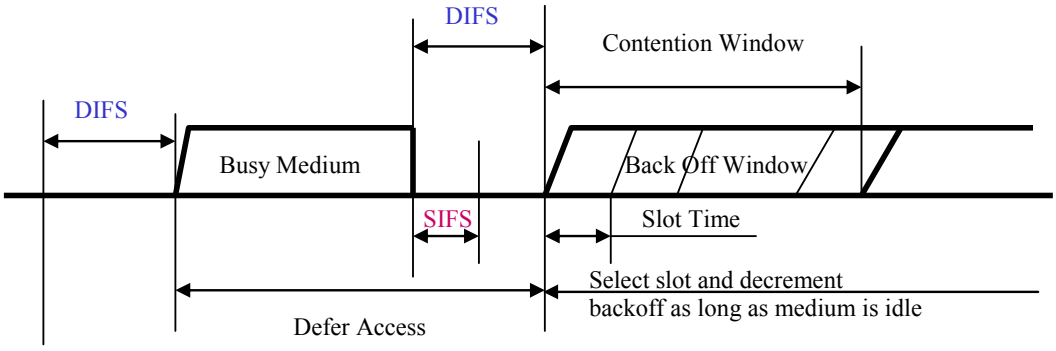

Figure 3.1 CSMA/CA

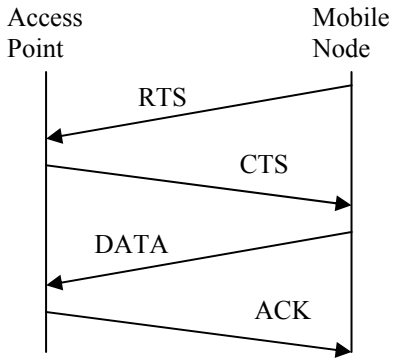

Figure 3.2 Four Way Handshake RTS-CTS Scheme

The basic access method is a two-way handshaking technique. A station with a packet to transmit persistently senses the channel and waits until a idle period equal to a distributed interframe space (DIFS) is detected. After an idle DIFS, the station waits for a random backoff interval before transmitting. This is a collision avoidance feature, which minimizes the probability of collision with packets transmitted from other stations. DCF has adopted a very efficient exponential backoff scheme. The time after DIFS is slotted and a station can transmit only at the beginning of each slot time as shown in Figure 3.1. Slot time (τ) is the time that a station takes to detect a transmission from another station and it depends on the physical layer. Slot time is the sum of the medium propagation delay, the receiver to transmitter turnaround time and the time taken to sense the state of the channel. A collision occurs only when two or more packets are transmitted in the same time slot.

At each packet transmission, the backoff time is uniformly chosen in the range *(0,w-1)*. The, value *w*, called the *contention window*, at the first transmission attempt is equal to the minimum contention window CW_{min}. After each unsuccessful attempt, w is doubled, up to a maximum value $CW_{max} = 2^{m}CW_{min}$. $CW_{min,}$ CW_{max} and *m*, the number of retry attempts are PHY-specific. The backoff interval is equal to the product of the selected random contention window CW and slot time. The backoff time counter is decremented as long as an idle channel is detected, frozen when the channel is sensed busy and reactivated again when the channel is sensed idle again for a time period more than DIFS. After the backoff timer expires, the station transmits the packet. Unlike CSMA/CD, CSMA/CA cannot detect a collision and has to rely on a *positive acknowledgement* (ACK) from the destination station to signal successful packet reception. At the end of a successfully transmitted packet, the destination station transmits ACK to the source station after a period of time called *short interframe space* (SIFS), which is shorter than DIFS. If the transmitting station does not receive the ACK within a specified ACK timeout, or it detects the transmission of another packet on the channel, it reschedules the packet transmission according to the above backoff scheme shown in Figure 3.3.

DCF defines an additional four-way handshaking technique to be optionally used for a packet transmission, known by the name RTS/CTS shown in Figure 3.4. A station that wants to transmit a packet, waits for an idle DIFS and follows the backoff rules explained above, and then, instead of the packet, first transmits a special short frame

called *request to send* (RTS). When the receiving station detects an RTS frame, it responds, after a SIFS, with a *clear to send* (CTS) frame. If the CTS frame is correctly received, the transmitting station is ready to transmit its packet after a SIFS.

The RTS/CTS scheme also handles the problem of system degradation due to hidden terminals. The RTS and CTS frames carry information regarding the length of the packet to be transmitted. This information can be read by all stations, which then update their *network allocation vector* (NAV). NAV contains specific information about the period of time the channel would be sensed busy. Thus a hidden station can suitably delay transmission and avoid collision, by detecting one of the RTS and CTS frames. The RTS/CTS scheme is very effective in terms of system performance for large packets, by reducing the length of frames involved in the contention process. For a more detailed explanation of the Basic Access and RTS-CTS scheme refer to the 802.11a standard [4].

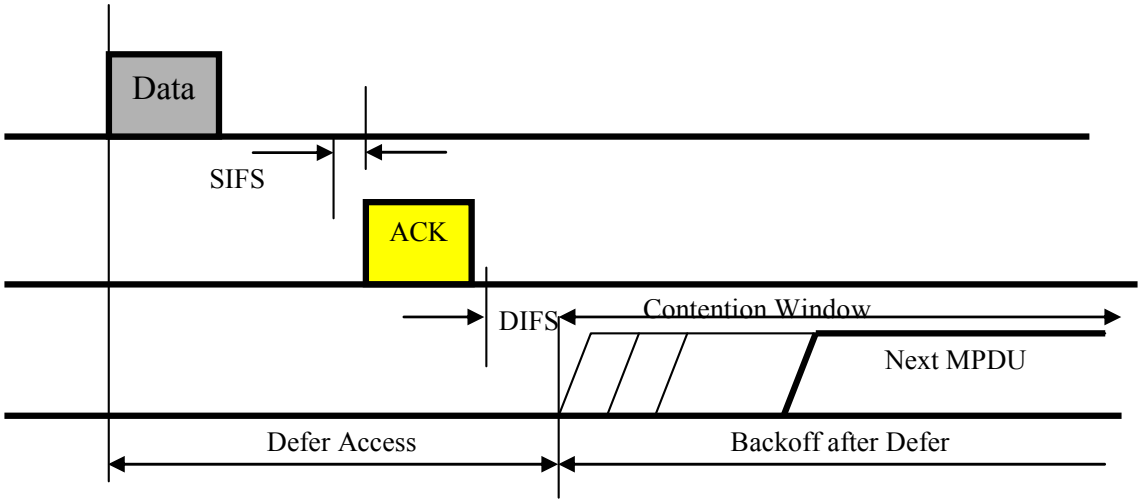

Figure 3.3 Basic Access Mechanism

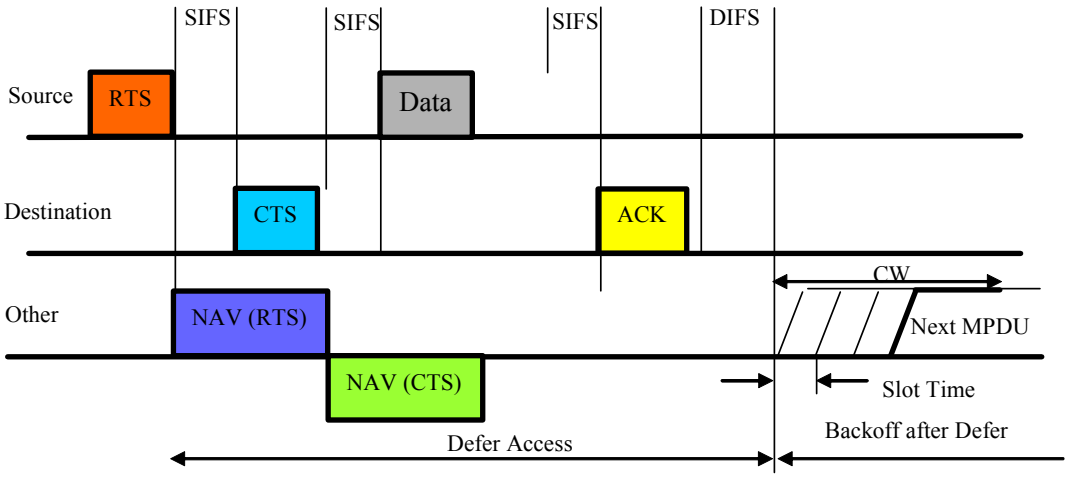

Figure 3.4 RTS/CTS Mechanism

3.3 Performance Analysis of the Distributed Co-ordination Function

This analysis is based on Bianchi's Model [41], [42]. The analysis is carried out as follows. First the behavior of a single station is analyzed using a Markov model [44], and two critical probabilities are obtained, which are independent of the DCF mechanism employed: stationary probability that the station transmits a packet in a generic slot time (q) and the probability that a transmitted packet collides (p). Then, by studying the events that can occur within a generic slot time, the saturation throughput of both Basic and RTS/CTS access methods can be expressed as function of the probability q. Finally the packet delay can be calculated based on the model above.

3.3.1 Markov Model

Consider a fixed number of n contending wireless stations operating under saturation conditions. Let $b(t)$ be the stochastic process representing the size of the back off window for a given station at slot time t (the time is stopped when the channel is sensed busy). The station transmits when the back off time reaches zero. At each transmission, the back off time is uniformly chosen in the range $(0,w-1)$. At the first transmission attempt, $w=W$, namely the minimum back off window. After each unsuccessful transmission, is doubled, up to a maximum value 2^mW. The maximum number of retry attempts is m. Let $W_i=2^iW$, where i lies in the range $(0,m)$, is called "backoff stage," and let $s(t)$ be the stochastic process representing the back off stage $(0,\ldots,m)$ of the station at time t.

The key approximation in Bianchi's model is, that at each transmission attempt and regardless of the number of attempts at retransmission, the probability p that a transmitted packet collides is constant and independent of the state $s(t)$ of the station (this is more accurate when W and n are larger). In this condition, it is possible to model the bi-dimensional process $\{s(t),b(t)\}$ with a discrete-time Markov chain illustrated below in Figure 3.5.

In this Markov chain, the only non null one-step transition probabilities are

$$
\begin{aligned}
&P\{i,k \mid i,k+1\} = 1, && k \in (0, W_i - 2) \,\&\, i \in (0,m) \\
&P\{0,k \mid i,0\} = \frac{1-p}{W_0}, && k \in (0, W_0 - 1) \,\&\, i \in (0,m) \\
&P\{0,k \mid i-1,0\} = \frac{p}{W_i}, && k \in (0, W_i - 1) \,\&\, i \in (1,m) \\
&P\{m,k \mid m,0\} = \frac{p}{W_m}, && k \in (0, W_m - 1)
\end{aligned}
\tag{3.1}
$$

Let

$$
b_{i,k} = lim_{t\to} P\{ s(t) = i, b(t) = k \}, i \in (0,m) \,\&\, k \in (0, W_i - 1) \tag{3.2}
$$

be the stationary distribution of the chain.

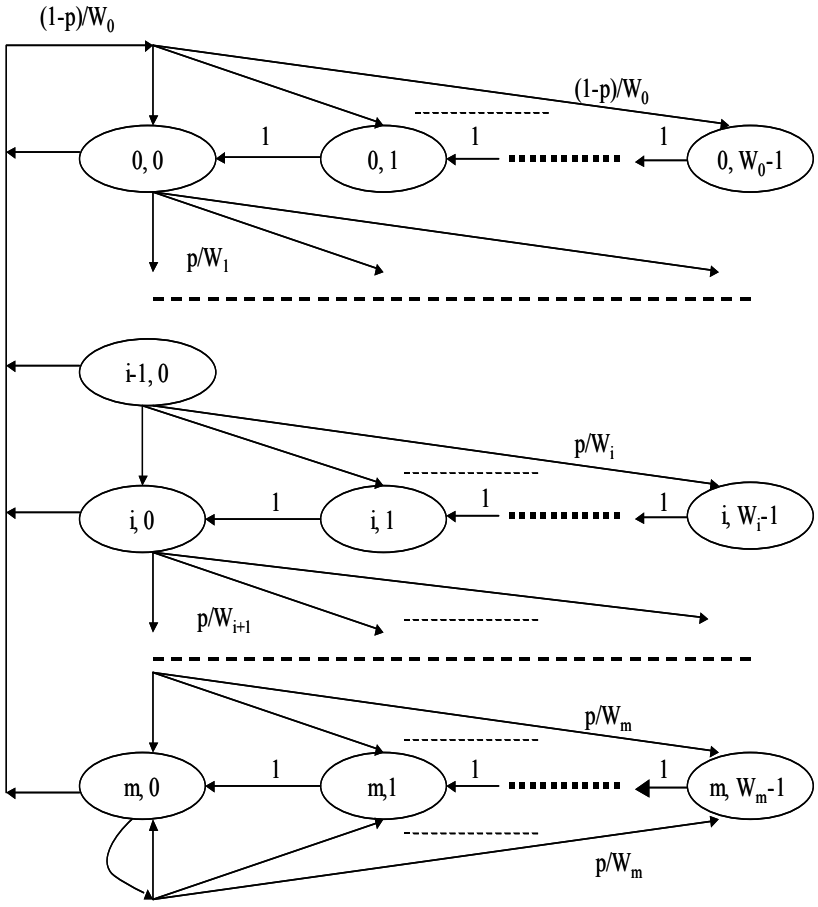

Figure 3.5 Markov Chain Model for the Backoff Window Size

Owing to the chain regularities, the following relations hold

$$b_{i,0} = p^i b_{0,0}, \quad i \in (0, m-1); \quad b_{m,0} = \frac{p^m}{1-p} b_{0,0}; \quad b_{i,k} = \frac{W_i - k}{W_i} b_{i,0} \tag{3.3}$$

The value of $b_{0,0}$ is determined by imposing the normalization condition $\sum_{i=0}^{m} \sum_{k=0}^{W_i - 1} b_{i,k} = 1$.

From which

$$b_{0,0} = \frac{2(1-2p)(1-p)}{(1-2p)(W+1) + pW(1-(2p)^m)} \tag{3.4}$$

Let q be the probability that a station transmits in a generic slot time. As any transmission occurs when the back off window is equal to zero, regardless of the back off stage, it is

$$q = \sum_{i=0}^{m} b_{i,0} = \frac{b_{0,0}}{1-p} = \frac{2(1-2p)}{(1-2p)(W+1) + pW(1-(2p)^m)} \tag{3.5}$$

However in general, q depends on the conditional collision probability p. To finally compute the probability p, that a transmitted packet collides, note that p is the probability that, in a time slot, at least one of the remaining $n-1$ stations transmits.

$$p = 1 - (1 - q)^{n-1} \tag{3.6}$$

Equation (3.5) and (3.6) represent a nonlinear system with two unknown's p and q can be solved using numerical techniques.

3.3.2 Throughput Analysis

Given n active stations contend on the same channel, and each transmits with a probability q, the probability P_{tr} that there is at least one transmission in a considered slot

time is given by

$$P_{tr} = 1-(1-q)^n \tag{3.7}$$

Given that a transmission has occurred the probability P_s, that the transmission is successful is given by

$$P_s = \frac{nq(1-q)^{n-1}}{P_{tr}} = \frac{nq(1-q)^{n-1}}{1-(1-q)^n} \tag{3.8}$$

Let u be the random variable representing the number of consecutive idle slots between two consecutive transmissions on the channel

$$E[u] = \frac{1}{P_{tr}} \text{ -1} \tag{3.9}$$

Finally the normalized system throughput S can be determined, defined as the fraction of time the channel is used to successfully transmit payload bits. As the instants of time right after the end of a transmission are renewal points, it is sufficient to analyze a single renewal interval between two consecutive transmissions, and express as the ratio

$$\begin{aligned} S &= \frac{E[\text{time for successful tranmission in interval}]}{E[\text{length of a revewal interval}]} \\ &= \frac{P_s E[P]}{E[v] + P_s T_s + (1-P_s)T_c} \end{aligned} \tag{3.10}$$

where $E[P]$ is the average packet length, T_S is the average time the channel is sensed busy because of a successful transmission, and T_C is the average time the channel is sensed busy by the stations during a collision. The times $E[P]$, T_S and T_C must be measured in slot times, as this is the time unit of $E[u]$.

To conclude the analysis, it remains only to specify the values T_S and T_C . Let $H=PHY_{hdr}+ MAC_{hdr}$ be the packet header, and d be the propagation delay. For the basic access method it is

$$T_S^{B} = H + E[P] + SIFS + d + ACK + DIFS + d$$

$$T_C^{B} = H + E[P^*] + DIFS + d \quad (3.11)$$

where $E[P^*]$ is the average length of the longest packet payload involved in a collision, in the case all packets have the same fixed size, $E[P^*]= E[P] =P$. T_C. is the time in which the channel is sensed busy by the *non-colliding station*s. For the RTS/CTS access method,

$$\begin{aligned} T_S^R &= RTS + SIFS + d + CTS + SIFS + d + H + ... \\ &.....E[P] + SIFS + d + ACK + DIFS + d \\ T_C^R &= RTS + DIFS + d \end{aligned} \quad (3.12)$$

3.3.3 Delay Analysis

The packet delay is another critical parameter in performance evaluation of the MAC layer [12]. For this another probability P_a is calculated, the probability that a specific station in n active stations transmits successfully

$$P_a = \frac{P_s}{n} = \frac{q(1-q)^{n-1}}{1-(1-q)^n} \quad (3.13)$$

R is the number of attempts at resensing the channel and T_f the expected time between two consecutive attempts at channel sensing. Then

$$R = \frac{1}{P_a} - 1$$
$$T_f = \left(\frac{P_s - P_a}{1 - P_a}\right) T_s + \left(\frac{1 - P_s}{1 - P_a}\right) T_c \tag{3.14}$$

The average delay time equals the average renewal cycle time plus the successful transmission time for the packet.

$$D = R(T_f + E(u)) + T_s \tag{3.15}$$

2.4 Performance of CSMA/CA MAC Layer in OWSS WLANs

In this analysis a robust transfer of the header and the preamble has been adopted; i.e., the PHY preamble (96 bits) and header (32 bits) are BPSK modulated with the concomitant transfer rate of only 18 Mbps. The use of the strategy shown in Figure 3.6 enhances the probability that even the far away stations receive the handshaking messages reliably so as to update their NAV (Network Allocation Vector) [4] for CSMA/CA access. Figure 3.6 also shows the inherent plumes of the OWSS pulses; as can be seen, all of these plumes are hidden except for the very last one.

A system throughput and delay analysis was carried out for OWSS based on Bianchi's Model. The numerical results are obtained according to the system parameters listed in Table 3.1. From the throughput analysis in Figure 3.7, it is evident that for a large number of stations, the RTS-CTS scheme performs significantly better than the basic access scheme. For the basic access scheme the throughput has an exponentially decaying profile, whereas for RTS-CTS it is generally constant at about 66%. The

average packet delay time, plotted in Figure 3.8, is proportional to the number of stations when the number of stations is small. However, it increases rapidly for large number of stations. At 20 stations, the packet delay is around 5 ms for both RTS-CTS and basic access; at 50 stations it increases to 12.5 ms for RTS-CTS and 15 ms for basic access.

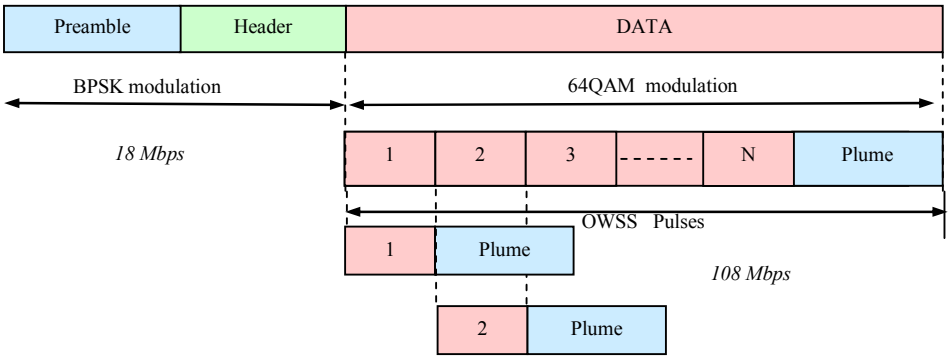

Figure 3.6 OWSS Frame Format

Table 3.1 MAC Attributes of OWSS

Attribute	Value
OWSS preamble	96 bits
OWSS header	48 bits
RTS size	160 bits
CTS size	128 bits
ACK size	112 bits
MAC header	272 bits
SIFS time (SIFS)	2 μs
DIFS time (DIFS)	9 μs
SLOT time (τ)	5 μs
Retry Attempts (m)	5
Payload	2312 bytes
CW_{MIN} (W)	32

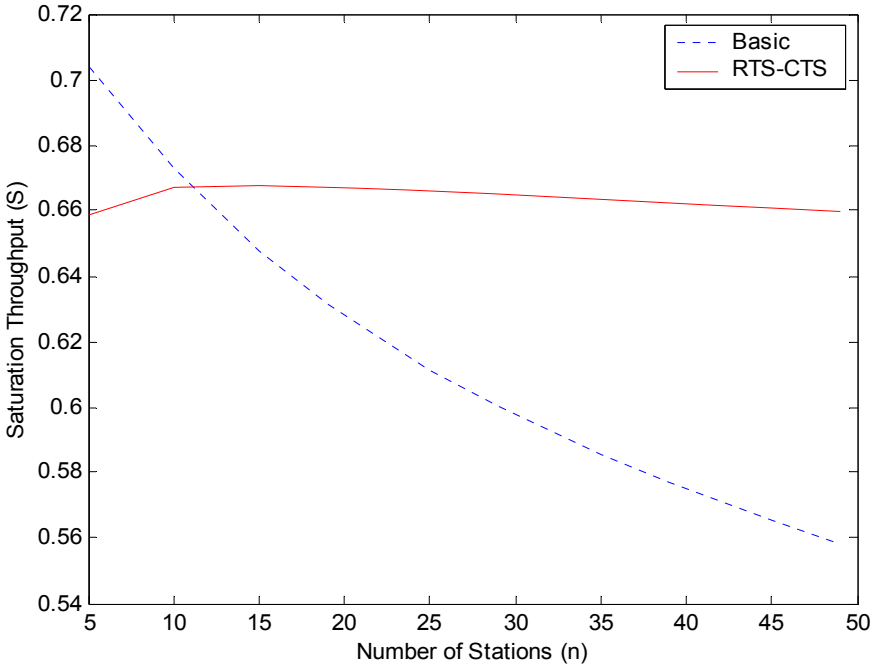

Figure 3.7 System Throughput for 108 Mbps OWSS WLAN

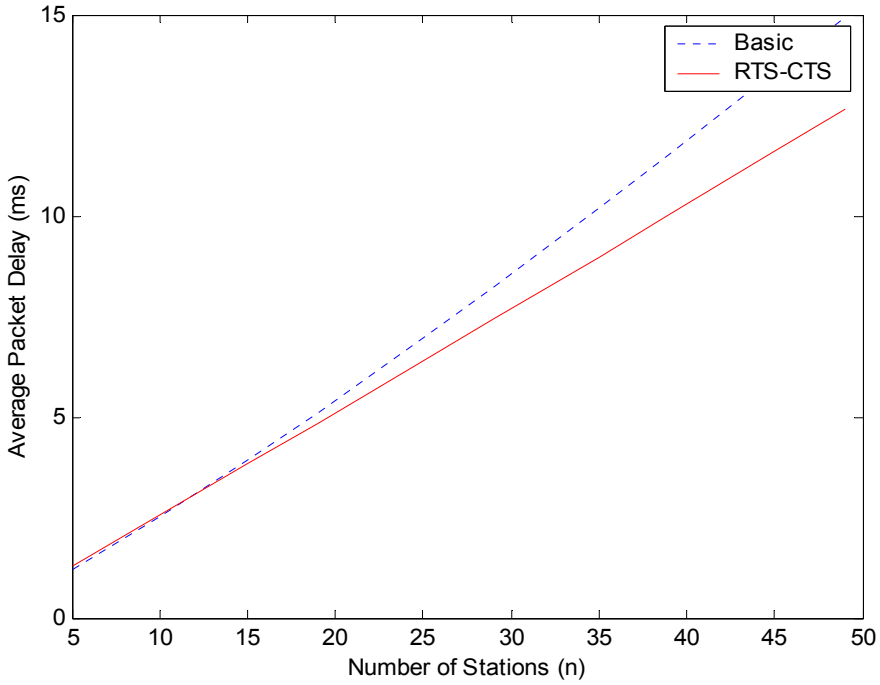

Figure 3.8 Average Delay for 108 Mbps OWSS WLAN

3.5 Conclusion

The OWSS signaling system with bit rates of 108 Mbps and beyond is directed at the next generation of high speed WLANs. OWSS offers multiplexing capability both at the PHY and MAC layers. However, multiplexing at the MAC layer is more preferable, as it would enable full rate shared access of the bandwidth (in this case 108 Mbps) to bursty users. Towards this end, OWSS will use a CSMA/CA based MAC protocol similar to the IEEE 802.11a standard to access the medium. A frame format for OWSS data packets in the MAC layer and MAC attributes of OWSS in terms of DCF parameters are proposed. Using a simple theoretical model for performance analysis, the MAC layer of OWSS has indicated a saturation throughput of 66% and an average packet delay of 5 ms using RTS-CTS – for a moderate number of stations (say, less than 50).

CHAPTER 4

SPECTRAL CHARACTERISTICS OF THE OWSS SIGNAL

Unlike the pulses used in OFDM [6] and TDMA [1], the OWSS pulses have both a wide time support and a wide frequency support, thereby lending the transmitted signal to effective multipath equalization at the receiver. However intrinsic to the design of the transmission system is the specification of the bandpass filter at its front end and the need to meet the emission mask requirements. For both these specifications, the study of the spectral characteristics of the OWSS signal is critical. The spectrum of a WLAN transmission system is one of its most important characteristics. It provides information about spectral leakages by the transmitted signal into adjacent bands. This chapter elaborates on the beneficial spectral properties of the OWSS transmitted signal. It shows that the baseband spectrum is perfectly flat, and that the passband signal requires a bandwidth 30-40% less than that required by OFDM. As an example, for 54 Mb/s operation, OWSS requires only 13 MHz bandwidth compared to 20 MHz for 802.11a OFDM [4], [5]. This is due primarily to the avoidance of overhead (prefix and channel coding), while still achieving BERs of 10^{-4} to 10^{-5} (at practical delay spreads of 50-100 ns and SNRs of 19-22 dB), and a sharp rolloff of the spectrum. The analysis also confirms that the broadband nature of the OWSS baseband signal is preserved in the passband. This enables the OWSS system to transmit data successfully over a frequency

selective multipath channels [1] with deep fades, unlike comparatively narrowband systems like OFDM. OWSS also extends to higher bit rates such as 108 Mbps, in a bandwidth efficient manner.

4.1 Baseband Spectrum of OWSS Signal

Assuming only a single super-symbol for OWSS and that all M virtual channels are active. The corresponding baseband signal in the time and frequency domains are given by

$$\begin{aligned} s_0(t) &= \sum_{i=0}^{M-1} A^{(i)} \psi^{(i)}(t) \\ S_0(f) &= \sum_{i=0}^{M-1} A^{(i)} \underline{c}^{(i)T} \underline{\Phi}(f) \end{aligned} \tag{4.1}$$

Therefore the power of the baseband signal is

$$\begin{aligned} E|S_0(f)|^2 &= \zeta^2 \sum_{i=0}^{M-1} \underline{\Phi}^H(f) \underline{c}^{(i)} \underline{c}^{(i)T} \underline{\Phi}(f) \\ &= \zeta^2 \underline{\Phi}^H(f) [M \cdot I_M] \underline{\Phi}(f) \\ &= \zeta^2 M \sum_{i=0}^{M-1} \left| \Phi^{(i)}(f) \right|^2 \\ &= M\zeta^2 \end{aligned} \tag{4.2}$$

where I_M is an identity matrix of size $M \times M$ and $\zeta^2 \underline{\Delta} E\,|\,A_i\,|^2$. For example, for 64QAM, $\zeta^2 = 42$. Note that in (4.2) the power complementary properties of the OWDM pulses is used, (see top trace of Figure 4.1), and the fact that the Hadamard [25] codes are orthogonal; indeed orthonormal if the code vectors are normalized to unit energy. In the

latter case, the factor M on the right hand side of (4.2) may be replaced by unity. Clearly, the baseband spectrum is flat, regardless of the value of *M*. A simulated spectrum is shown in the lower trace of Figure 4.1.

It follows in an analogous manner that the theoretical baseband spectrum of the complete signal, with an infinite symbol stream,

$$s(t)=\sum_{n}\sum_{i=0}^{M-1} A_n^{(i)}\psi^{(i)}(t-nT)=\sum_{n}\underline{A}_n^{T}\underline{\psi}(t-nT) \qquad (4.3)$$

is also flat. Here, the vector of symbols $A_n = [A_n^{(o)} \quad A_n^{(1)} \quad \cdots \quad A_n^{(M-1)}]^T$ is called the *n*-th supersymbol.

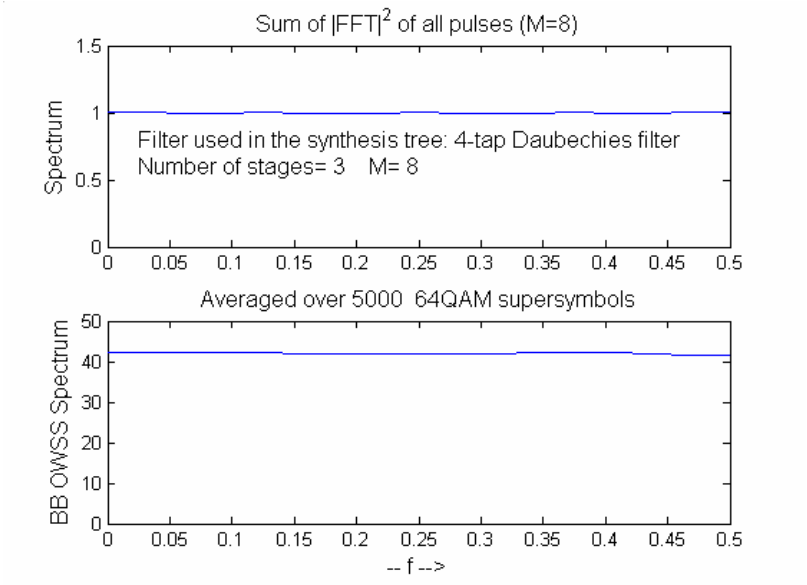

Figure 4.1. Baseband Spectrum of OWSS

4.2 Passband Spectrum of the OWSS Signal

In a typical WLAN system, the transmitted passband RF signal [44] is analog while the baseband signal is a discrete time signal generated by DSP [45]. Therefore the

baseband signal must be converted into an analog signal. The passband analog OWSS signal used for spectral analysis is given by

$$x(t) = \mathrm{Re}\left(\sum_{i=0}^{M-1} s^{(i)}(t)\, e^{j\omega_c t} \right) \tag{4.4}$$

As passband modulation is performed by a complex analog carrier signal (with frequency f_c), D/A conversion of the discrete time baseband OWSS signal is required. This can be achieved by means of a simple passband OWSS transmission system for spectral analysis, illustrated in Figure 4.2. This analog signal is produced through an upconversion process. Prior to upconversion, a pseudo D/A [45] conversion (upsampling by a factor U followed by low pass filtering) of the discrete time baseband signal is performed. Thereupon, in the simulations for the passband spectrum, an FFT is performed, its magnitude-square calculated, then smoothed (using a moving average filter [45] of length W as shown in Figure 4.3), and finally shifted to the carrier frequency (for example, 5.785 GHz).

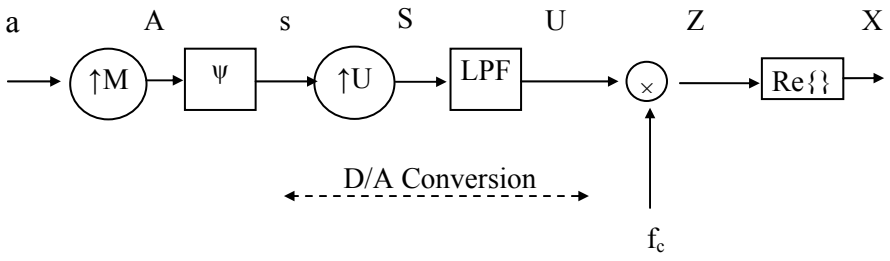

Figure 4.2 Simple Passband OWSS Transmission System for Spectral Analysis

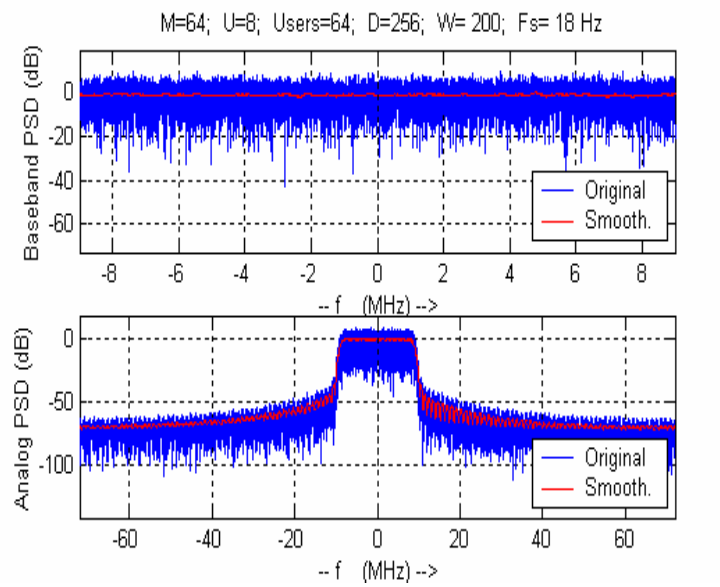

Figure 4.3 Simulated Baseband and Passband Spectrum of OWSS Signal

4.2.1 Passband Spectrum of 108 Mbps OWSS

The 108 Mbps OWSS system has a sampling rate of 18 Msps and uses a 64-QAM constellation. The passband spectrum of the 108 Mbps OWSS transmitted signal is shown in Figure 4.4. The spectral plot is obtained for M=64 (all virtual channels or users active). For D/A conversion, a combination of upsampling, by U = 8, JIF filtering [61] (LPF), followed by smoothing (W = 200) is used. The solid line shows the passband spectrum and the suggested emission mask is shown by the dotted line. The response of the filter was finally shifted to the carrier frequency of 5.785 GHz. The OWSS spectrum for 108 Mbps has a -3dBr passband bandwidth of about 16 MHz, -10 dBr bandwidth of 18 MHz and -40dBr bandwidth of 25 MHz. Also notice the sharp roll off at the edges of the spectrum, indicating a low spectral leakage into adjacent bands. An emission mask is also suggested, shown by a dotted line. The emission mask has been

specified generously to account for nonlinearities and impairments. However certain changes may be necessary to account for PA nonlinearities. The resultant spectrum bandwidth and suggested emission mask is tabulated in Table 4.1.

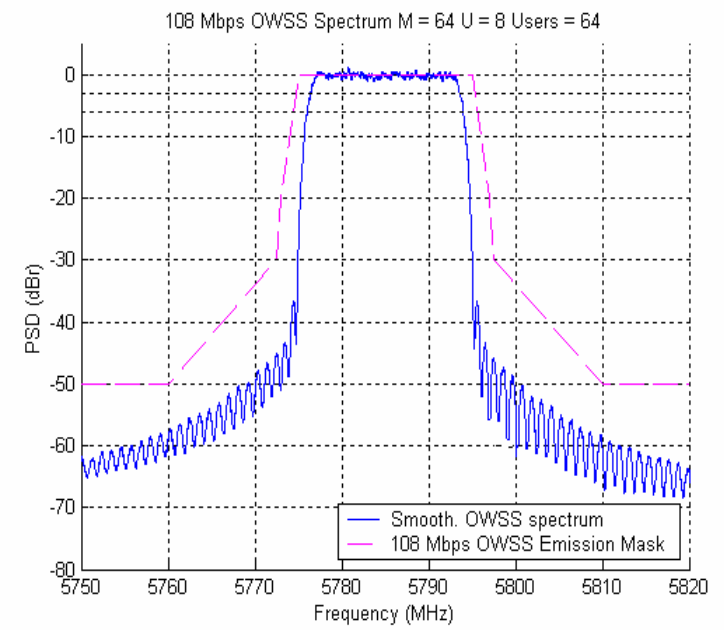

Figure 4.4 Spectrum and Emission Mask for 108 Mbps OWSS Signal

Table 4.1 Spectrum and Emission Mask BW of 108 Mbps OWSS Signal

Average Spectral Density (-dBr)	Spectrum BW (MHz)	Suggested Mask BW (MHz)
0	15.5	20
3	17.2	
6	18	
10	18.6	
20	19.6	
30	20.1	25
40	21.7	
50	30	50

4.2.2 Bandwidth Efficiency of OWSS vis-à-vis OFDM

Now the bandwidth efficiency of OWSSS vis-à-vis OFDM will be compared by studying the passband spectrum and emission masks of both the signaling schemes for 54 Mbps operation. Figure 4.5 compares the passband spectra and emission masks of 60 Mbps (10 Msps sampling rate and 64QAM modulation) OWSS and 54 Mbps 802.11a OFDM system. 60 Mbps OWSS gives a net rate of about 54 Mbps with adaptive loading (use of lower constellation training symbols for equalization in poor channels) and a comparable BER. The spectral plot for OWSS shown in Figure 1.5 is obtained for M=64 (all virtual channels active). For D/A conversion, a combination of upsampling, by U = 8, 129 tap JIF filtering [61] (LPF), followed by smoothing (W = 200) is used. The spectrum and emission mask for 802.11a OFDM is specified in the standard. An an emission mask for 54 Mbps OWSS is also suggested. As is evident from the plots, OWSS spectrum requires only 9.5 MHz for OFDM's 16.3 MHz at –3 dBr and 10.3 MHz for OFDM's 17 MHz at –10dBr. This represents a spectrum bandwidth efficiency of about 40% for OWSS over OFDM. At -10 dBr, OWSS emission mask requires only 12 MHz bandwidth as compared to 20 MHz for 802.11a OFDM emission mask [5], [6]. This represents a significant bandwidth advantage of roughly 40% for both the spectrum and the emission mask. See Table 4.2 and Table 4.3 for details. This advantage arises due to (1) the avoidance of the prefix, channel coding, and guard zero-carriers in OWSS and (2) a compact brick-wall like characteristic of the baseband OWSS spectrum. PA non-linearities and other impairments such as timing and carrier phase errors have been ignored in this simulation, though the emission mask for 54 Mbps OWSS has been defined generously to account for such impairments.

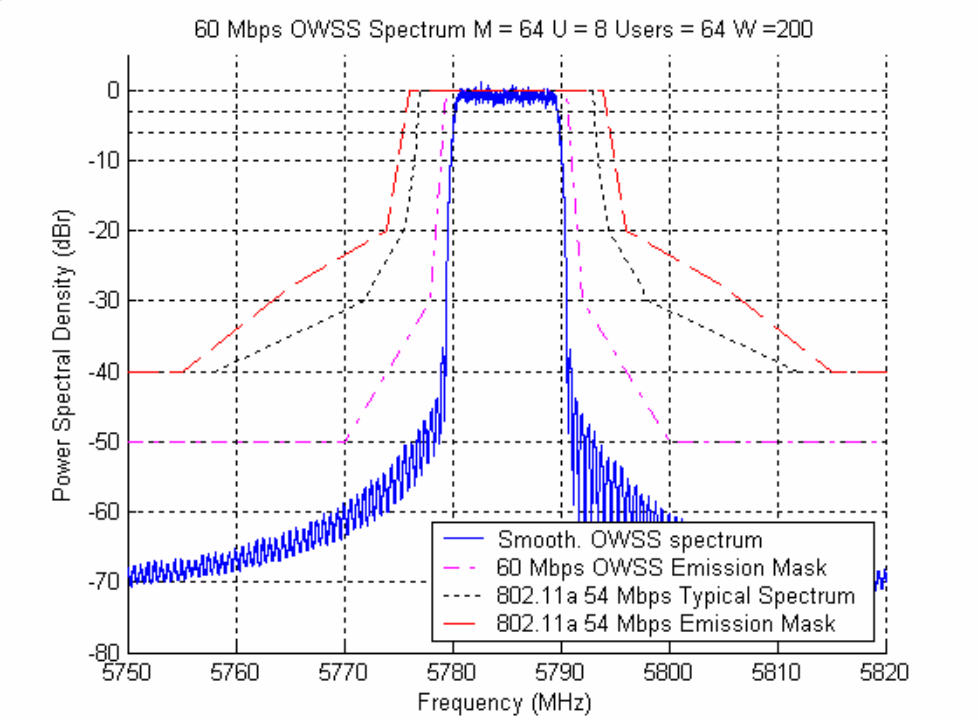

Figure 4.5 Comparison of OWSS and 802.11a OFDM.

Table 4.2 Comparison of 54 Mbps OWSS and 802.11a OFDM Spectrums

Average PSD (-dBr)	BW 60 Mbps OWSS Spectrum (MHz)	BW 54 Mbps OFDM Spectrum (MHz)	Efficiency (%)
-3	9.6	16.4	41.46%
-6	10	16.7	40.12%
-10	10.3	17	39.41%
-20	10.8	19	43.15%
-30	11.2	26	57%
-40	12	56	78.5%

Table 4.3 Comparison of OWSS and 802.11a OFDM Emission Masks

Average PSD (-dBr)	BW 60 Mbps OWSS Mask (suggested) (MHz)	BW 54 Mbps OFDM Mask (MHz)	Efficiency (%)
0	11	18	39 %
-10	12	20	40 %
-20	13	22	41 %
-28	14	40	65 %
-40	22	60	63 %

4.3 Compensation of PA Non-Linearity in OWSS WLAN systems

PA nonlinearity in the transmitter leads to spectral broadening in the passband which can exacerbate adjacent channel interference [71]. This spectral regrowth depends on the level of output backoff and can severely affect the performance of the system. Backoff [72] is an important parameter for a practical power amplifier to attain an acceptable level of out of band radiation. Backoff is used to shift the operating point of a non-linear PA so as to operate it in the linear (actually, less nonlinear) region. To simulate the PA, a Rapp Model [72] is used for AM/AM conversion given by $f(A) = A \Big/ \left(1 + A^{2p}\right)^{\frac{1}{2p}}$ where A is the input amplitude. A good approximation to existing amplifiers is obtained by choosing p in range of 2 to 3. We chose p=2.2. Figure 4.6 illustrates the effect of PA non-linearity on the passband spectra of 108 Mbps (18 Msps sampling rate, 64 active users, 64QAM modulation and smoothing window W=200) OWSS. The figure also shows the spectral regrowth for backoff values of -10dB,

-7dB and -5dB on the 108 Mbps OWSS spectrum. It is observed that for -6 dB backoff, any significant distortion occurs only at -28 dBr. Notice that the 108 Mbps OWSS bandwidth has broadened from 22 MHz (linear) to 26 MHz (6 dB backoff) at -30 dBr, and from 26 MHz (linear) to 54 MHz (6 dB backoff) at -40 dBr.

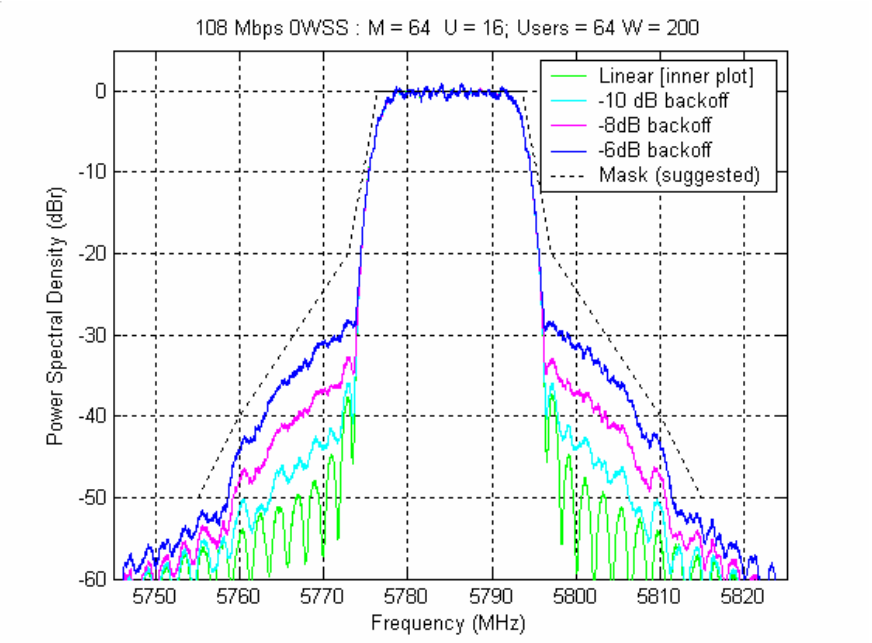

Figure 4.6 Passband 108 Mbps OWSS spectrum with PA Non-linearity using Rapp Model

To compensate for this spectral regrowth, a novel pre-distortion [70], [73] scheme is employed based on the inverse function [70] of the Rapp PA Model which is illustrated in Figure 4.7. The analog OWSS signal is normalized and appropriate backoff is applied. The magnitude and phase are extracted from the signal and the magnitude is clipped (if required) and passed through the inverse Rapp function model given by

$g(A) = A \Big/ \left(1 - A^{2p}\right)^{\frac{1}{2p}}$. The pre-distorted magnitude is then combined with the phase to get the pre-distorted OWSS signal. This signal is then modulated by a carrier frequency

and the Rapp model *f(A)* is applied to simulate the effect of PA nonlinearity. Figure 4.8 shows the effect of pre-distortion on the OWSS signal for 6 dB backoff. As can be seen, with compensation (using pre-distortion) any significant distortion occurs only at -38 dBr as compared to -28 dBr without compensation. This represents a significant improvement of 10 dB [70] in spectral regrowth distortion levels in the passband for the 108 Mbps OWSS signal. The 108 Mbps OWSS bandwidth with 6 dB backoff shows no broadening at -30 dBr and has broadened to only 30 MHz at -40 dBr, compared to 54 MHz (without pre-distortion).

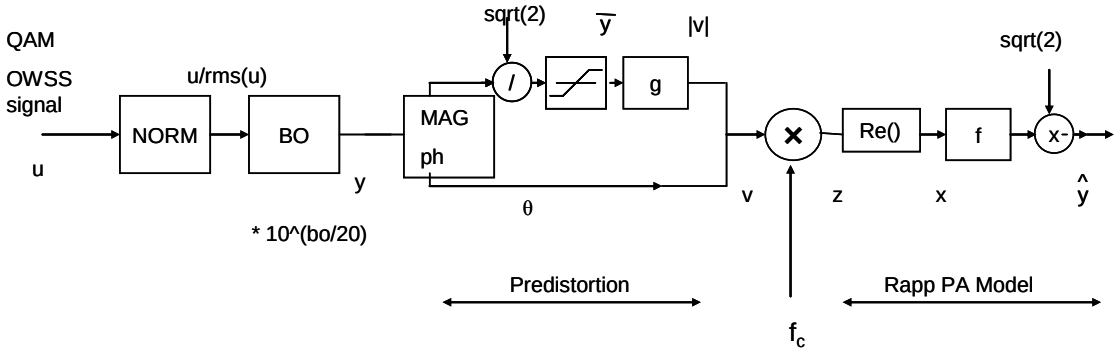

Figure 4.7 Novel Pre-distortion Scheme for PA Non-Linearity Compensation

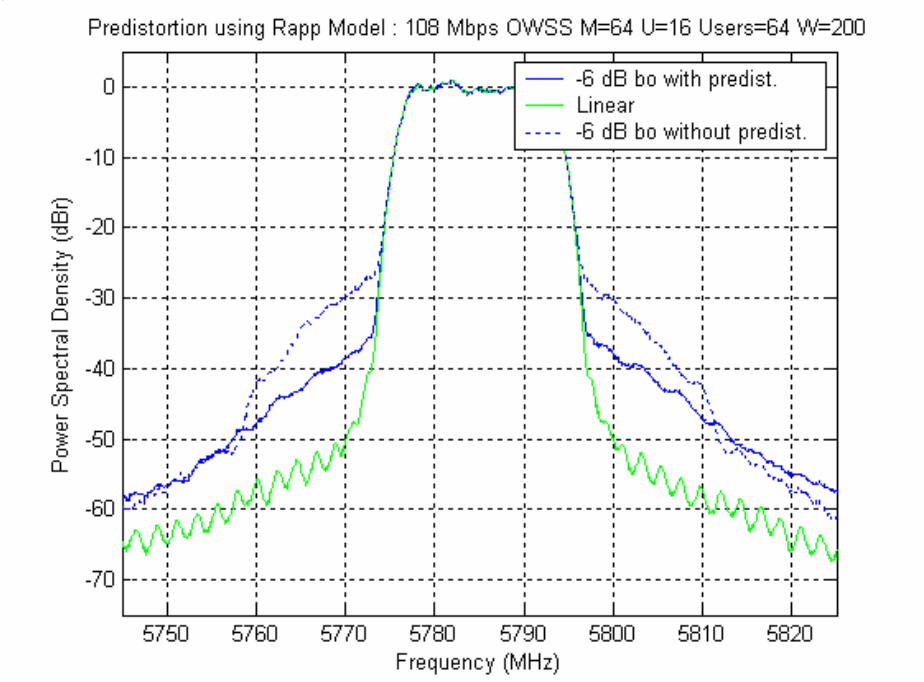

Figure 4.8 Compensated 108 Mbps Passband Spectrum using Pre-Distortion

4.4 Conclusion

OWSS can avoid substantial overhead penalties through the elimination of the prefix, the guard zero-carriers, and channel. coding, while still providing a desired BER performance at practical SNRs. It was shown that the theoretical baseband spectrum is perfectly flat, and the passband spectrum offers a 30-40% bandwidth advantage over 802.11a OFDM. OWSS readily extends to higher bit rates, such as 108 Mb/s, in a bandwidth efficient manner. PA nonlinearity can lead to spectral regrowth in the passband spectrum of the OWSS signal. This spectral regrowth which increases with the output backoff level, can be compensated to a large extent using a pre-distortion scheme based on the Rapp model. At 6 dB backoff in 108 Mbps OWSS, this scheme yields an improvement of 10 dB in spectral regrowth distortion levels.

CHAPTER 5

PERFORMANCE LIMITS OF THE OWSS WLAN SYSTEM

OWSS WLAN System is based on a new family of pulses which have both a wide time support and a wide frequency support, and is 30–40% more bandwidth efficient than OFDM. As a consequence of the wide frequency support, effective equalization [44] in a multipath environment [1] can be achieved using a Forward Equalizer–Decision Feedback Equalizer (FE–DFE) structure [29], [30] together with the LMS adaptation algorithm [29] as explained in Chapter 2. The purpose of this chapter is to explore the fundamental limits to OWSS performance. Towards this purpose, a multi-level matrix formulation [27], [31] is employed to model the signal processing system. The total minimum mean-square error (TMSE) [44] for the FE–DFE structure is derived in a closed form, and thereupon minimized rigorously. The TMSE governs the BER performance of the system, and is the sum of the MSE of the unequalized residual error and the MSE due to the channel noise amplified by the FE. Simulation results on a 108 Mbps system will demonstrate the effectiveness of this theory.

Although a symbol-level formulation is generally performed in the equalization literature, the problem is formulated at the chip level for the following reason. The peak of the channel response can occur at instants that are not integer multiples of the super-symbol interval, and therefore the best delay for optimum detection in the FE-DFE is not

necessarily an integer multiple of the symbol interval. A down-sampled low rate symbol-interval formulation could actually easily miss the real optimum. Since the goal of this paper is to explore the fundamental limits to the performance, a chip-level formulation will be studied. The matter of reduced complexity can be addressed in the future.

5.1 Multi Level Matrix Formulation of OWSS Receiver

The OWSS transmitter-receiver system is illustrated in Figure 5.1. The equalizer structure consists of two adaptive FIR [45] components: FE and DFE. LMS algorithm [29] is used as the adaptation mechanism to update the FE and DFE. The receiver also uses an OWSS correlator, an upsampler and a decision device (slicer) [44]. The output of the equalizer is correlated with a user specific OWSS pulse, thus generating a statistic for detection. Note also that the correlator generates its output every Mth sample, or chip. Therefore, the decision device and error computations operate at a lower rate compared to the equalizer. The OWSS Receiver is thus a multi rate signal processing system [51]. Since the DFE operates at the same speed as the FE, an upsampler is needed as shown in the figure. Initially, the coefficients of FE and DFE are obtained through a training phase (using a previously stored sequence of symbols, and the LMS algorithm for update). Subsequently, the receiver goes into a maintenance mode. Of course, the equalizer coefficients are updated in this mode as well. The training phase begins with an arbitrary set of equalizer weights. These weights tend to converge so as to minimize the MSE. The final weights obtained at the end of the training are then used to initialize the maintenance phase.

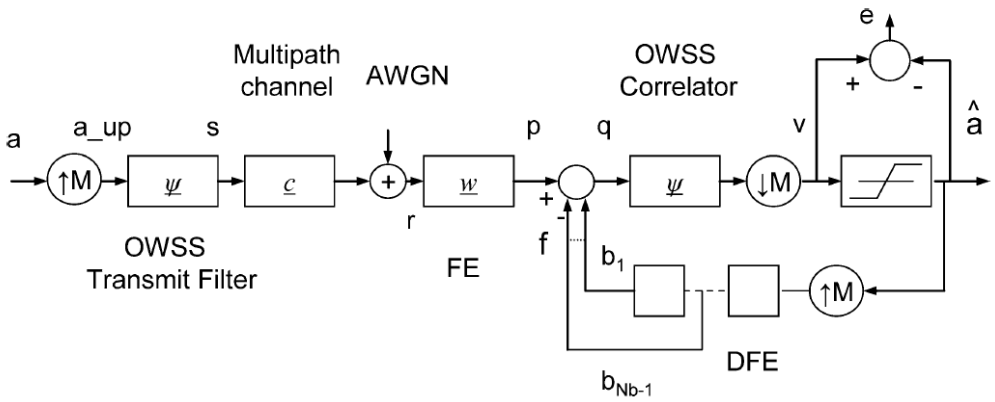

Figure 5.1 OWSS Transreceiver System

After the FE-DFE, the equalized output is fed to the slicer to recover the QAM symbols. To minimize its receiver BER, the TMSE (Total Mean Square Error) needs to be minimized, which is the subject of the discussion below. The TMSE governs the BER performance of the system, and is the sum of the MSE of the unequalized residual error and the MSE due to the channel noise amplified by the FE. The TMSE will be derived in closed form using a multi level matrix formulation [27], and thereupon minimized rigorously to give an estimate of the optimum FE and DFE weights.

5.1.1 TMSE in the OWSS Receiver

The definitions of the QAM symbol vector $\underline{a}$ (of length D), OWSS transmit filter $\underline{\psi}$ (*L taps, assumed to be an integer multiple of M by zero padding if necessary*), multipath channel $\underline{c}$ (N_c taps), FE $\underline{w}$ (*N_w taps*) and DFE $\underline{b}$ (*N_b taps*) are given below

$$\begin{aligned}
&\underline{a} = \begin{bmatrix} a_0 & a_1 & a_2 & \dots & a_{D-1} \end{bmatrix}^T; \qquad \underline{\psi} = \begin{bmatrix} \psi_0 & \psi_1 & \psi_2 & \dots & \psi_{L-1} \end{bmatrix}^T; \\
&\underline{c} = \begin{bmatrix} c_0 & c_1 & c_2 & \dots & c_{N_c-1} \end{bmatrix}^T; \qquad \underline{w} = \begin{bmatrix} w_0 & w_1 & w_2 & \dots & w_{N_w-1} \end{bmatrix}^T; \\
&\underline{b} = \begin{bmatrix} b_0 & b_1 & b_2 & \dots & b_{N_b-1} \end{bmatrix}^T
\end{aligned} \tag{5.1}$$

The symbol stream upsampled by a factor M (of length $MD=M \times D$) is given by

$$\underline{a}_{up} = \begin{bmatrix} a_0 & [0..0]_{1\times M-1} & a_1 & [0..0]_{1\times M-1} & a_2 & [0..0]_{1\times M-1} & ..... & a_{D-1} & [0..0]_{1\times M-1} \end{bmatrix}^T \tag{5.2}$$

The symbol matrix input A_1 to the FE, OWSS filter matrix H_1, multipath channel matrix C and the adaptive white Gaussian noise (AWGN) matrix N are given by

$$A_1 = \begin{bmatrix} & 0 & \cdots & 0 \\ \underline{a}_{up} & & \cdots & 0 \\ — & \underline{a}_{up} & \ddots & \vdots \\ & — & & a_0 \end{bmatrix}_{MD\times MD} ; H_1 = \begin{bmatrix} & 0 & \cdots & 0 \\ \underline{\psi} & & \cdots & 0 \\ — & \underline{\psi} & \ddots & \vdots \\ & — & & \psi_0 \end{bmatrix}_{MD\times MD} ;$$

$$C = \begin{bmatrix} & 0 & \cdots & 0 \\ \underline{c} & & \cdots & 0 \\ — & \underline{c} & \ddots & \vdots \\ & — & & c_0 \end{bmatrix}_{MD\times N_w} ; N = \begin{bmatrix} n_0 & 0 & \cdots & 0 \\ n_1 & n_0 & \cdots & 0 \\ \vdots & \vdots & \ddots & \vdots \\ n_{MD-1} & n_{MD-2} & \cdots & n_0 \end{bmatrix}_{MD\times N_w} \tag{5.3}$$

The output of the FE, including the contribution of noise, is

$$\underline{p} = \left(A_1 H_1 C + N\right)\underline{w} = A_1 G_1 \underline{w} + N\underline{w} \text{ where } G_1 = H_1 C. \tag{5.4}$$

The symbol matrix input to the DFE (with delay L due to the correlator) and the OWSS correlator-downsampler matrix H_2 are given by

$$A_2 = \begin{bmatrix} & 0 & 0 & \cdots & 0 \\ \underline{0}_{L\times 1} & & & \cdots & 0 \\ \underline{a}_{up} & \underline{0}_{L\times 1} & & \cdots & \vdots \\ \_\_ & \underline{a}_{up} & : & \ddots & \underline{0}_{L\times 1} \\ & \_\_ & & \cdots & a_0 \end{bmatrix}_{MD\times Nb} ;$$

$$H_2 = \begin{bmatrix} \underline{\psi}^T & | & \underline{0}_{1\times M} & \cdots & \underline{0}_{1\times M} \\ \underline{0}_{1\times M} & | & \underline{\psi}^T & | & \cdots & \underline{0}_{1\times M} \\ \underline{0}_{1\times M} & \underline{0}_{1\times M} & | & \underline{\psi}^T & | & \underline{0}_{1\times M} \\ & & & & \ddots & \\ \underline{0}_{1\times M} & \underline{0}_{1\times M} & \underline{0}_{1\times M} & & \underline{\psi}^T_{1\times M} \end{bmatrix}_{D\times MD} \tag{5.5}$$

The output of the DFE is given by

$$\underline{f} = A_2 \underline{b} \tag{5.6}$$

The input to the slicer (decision device), from the correlator, after the sliding correlation and downsampling operation is

$$\begin{aligned} \underline{v} &= H_2 \underline{q} \\ &= H_2 \left(\underline{p} - \underline{f} \right) \\ &= H_2 \left(A_1 G_1 \underline{w} + N \underline{w} - A_2 \underline{b} \right) \end{aligned} \tag{5.7}$$

The error signal $\underline{e}$ (assuming perfect detection of QAM symbols, $\hat{a} = a$) is

$$\underline{e} = \underline{v} - \underline{a} \tag{5.8}$$

Neglecting the effect of noise temporarily, the error signal can be expressed as follows

$$\begin{aligned} \underline{e} &= H_2 \left[A_1 G_1 \underline{w} - A_2 \underline{b} \right] - \underline{a} \\ &= V_1 \underline{w} - V_2 \underline{b} - \underline{a} \end{aligned}$$

where $V_1 = H_2 A_1 G_1$ and $V_2 = H_2 A_2$. (5.9)

Correspondingly, the TMSE is given by

$$\mathcal{E} = E\left(\left\|\underline{e}\right\|^2\right) = E\left(\underline{e}^H \underline{e}\right) \tag{5.10}$$

5.1.2 Optimum FE-DFE receiver

Now, to find the optimum FE-DFE [27] to minimize the MSE, $\mathcal{E}$ is differentiated with respect to $\underline{w}$ and $\underline{b}$ and set the two terms to zero.

$$\begin{aligned}
\nabla_{\underline{w}}\mathcal{E} &= E\left[2V_1^H\left(V_1\underline{w} - V_2\underline{b} - \underline{a}\right)\right] \\
&= 2E(V_1^H V_1)\underline{w} - 2E(V_1^H V_2)\underline{b} - 2E(V_1^H\,\underline{a}) = 0 \\
\nabla_{\underline{b}}\mathcal{E} &= E\left[2V_2^H\left(V_1\underline{w} - V_2\underline{b} - \underline{a}\right)\right] \\
&= 2E(V_2^H V_1)\underline{w} - 2E(V_2^H V_2)\underline{b} - 2E(V_2^H\,\underline{a}) = 0
\end{aligned} \tag{5.11}$$

In matrix-vector form, the above equations can be written as

$$\begin{aligned}
&\begin{bmatrix} E(V_1^H V_1) & -E(V_1^H V_2) \\ E(V_1^H V_2) & E(V_2^H V_2) \end{bmatrix}\begin{bmatrix} \underline{w} \\ \underline{b} \end{bmatrix} = \begin{bmatrix} E(V_1^H\,\underline{a}) \\ E(V_2^H\,\underline{a}) \end{bmatrix} \\
&\qquad\Downarrow \\
&\begin{bmatrix} Q_2 & -Q_3 \\ Q_3^H & Q_4 \end{bmatrix}\begin{bmatrix} \underline{w} \\ \underline{b} \end{bmatrix} = \begin{bmatrix} Q_1^H \\ 0 \end{bmatrix}
\end{aligned} \tag{5.12}$$

Hence the optimum *FE* and *DFE* can be estimated (for the noiseless case) as follows

$$\begin{bmatrix} \underline{w} \\ \underline{b} \end{bmatrix} = \begin{bmatrix} Q_2 & -Q_3 \\ Q_3^H & Q_4 \end{bmatrix}^{-1}\begin{bmatrix} Q_1^H \\ 0 \end{bmatrix} \tag{5.13}$$

Here,

$$\begin{aligned}
Q_1 &= E(\underline{a}^H H_2 A_1 G_1); \\
Q_2 &= E(G_1^H A_1^H R A_1 G_1) = G_1^H E(A_1^H R A_1) G_1 = G_1^H F_1 G_1 \\
Q_3 &= E(G_1^H A_1^H R A_2) = G_1^H E(A_1^H R A_2) = G_1^H F_2; \\
Q_4 &= E(A_2^H R A_2) = E(A_1^H R A_2) = F_3
\end{aligned} \tag{5.14}$$

A symbol correlator matrix for M symbols is shown below

$$P_{all} = \begin{bmatrix} \psi^T & \underline{0} & \underline{0} & \cdots & \underline{0} \\ \underline{0} & \psi^T & \underline{0} & \cdots & \underline{0} \\ \underline{0} & \underline{0} & \psi^T & \cdots & \underline{0} \\ \vdots & \vdots & \vdots & \vdots & \vdots \\ \underline{0} & \underline{0} & \underline{0} & \cdots & \psi^T \end{bmatrix}_{M \times (M-1)L+M} \tag{5.15}$$

Blocks p of size $M \times M$ are extracted. Now let $m = L/M$. (Note L should be a multiple of M). So p_i blocks of size $M \times M$, ($i = 1, 2, ...I$) where $I = m + (M-1)$ will be created. Also let $I_p = I/m$. Additional p blocks p_i ($i = I+1$, $...I+(I_p - 1) \times M$) = $Z_{M \times M}$ are then defined, so as to complete the polyphase sequences given below

$$\begin{bmatrix} 1 & 2 & 3 & \cdots & I \\ 1+M & 2+M & 3+M & \cdots & I+M \\ 1+2M & 2+2M & 3+2M & \cdots & I+2M \\ \vdots & \vdots & \vdots & \vdots & \vdots \\ 1+(I_p-1)M & 2+(I_p-1)M & 3+(I_p-1)M & & I+(I_p-1)M \end{bmatrix} \tag{5.16}$$

Now using the above polyphase sequences, R can be expressed (neglecting edge effects) as

$$R = H_2^H H_2$$

$$= \begin{bmatrix} p_1^T & & & & & & & \\ p_2^T & p_1^T & & & & & & \\ p_3^T & p_2^T & p_1^T & & & & & \\ \vdots & \vdots & \vdots & \ddots & & & & \\ p_1^T & \vdots & \vdots & & \ddots & & & \\ 0 & p_1^T & \vdots & & & \ddots & & \\ \vdots & \vdots & p_1^T & & & & \ddots & \\ 0 & 0 & 0 & & & & & p_1 \end{bmatrix} \begin{bmatrix} p_1 & p_2 & p_3 & \cdots & p_1 & 0 & & 0 \\ & p_1 & p_2 & \cdots & \cdots & p_1 & 0 & 0 \\ & & p_1 & \cdots & \cdots & \cdots & p_1 & 0 \\ & & & \ddots & & & & \vdots \\ & & & & \ddots & & & \vdots \\ & & & & & \ddots & & \vdots \\ & & & & & & \ddots & \vdots \\ & & & & & & & p_1 \end{bmatrix}$$

$$= \begin{bmatrix} K_1 & J_{1,1} & \cdots & \cdots & \cdots & \cdots & J_{1,I-1} & \\ J_{1,1}^T & K_2 & J_{2,1} & \cdots & \cdots & \cdots & J_{2,I-2} & \\ \vdots & J_{2,I-1}^T & \ddots & \ddots & \ddots & \ddots & & \\ \vdots & \vdots & \ddots & K_M & J_{M,1} & \cdots & J_{M,I-M} & \\ \vdots & \vdots & \ddots & J_{M,1} & K_1 & & & \\ \vdots & \vdots & \ddots & & & \ddots & & \\ J_{1,I-1}^T & J_{2,I-2}^T & & J_{M,I-M} & & & \ddots & \\ & & & & & & & K_M \end{bmatrix}_{MD\ X\ MD} \tag{5.17}$$

Note the repeating blocks whose components are given below

$$\begin{aligned} K_i &= \sum_{k=0}^{I_p} p_{i+k*M}^T p_{i+k*M}; \\ J_{i,j} &= \sum_{k=0}^{I_p} p_{i+k*M}^T p_{i+j+k*M}; \qquad i = 1, 2, \ldots, M, j = 1, 2, \ldots, I-1 \end{aligned} \tag{5.18}$$

The matrix Q_1 can be expressed statistically in terms of symbol energy ζ

$$\begin{aligned} Q_1 &= E(\underline{a}^H H_2 A_1) G_1 \\ &= \zeta^2 \left[D\psi_0 \quad .. \quad D\psi_{M-1} \quad (D-1)\psi_M \quad .. \quad (D-1)\psi_{2M-1} \quad .. \quad (D-I)\psi_{(I+1)M-1} \right] G_1 \end{aligned} \tag{5.19}$$

The matrix Q_2 is given by

$$Q_2 = G_1^H E(A_1^H R A_1) G_1 = G_1^H F_1 G_1 \tag{5.20}$$

The diagonal and off diagonal terms of the matrix $F_1 = E(A_1^{\mathrm{H}} R A_1)$ are given by

$$F_1(i,i) = \zeta^2 \left[\left(\frac{D}{M} - \left\lceil \frac{i}{M} \right\rceil + 1 \right) \sum_{n=1}^{M} K_n - \sum_{n=mod(i/M)-1} K_n \right]$$

$$F_1(i,i+j) = \zeta^2 \left[\left(\frac{D}{M} - \left\lceil \frac{i}{M} \right\rceil + 1 \right) \sum_{n=1}^{M} J_{n,j} - \sum_{j} J_{M-(mod(i/M)-1),j} - \sum_{n=mod(i/M)-1} J_{n,j} \right]$$

$$F_1(i+j,i) = \zeta^2 \left[\left(\frac{D}{M} - \left\lceil \frac{i}{M} \right\rceil + 1 \right) \sum_{n=1}^{M} J^T_{n,j} - \sum_{j} J^T{}_{M-(mod(i/M)-1),j} - \sum_{n=mod(i/M)-1} J^T{}_{n,j} \right]$$

$$given\ i = 1,2,....,D,\ j = 1,2,...,I-1\ and\ i+j <= D$$

$$else\ F_1(i,i+j) = F_1(i+j,i) = Z_{M\ X\ M},\ where\ Z\ is\ a\ zero\ matrix$$

$$when\ given\ i = 1,2,....,D\ then\ j > I-1, i+j <= D$$

(5.21)

The matrix Q_3 can also be defined as

$$Q_3 = G_1^H E(A_1^H R A_2) = G_1^H F_2 \tag{5.22}$$

Note that the matrix A_1 is $MD \times MD$ (i.e., $D \times D$ blocks), and the matrix A_2 is $MD \times Nb$, ($D \times n_b$ blocks) therefore the final matrix is of size $MD \times N_b$ (i.e., $D \times n_b$ blocks), where $n_b \cdot Nb/M$. Also note that the first $l \cdot L/M$ block rows of A_2 are zero rows. Then $F_2 = E(A_1^{\mathrm{H}} R A_2)$ can be obtained from F_1 by removing the first l block columns from F_1 , extracting the next n_b block columns and removing the remaining block columns.

The matrix Q_4 can also be determined similarly

$$Q_4 = E(A_2^H R A_2) = F_3 \tag{5.23}$$

The final matrix F_3 is of size $N_b \times N_b$ (i.e., $n_b \times n_b$ blocks), Also note that the first l block rows of A_2 are zero rows. Then F_3 is a submatrix of F_2 and can be obtained from F_2 by removing the first l block rows from F_2 , extracting the next n_b block rows and removing the remaining block rows.

Now to consider the effect of AWGN, another matrix Q_5 will be incorporated in the estimation, from (5.13). Thus the optimum *FE* and *DFE* can be estimated (for the AWGN case) as follows

$$\begin{bmatrix} \underline{w} \\ \underline{b} \end{bmatrix} = \begin{bmatrix} Q_2 + Q_5 & -Q_3 \\ Q_3^H & Q_4 \end{bmatrix}^{-1} \begin{bmatrix} Q_1^H \\ 0 \end{bmatrix} \tag{5.24}$$

The matrix Q_5 is similar to Q_1 and uses AWGN energy σ.

$$\begin{aligned} &Q_5 = E\left(N^H H_2^H H_2 N\right) = \left[RS_N\right]_{MD\times MD}; \\ &where\ S_N = diag\left[\left(MD\sigma^2\ MD-1\sigma^2 \cdots \sigma^2\right)\right]_{MD\times MD} \end{aligned} \tag{5.25}$$

5.2 Simulation Results on the Performance Limits

5.2.1. Experiment 1 (100 ns Delay-Spread Channel):

Consider a 108 Mbps, 64 QAM (18 Msps), four users (M=4, L=12) OWSS system over a 100 ns rms delay-spread multipath channel [1]. A Naftali channel model [62], [63] is used which results in a 9-tap structure. The receiver's FE-DFE are optimized for N_w = 4 and N_b = 8. Adaptive loading [64], [65] is also used based upon the total mean-squared error. That is, if the TMSE is below a threshold thr_{64}, 64QAM transmission is used; if it is at or above thr_{64} but below another threshold thr_{16}, 16QAM transmission is used; otherwise QPSK transmission is used. Table 5.1 shows the bit error rate for two scenarios. In the first case delayed decision is used which is simulated by accepting only those channels for which the peak occurs at the zero-th bin; this is a simplified approach which can be made more rigorous either by incorporating the delay into the algorithm itself, or by LMS algorithm [3]. This delay is bounded by the channel memory, i.e., eight samples. The second case is where the decision is not delayed. Also shown are the

aggregate bit rates as a result of the adaptive strategy. The results are given for the following SNRs: Eb/No = 19 dB, 22 dB, and 25 dB with a 2:1 selection diversity at the receiver. Due to a very sharp roll-off of the spectrum, a bandwidth expansion ratio of just 1.1, and a corresponding bandwidth of 18*1.1=19.8 MHz are assumed in the calculation of the spectral efficiency. Figure 5.2 shows the BER curve for fixed 64QAM symbol constellation. Note that this represents the performance in the limit.

5.2.2 Experiment 2 (50 ns Delay-Spread Channel)

Consider again a 108 Mbps, 64 QAM (18 Msps), four user (M=4) OWSS system. However, now a 50 ns rms delay-spread multipath channel (5 taps) will be considered. As before, an adaptive loading strategy is used based upon the total mean-squared error. The equalizer parameters are N_w=7, N_b=4. Table 5.2 shows the bit error rate for the situation where delayed decision is used which is simulated by accepting only those channels for which the peak occurs at the zero-th bin. This is a simplified approach which can be made more rigorous either by incorporating the delay into the algorithm itself, or by LMS algorithm.

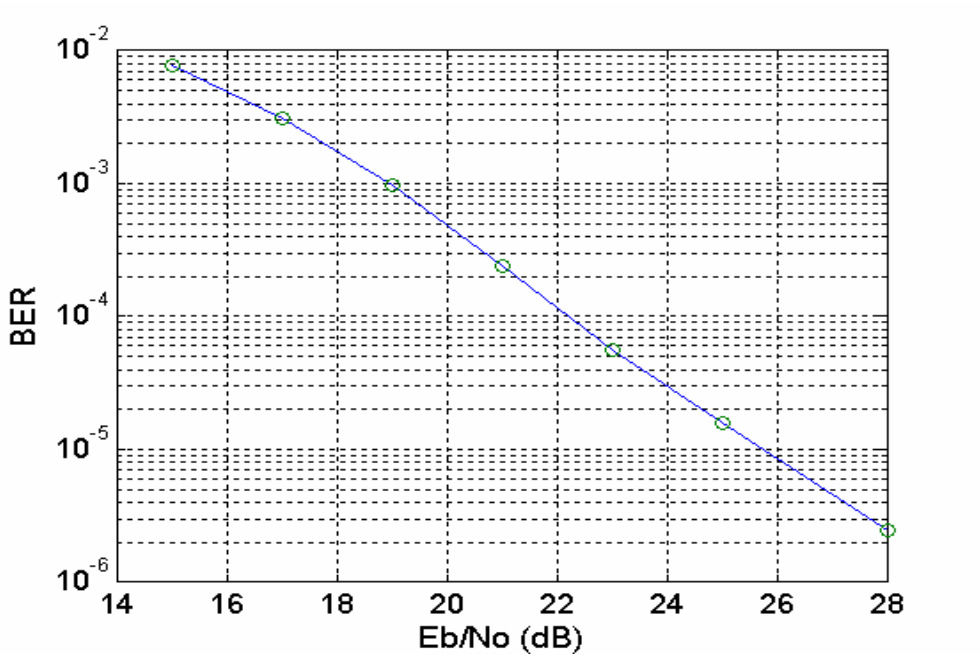

Figure 5.2 BER for 108 Mbps 64QAM with 2:1 Selection Diversity (over 100 ns Delay-Spread Channels)

It is also useful to remark that *Maximal Ratio Combining* (MRC) [9] on a diversity of 2:1 is used at the receiver. Using this scheme in a 50ns delay spread channel, a low BER of 10^{-5} is achieved at an Eb/No of 19 dB, for an aggregate bit rate of 103.3 Mbps and a spectral efficiency of 5.2 bits/s/Hz. Of course, this represents performance in the limit.

Table 5.1 Simulation Results with Adaptive Loading for 100 ns Delay-Spread Channels

Decision	Eb/No (dB)	64QAM (%)	thr_{64} TMSE	16QAM (%)	thr_{16} TMSE	QPSK (%)	Aggregate bit rate (Mbps)	BER	Bits/s /Hz
Delayed	19 dB	59	0.15	12	0.2	29	82.8	7×10^{-6}	4.2
	22 dB	82	0.15	14	0.2	4	100.1	6×10^{-6}	5.0
	25 dB	90	0.1	7	0.15	3	103.3	3×10^{-7}	5.2
Not Delayed	19 dB	28	0.15	13	0.2	59	60.8	3×10^{-3}	3.1
	22 dB	51	0.15	10	0.2	39	76.3	6×10^{-4}	3.8
	25 dB	58	0.1	17	0.15	25	83.9	2×10^{-5}	4.3

Table 5.2 Simulation Results with Adaptive Loading for 50 ns Delay-Spread Channels

Decision	Eb/No (dB)	64QAM %	thr_{64} TMSE	16QAM %	thr_{16} TMSE	QPSK %	Aggregate bit-rate (Mbps)	BER	Bits/s/ Hz
Delayed	19 dB	91.5	0.2	4.5	0.25	5	103.3	10^{-5}	5.2

5.3 Conclusions

This chapter has presented a theoretical basis for understanding the limits to the performance of OWSS systems. Multi-level matrix formulation was used in determining the optimum receiver for OWSS. Experiments on 108 Mbps (64 QAM) indicate that a BER of 10−5 and spectral efficiencies up to 5.2 bits/s/Hz can be achieved for 50 ns delay spread channels at an SNR of 19 dB. This illustrates the effectiveness of this multi-level matrix formulation in determining the optimum receiver for OWSS. For practical implementation, future work should attempt an analogous development on a symbol interval basis.

CHAPTER 6

A Novel MIMO-STC-OFDM WLAN System

6.1 Introduction

Fourth generation (4G) wireless technology [2] will provide high bit-rate multimedia communication capability, thereby enabling numerous advanced services that will significantly benefit the industry, business, government, and the society in general. For example, info stations will become pervasive as are today's beverage-vending machines, and high-quality mobile video communication will become widespread as is today's cell telephony. Such path breaking changes are expected to have a major economic impact, nationally as well as globally. This chapter presents a novel MIMO STC-OFDM technique [33]-[35] targeted towards 4G data rates, and at the same time achieve both high spectral efficiency and high performance (high data rate and low BER) over frequency selective channels. This new system is accomplished by a combination, or layering [36], of MIMO OFDM [12]-[16] (for high spectral efficiency), group transmit signals and antennas (for reduced complexity) [37], space time block coding [38], [39] (for reliability), array processing at the receiver [37] (for interference suppression on a per carrier basis), and a new Least Squares (LS) decoding scheme (for high performance) [33]. The overall approach is portrayed graphically in Figure 6.1.

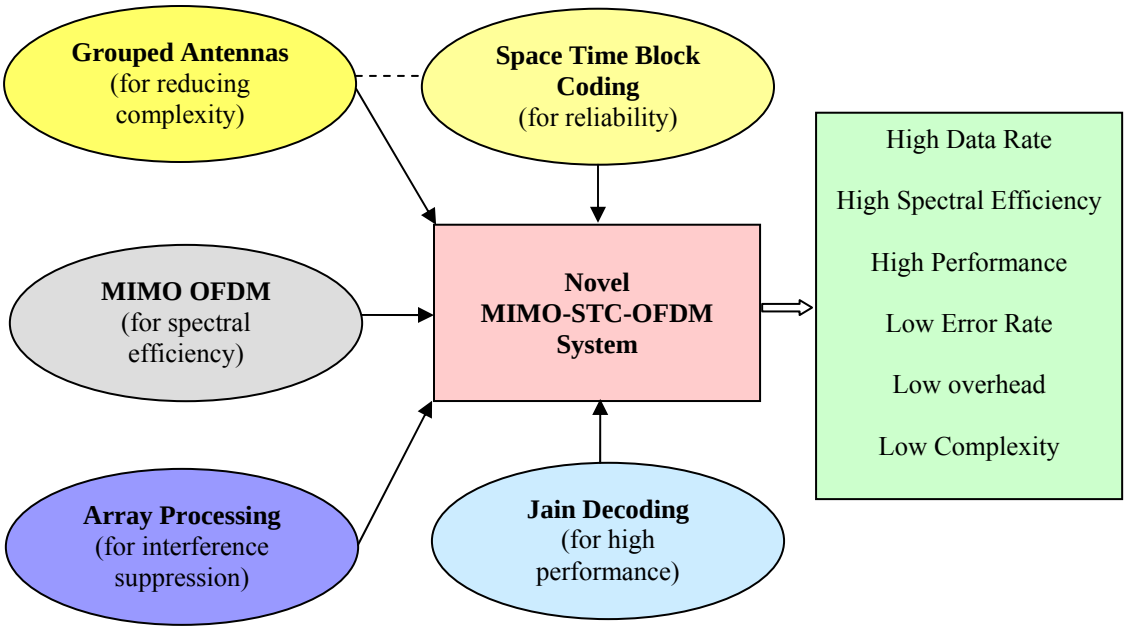

Figure 6.1 The Overall Approach

Originally proposed by Tarokh et al. [37] for flat fading MIMO systems, the group coding of transmit antennas reduces the complexity of receivers in space time coded MIMO systems. It partitions transmit antennas into small groups. The received signals are then processed by a technique called *group interference suppression method* or *array processing*. By using interference suppression on a per carrier basis after the FFT at the receiver, as suggested by Boubaker et al [57], the technique also lends itself to frequency selective multipath channels. Finally, a novel decoding scheme is employed. It uses samples from frequencies that are $K/2$ apart, where K is the total number of FFT frequencies, in order to introduce another element of diversity, and then uses least squares estimation to yield reliable statistics for symbol detection. Note that this diversity is achieved without any cost. The frequency diversity is illustrated in Figure 6.2.

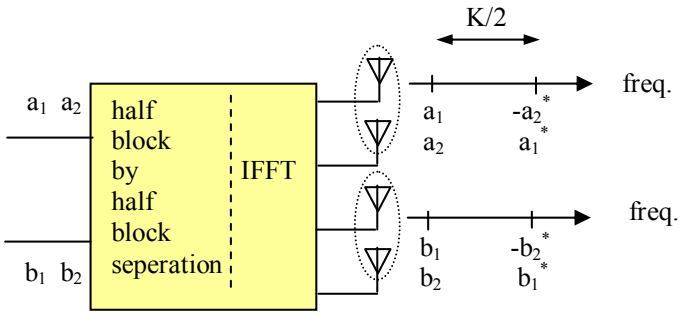

Figure 6.2. Frequency Diversity in New System

At 22 dB, this new scheme achieves a BER of 4 x 10^{-5}, without coding or interleaving. The data rate achieved, over a bandwidth of 20 MHz, is 144 Mbps with a corresponding spectral efficiency of 7.2 bits/s/Hz. If channel coding and interleaving gains of 8 dB and 4 dB, respectively, are assumed the proposed technique can achieve a BER of 4 x 10^{-5} at 10 dB and a BER of 10^{-5} at about 13 dB. However, the data rate would then be reduced to 108 Mbps with a spectral efficiency of 7.2 bits/s/Hz. In addition, the scheme is a relatively low complexity scheme, e.g., far lower compared to that in [66] which uses linear precoding and space frequency block coding.

6.2 Group Coded Antennas and Array Processing in Flat Fading Channels

In this section, the scheme proposed by Tarokh et al. [37] to reduce the complexity of receivers in space time coded MIMO systems, will be reviewed. It partitions the transmit antennas into small groups. The received signals are then processed by a technique called *group interference suppression* or *array processing*. It suppresses the signals from all other groups of antennas as interference, other than the specific group of interest which is to be decoded. Consider, for example, a 4×4 MIMO

system shown in Figure 6.3. The four transmit antennas are divided into two groups of two antennas each, and each of these groups uses the Alamouti STC code [39]. At the receiver the null space of the transpose of the second group's channel matrix is used to extract first group's signals (from the received signals). Conversely, the null space of the first group's channel matrix is used to extract second group's signals.

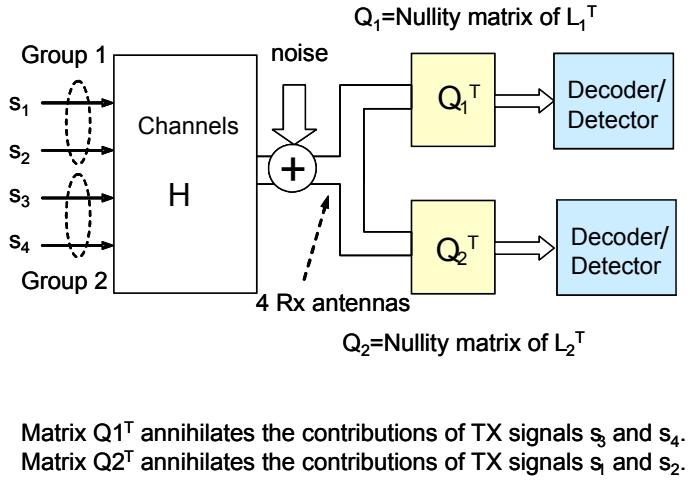

Figure 6.3 Grouped Antennas and Array Processing for 4 × 4 System

To elaborate on the theory, consider a MIMO system with N transmit and M receive antennas, with the model

$$\underline{r} = H\,\underline{s} + \underline{n} \tag{6.1}$$

Where the vector $\underline{s}$ denotes the transmitted signals, $\underline{r}$ the received signals, and $\underline{n}$ the AWGN. The $M \times N$ matrix $H = [h_{ij}]$, represents the multiple flat-fading channels.

Assume that the N transmit antennas at the transmitter are partitioned into q groups $G_1, G_2, \ldots, G_q$, comprising $N_1, N_2, \ldots, N_q$ antennas, respectively. Using array

processing, the transmitted signals from antenna group g ($g=1,2,..,q$) are decoded/detected separately while suppressing signals from all other groups. For simplicity, focus on the detection of signals from group 1. The channel matrix H is partitioned into two sub matrices, namely V_1 which consists of the first N_1 columns and L_1 which contains the remaining N-N_1 columns. Note that V_1 corresponds to the transmission of the desired group signals, and L_1 to the transmission of all other group signals, which may be interpreted as interference. To annihilate this interference, Tarokh et al. compute a set of orthonormal vectors in the null space of L_1^T assembled into a matrix Q_1. Multiplying both sides of (6.1) by its transpose

$$Q_1^T \underline{r} = Q_1^T H \underline{s} + Q_1^T \underline{n} \tag{6.2}$$

Since $Q_1^T L_1 = 0$, i.e., a zero matrix, (2) can be written as

$$Q_1^T \underline{r} = Q_1^T H_1 \underline{s}_1 + Q_1^T \underline{n} \tag{6.3}$$

where $\underline{s}_1$ represents the vector of all signals from group 1. Setting

$$\tilde{\underline{r}} = Q_1^T \underline{r}\,; \quad \tilde{H} = Q_1^T H_1\,; \quad \tilde{\underline{n}} = Q_1^T \underline{n} \tag{6.4}$$

equation (3) can be rewritten as

$$\tilde{\underline{r}} = \tilde{H}\, \underline{s}_1 + \tilde{\underline{n}} \tag{6.5}$$

Here all signal-streams out of transmit antennas $N_1 + 1$, …., N are suppressed. That is, the matrix Q_1^T annihilates the contributions of signals transmitted from N_1+1,.., N; similarly Q_2^T annihilates the contributions of signals transmitted from 1,..., N_1, and N_1+N_2+1,..., N ; and so on. Any of the various schemes could then be used for decoding/detection. The performance of the system can be enhanced considerably by

using space time codes on each group, codes that are often called component codes [37],[38]. Using array processing [37] each code is decoded separately while suppressing signals from the other component codes. This combination of component codes and array processing can provide reliable and high data rate communication.

6.3 Grouped Antennas and Array Processing in MIMO-OFDM.

6.3.1 Frequency Selective Channels in MIMO-OFDM.

Referring to Figure 6.3, consider an $N \times M$ MIMO-OFDM system with K sub-carriers. The MIMO channel is modeled as L tap frequency selective channel $h_{i,j}(l)$, with $l=0,1,...,L-1$, $i=1,2,..,M$ and $j=1,2,..,N$. Suppose $h_{i,j}(l)$ is the (i,j) th element of the matrix $H(l)$, then the discrete time MIMO baseband signal model at time instant n is given by

$$\underline{x}_{pfx}(n) = \sum_{l=0}^{L-1} H(l)\,\underline{s}_{pfx}(n-l) + \underline{w}(n) \tag{6.6}$$

where $\underline{x}_{pfx}(n)$ is the M dimensional received signal with prefix, $\underline{s}_{pfx}(n)$ is N dimensional transmitted signal with prefix and $\underline{w}(n)$ represents the additive noise. Here the underbar connotes a vector. This OFDM system utilizes K sub carriers per antenna transmission and a cyclic prefix of G samples to avoid the so-called "Inter-Block-Interference". The received MIMO OFDM symbol, after removal of the cyclic prefix, is given by

$$\underline{x} = \Gamma\,\underline{s} + \underline{w} \tag{6.7}$$

Here $\underline{s}$ is the transmitted vector of size $KN \times 1$ given by $\underline{s} = [\underline{s}(G)^T\ \underline{s}(G+1)^T\ ....\ \underline{s}(K+G-1)^T]^T$ with $\underline{s}(n)$ being an $N \times 1$ sub-vector of the nth sample. Similarly $\underline{x}$ is the $KM \times 1$ received vector given by

$\underline{x} = [\underline{x}(G)^T \ \underline{x}(G+1)^T \ .... \underline{x}(K+G-1)^T]^T$ with $\underline{x}(n)$ being an $M \times 1$ sub-vector of the nth sample. Γ is a $KM \times KN$ block circulant matrix of the form

$$\Gamma = \begin{bmatrix} \Gamma_0 & \Gamma_{K-1} & \Gamma_{K-2} & \cdots & \Gamma_1 \\ \Gamma_1 & \Gamma_0 & \Gamma_{K-1} & \cdots & \Gamma_2 \\ \Gamma_2 & \Gamma_1 & \Gamma_0 & \cdots & \Gamma_3 \\ \vdots & \vdots & \vdots & \ddots & \vdots \\ \Gamma_{K-1} & \Gamma_{K-2} & \Gamma_{K-3} & \cdots & \Gamma_0 \end{bmatrix} \tag{6.8}$$

where each individual block Γ_k, $k = 0, 1, 2, ..., K-1$, is of size $M \times N$. The $KM \times N$ dimensional first block-column of Γ is $B = [\, H(0)_{M\times N}{}^T \ H(1)_{M\times N}{}^T \ldots H(L-1)_{M\times N}{}^T \ Z_{M(K-L)\times N}{}^T \,]^T$, where Z represents a zero matrix. The transmitted signal can be represented as

$$\underline{s} = \left(F^H \otimes I_{N\times N}\right)\underline{a} \tag{6.9}$$

where F is a $K \times K$ FFT matrix (the superscript ^{H} denotes hermitian transpose), $\underline{a}$ is the $KN \times 1$ dimensional QAM symbol input given by $\underline{a} = [\underline{a}^{0T} \ \underline{a}^{1T} \ .... \underline{a}^{K-1T}]^T$, where $\underline{a}^k$ is an $N \times 1$ symbol vector of the kth subcarrier. Here $\otimes$ denotes the Kronecker product. At the receiver, after the removal of cyclic prefix and conversion to frequency domain the signal is given by

$$\begin{aligned} \underline{y} &= \left(F \otimes I_{M\times M}\right)\underline{x} = \left(F \otimes I_{M\times M}\right)\Gamma\left(F^H \otimes I_{N\times N}\right)\underline{a} + \left(F \otimes I_{M\times M}\right)\underline{w} \\ &= \hat{H}\,\underline{a} + \underline{n} \end{aligned} \tag{6.10}$$

where $\underline{y} = [\underline{y}^{0T} \ \underline{y}^{1T} \ .... \underline{y}^{K-1T}]^T$ is the frequency domain $KM \times 1$ vector, $\underline{n}$ is the additive frequency domain noise and $\hat{H}$ is a block diagonal matrix.

$$\hat{H} = \left(F \otimes I_{M\times M}\right)\Gamma\left(F^H \otimes I_{N\times N}\right) = \begin{bmatrix} H^0 & 0 & \cdots & 0 \\ 0 & H^1 & \cdots & 0 \\ \vdots & \vdots & \ddots & \vdots \\ 0 & 0 & \cdots & H^{K-1} \end{bmatrix} \tag{6.11}$$

The kth block diagonal element is the $N \times M$ MIMO channel of the kth sub-carrier and can be shown to be $H^k = \sum_{l=0}^{L-1} H(l) exp\left(-j\,2\pi \frac{k\,l}{K}\right)$. So for this sub-carrier the received frequency domain signal can be expressed as

$$\underline{y}^k = H^k \underline{a}^k + \underline{n}^k \tag{6.12}$$

As shown above, the resulting MIMO channel model in the frequency domain on a per sub-carrier basis is flat.

6.3.2. Array Processing for Frequency Selective Channels

In this section, the discussion on array processing is extended to MIMO-OFDM systems over frequency selective channels. Frequency domain equalization for frequency selective channels on a per sub-carrier basis was proposed by Boubaker et al. [57] in the context of a VBLAST-OFDM system. Their concept of per sub-carrier based MIMO processing is adapted, combined with array processing, thereby extending it to MIMO-OFDM systems in frequency selective channel environments. In the frequency domain each OFDM sub-carrier undergoes (very nearly) flat fading [6]-[8], and as such array processing can be used to separate group signals on a per sub-carrier basis. After group interference suppression, further processing such as equalization and decoding/detection can be carried out depending on the particular scheme.

Consider equation (13), where $H^k = [h_{ij}^k]$ the $M \times N$ k-th sub-carrier channel matrix. The channel matrix is partitioned into two sub matrices, namely the desired group matrix V^k_g and interferer group matrix $L^k_{g,}$ whereupon array processing is applied to separate out

the desired group of interest. Without loss of generality, further details are provided below only for group *1*.

$$V_1^k = \begin{bmatrix} h_{1,1}^k & h_{1,2}^k & \cdots & h_{1,N1}^k \\ h_{2,1}^k & h_{2,2}^k & \cdots & h_{2,N1}^k \\ \cdots & \cdots & \ddots & \cdots \\ h_{M,1}^k & h_{M,2}^k & \cdots & h_{M,N1}^k \end{bmatrix}; \quad L_1^k = \begin{bmatrix} h_{1,N1+1}^k & h_{1,N1+2}^k & \cdots & h_{1,N}^k \\ h_{2,N1+1}^k & h_{2,N1+2}^k & \cdots & h_{2,N}^k \\ \cdots & \cdots & \ddots & \cdots \\ h_{M,N1+1}^k & h_{M,N1+2}^k & \cdots & h_{M,N}^k \end{bmatrix} \tag{6.14}$$

Note that the columns of V_1^k and those of L_1^k when adjoined, form the complete matrix H^k. Similar definitions hold for other groups. Now let

$$Q_1^k = null((L_1^k)^T) \tag{6.15}$$

Then $Q^k{}_1^T$ can be used for group interference suppression to extract the signals of group *1,* while suppressing the contributions of all other groups. Multiplying both sides of (12) by its transpose

$$Q_1^k \underline{y}^k = Q_1^k H^k \underline{s}^k + Q_1^k \underline{n}^k \tag{6.16}$$

Since $Q_1^k L_1^k = 0$, i.e., a zero matrix, (16) can be written as

$$Q_1^k \underline{y}^k = Q_1^k H_1^k \underline{s}_1^k + Q_1^k \underline{n}^k \tag{6.17}$$

where $\underline{s}_1^k$ represents the vector of all signals from group 1. Setting

$$\underline{r}_1^k = Q_1^k \underline{y}^k \; ; \quad U_1^k = Q_1^k H_1^k \; ; \quad \underline{n}_1^k = Q_1^k \underline{n}^k \tag{6.18}$$

equation (3) can be rewritten as

$$\underline{r}_1^k = U^k{}_1 \underline{s}_1^k + \underline{n}_1^k \tag{6.19}$$

As shown in Figure 6.4, all signal-streams out of transmit antennas $N_1 + 1$, ..., N are suppressed. That is, the matrix $\mathbf{Q}_1^k$ annihilates the contributions of signals (for sub-carrier k) transmitted from N_1+1,.., N; similarly $\mathbf{Q}_2^k$ annihilates the contributions of signals

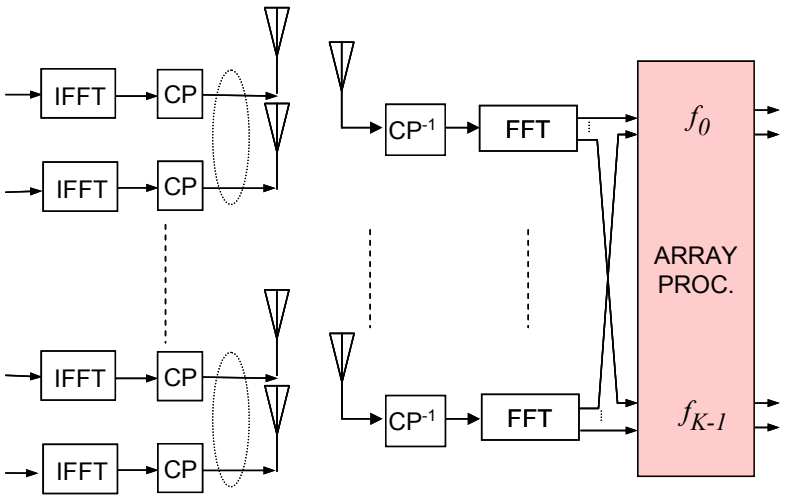

Figure 6.4 Array Processing in Frequency Selective MIMO-OFDM Channels

transmitted from 1,..., N_1, and $N_1+N_2+1,\ldots, N$; and so on. In general, $\boldsymbol{Q}_g^k$ is defined for the various other groups to facilitate signal extraction for group g.

It is interesting to observe that each group g could, in the limit, contain only one antenna, i.e., each antenna could be transmitting independently. In such a case the transmission capacity would increase by N times over a SISO OFDM system. However, such a system would suffer in terms of performance and reliability. A reasonable solution would be to introduce diversity by use of component codes and array processing, which would provide a reliable and performance oriented system with adequate increase in data rate.

6.4 Novel MIMO-STC-OFDM System

A new system is proposed here system which combines the concepts of grouped

antennas, component STC, array processing, MIMO OFDM and a new decoding algorithm. *The objective is to achieve both high spectral efficiency and high performance.* A block diagram of the system is shown in Figure 6.5. The approach is the following. The transmit antennas are divided into groups, each of which uses a component STC-OFDM (block) code. At the receiver each component code is decoded by *group interference suppression method* that suppresses signals from other antenna groups as interference. This is followed by reassembly of carriers and a novel Least Squares (LS) decoding process called Jain decoding to recover the original QAM symbols. For definitiveness, consider a 4×4 system (N=4, M=4). The transmit antennas are divided into two groups of two each and the input stream of D QAM symbols to each group is space time block coded using the block-by-half block Alamouti code [39].

$$\begin{bmatrix} \underline{a}^g(2n) & -\underline{a}^g{}^*(2n+1) \\ \underline{a}^g(2n+1) & \underline{a}^g{}^*(2n) \end{bmatrix} \tag{20}$$

where n is half-block index. Note that the underbar connotes a vector. Specifically, here the size of each of the symbol vectors is $K/2$. Also note that the symbol and its associate (complex conjugate of the symbol transmitted from the other antenna at the same time) are $K/2$ sub-carrier frequencies apart which provides frequency diversity over symbol-by-symbol scheme.

From (6.12), on a per sub-carrier basis the vector of received signals can be written as

$$\underline{y}^k = H^k \underline{s}^k + \underline{n}^k$$

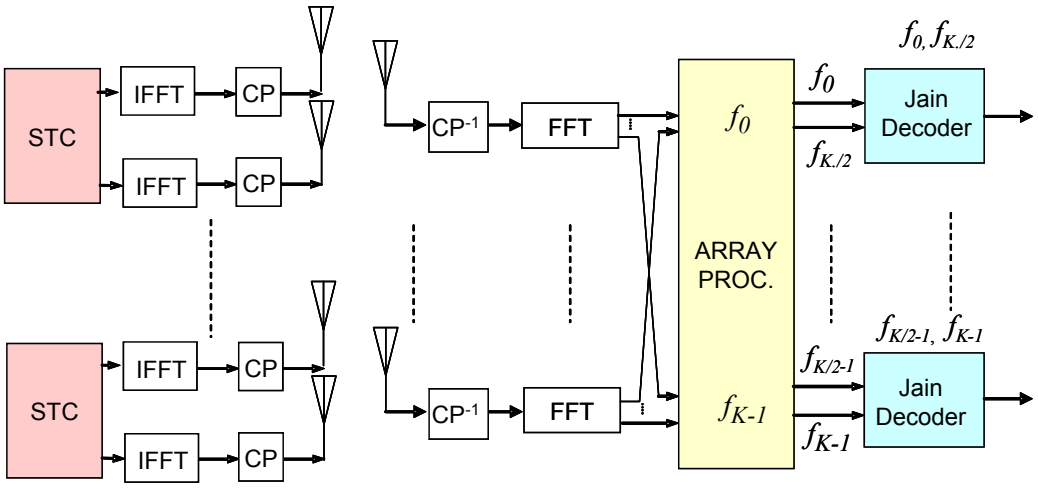

Figure 6.5 Novel MIMO-STC-OFDM system

where $\underline{s}^k$ is the transmitted signal vector, $\underline{n}^k$ the noise and $H^k=[h_{ij}{}^k]$ the $M\times N$ sub-carrier channel matrix. The channel matrix is partitioned into two sub matrices, namely the desired group matrix $V^k{}_g$ and the interferer group's matrix $L^k{}_g$. The array processing matrix $Q^k{}_g$ is applied to separate out the desired group of interest, as shown below

$$\underline{r}_g^k=Q_g^k\,\underline{y}_g^k; \qquad U_g^k=Q_g^k H_g^k \tag{6.21}$$

Now considering the structure of the Alamouti space time block code, the symbol and its conjugate are $K/2$ sub-carrier frequencies apart. This fact is used in the novel LS decoding scheme. The group index (g) details have been omitted below and only two symbols a_1 and a_2 are considered which are carried over frequencies that are $K/2$ sub-carrier frequencies apart in a single group.

$$\begin{aligned} &\underline{r}^k=U^k\begin{bmatrix}a_1\\a_2\end{bmatrix}+\underline{n}_1; \qquad \underline{r}^{k+\frac{K}{2}}=U^{k+\frac{K}{2}}\begin{bmatrix}-a_2^*\\a_1^*\end{bmatrix}+\underline{n}_2 \\ &\underline{r}^{*k+\frac{K}{2}}=U^{*k+\frac{K}{2}}\begin{bmatrix}-a_2\\a_1\end{bmatrix}+\underline{n}_2^*; \qquad \tilde{\underline{r}}^{k+\frac{K}{2}}=\tilde{U}^{k+\frac{K}{2}}\begin{bmatrix}a_1\\a_2\end{bmatrix}+\underline{n}_2^* \end{aligned} \tag{6.22}$$

The above terms can be grouped below as

$$\begin{bmatrix} \underline{r}^{k} \\ \tilde{\underline{r}}^{k+\frac{K}{2}} \end{bmatrix} = \begin{bmatrix} U^{k} \\ \tilde{U}^{k+\frac{K}{2}} \end{bmatrix} \begin{bmatrix} a_1 \\ a_2 \end{bmatrix} + \begin{bmatrix} \underline{n}_1 \\ \underline{n}_2^{*} \end{bmatrix} \tag{6.23}$$

(6.22) and (6.23) can also be explained in detail as follows

$$\underline{r}^{k} = \underbrace{\begin{bmatrix} h_{11} & h_{12} \\ h_{21} & h_{42} \end{bmatrix}}_{U^{k}} \begin{bmatrix} a_1 \\ a_2 \end{bmatrix} + \underline{n}_1 \qquad \underline{r}^{k+\frac{K}{2}} = \underbrace{\begin{bmatrix} h_{31} & h_{32} \\ h_{41} & h_{42} \end{bmatrix}}_{U^{k+\frac{K}{2}}} \begin{bmatrix} -a_2^{*} \\ a_1^{*} \end{bmatrix} + \underline{n}_2$$

$$\underline{r}^{*k+\frac{K}{2}} = \underbrace{\begin{bmatrix} h_{31}^{*} & h_{32}^{*} \\ h_{41}^{*} & h_{42}^{*} \end{bmatrix}}_{U^{*k+\frac{K}{2}}} \begin{bmatrix} -a_2 \\ a_1 \end{bmatrix} + \underline{n}_2^{*} \qquad \tilde{\underline{r}}^{k+\frac{K}{2}} = \underbrace{\begin{bmatrix} h_{32}^{*} & -h_{31}^{*} \\ h_{42}^{*} & h_{41}^{*} \end{bmatrix}}_{\tilde{U}^{k+\frac{K}{2}}} \begin{bmatrix} a_1 \\ a_2 \end{bmatrix} + \underline{n}_2^{*}$$

$$\begin{bmatrix} \underline{r}^{k} \\ \tilde{\underline{r}}^{k+\frac{K}{2}} \end{bmatrix} = \begin{bmatrix} h_{11} & h_{12} \\ h_{21} & h_{22} \\ h_{32}^{*} & -h_{31}^{*} \\ h_{42}^{*} & h_{41}^{*} \end{bmatrix} \begin{bmatrix} a_1 \\ a_2 \end{bmatrix} + \begin{bmatrix} \underline{n}_1 \\ \underline{n}_2^{*} \end{bmatrix}$$

$$= \underbrace{\begin{bmatrix} U^{k} \\ \tilde{U}^{k+\frac{K}{2}} \end{bmatrix}}_{U} \begin{bmatrix} a_1 \\ a_2 \end{bmatrix} + \begin{bmatrix} \underline{n}_1 \\ \underline{n}_2^{*} \end{bmatrix}$$

The above equation can also be written as

$$\underline{R} = U\underline{a} + \underline{n} \tag{6.24}$$

Finally frequency domain equalization is carried out using the pseudo-inverse and slicing is done to recover the received QAM symbols.

$$\underline{d} = pinv(U) * \underline{R} \quad \Rightarrow \quad \hat{\underline{a}} = slicer(\underline{d}) \tag{6.25}$$

Although a 4 × 4 system with groups of 2 antennas and Alamouti coding has been discussed, however larger systems using various space time block coding schemes are possible. To compare the *weak diversity* (symbol by symbol separation) and *strong diversity*

(half block by half block), the conditioning of the array processed 2×2 channel matrix (U^k) is studied by comparing their eigenvalues. Recall that the minimum eigenvalue [68] of a matrix is a direct measure of its conditionality. Figure 6.6a shows the minimum eigenvalues for the *weak diversity* case while Figure 6.6b shows results for the *strong diversity* scheme. For iteration no. 7, in Figure 6.6a, , the minimum (over K sub carriers) channel eigenvalues for the symbol-by-symbol case are poor, less than 0.2, for both symbols, while in Figure 6.b, the associate symbol which is $K/2$ sub-carrier frequencies apart has a good minimum eigenvalue of 0.7. As another example, for iteration no. 9, the minimum eigenvalues for the *weak diversity* case are below 0.4 for both symbols, while in the strong diversity case (Figure 6b), the associate symbol has a minimum eigenvalue of 1.5. Thus the half-block by half block based system provides distinct performance advantage over the symbol-symbol scheme.

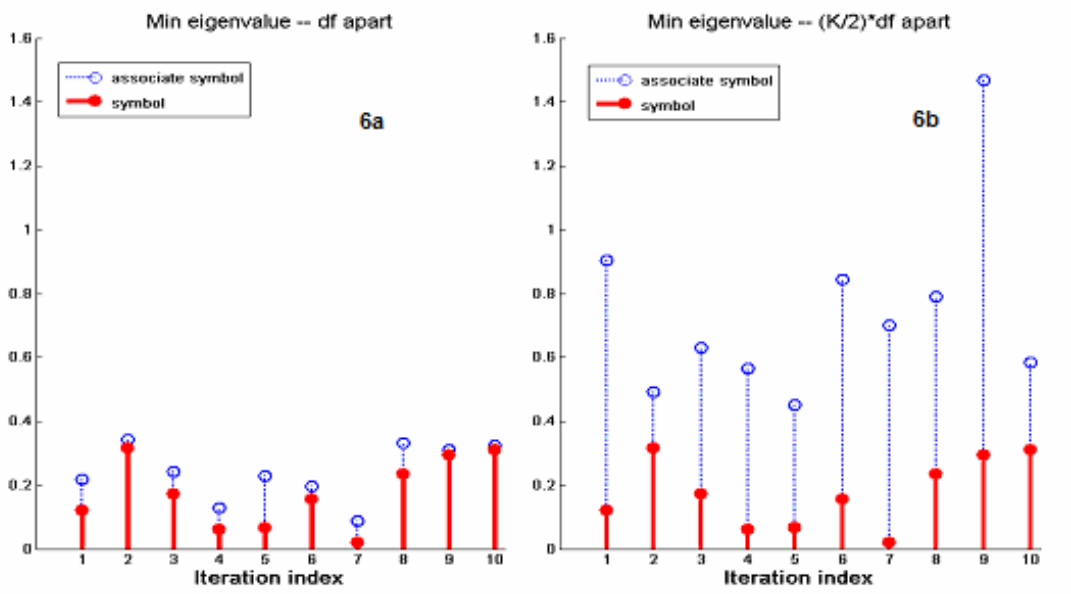

Figure 6.6 Eigen Value Analysis of Frequency Diversity for Novel MIMO-STC-OFDM System

6.5 Performance of the New MIMO-STC-OFDM System

6.5.1 Simulation Results

Simulation results on a 4 × 4 system using the new scheme, Alamouti code with 2 groups of 2 transmit antennas each are shown in Figure 6.7. The new scheme clearly outperforms VBLAST techniques in performance. For a 64-QAM symbol constellation, and 50ns delay spread Naftali channel [62], [63] (5 tap) model, to achieve BER = 10^{-3}, Group STC-OFDM with Array Processing and Jain Decoding requires only 17 dB (Eb/No) compared to 30dB (Eb/No) for an uncoded 802.11a based 64-QAM OFDM system. At 19 dB (Eb/No) this new system achieves BERs on the order of 3×10^{-4}, and at 22 dB on the order of 4×10^{-5}. The spectral efficiency is 9.6 bits/s/Hz (assuming that only 48 carriers are used for data), which is more than two times that of an 802.11a SISO OFDM system. The data rate becomes 144 Mbps. The bandwidth used is 20 MHz. Higher spectral efficiencies could be attained with larger systems, say 6 × 4.

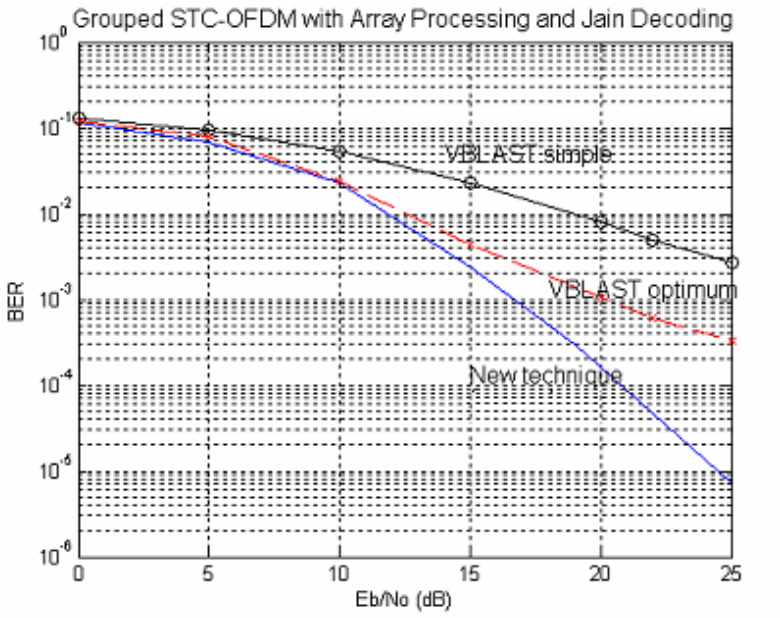

Figure 6.7 MIMO-STC-OFDM Simulation Results

6.5.2. Comparison with Other MIMO-OFDM techniques

To compare the novel MIMO STC-OFDM technique with others, the following figure of merit is proposed:

$$FOM = Spectral\ Efficiency \times (-\log_{10} BER) - \alpha \times Eb/No_{dB}$$

where α is a suitable positive number.

van Zelst's MIMO space division multiplexed (SDM) OFDM [13] has a spectral efficiency of 1.2 bits/sec/Hz and a BER of 3×10^{-4} at Eb/No of 3 dB; correspondingly for α = 0.2, FOM = 11.Shao's MIMO space frequency block coded (SFBC) OFDM [66] has a spectral efficiency of 4.8 bits/sec/Hz with a corresponding BER of 5×10^{-5} at Eb/No of 19 dB; correspondingly for α = 0.2, FOM = 44. The new technique with spectral efficiency of 7.2 bits/sec/Hz and BER of 3×10^{-4} at Eb/No of 19 dB, has a FOM = 55. Comparison with other MIMO-OFDM schemes for WLANs based on the Figure of Merit is provided in Table 6.1. This is a preliminary Figure of Merit (FOM) definition; and can be studied further for its strengths and weaknesses.

6.5.3 Benefits of Channel coding and Interleaving

In the previous section, a bandwidth of 20 MHz has been used which provisions a rate 3/4 channel coding. Therefore, the benefit of channel coding must be taken into account. Further, interleaving/deinterleaving can be incorporated at the transmitter/receiver which can yet improve the performance. Table 6.2 gives the predicted performance estimates using the upper limits GC ≤ 8 dB and GI ≤ 6 dB. Admittedly, the BER numbers in this table are only approximate estimates, but they do point to the attainable levels of performance.

Table 6.1 Comparison of the New MIMO-STC-OFDM System with Other MIMO-OFDM Systems

Author	System	Const.	Eb/No (dB)	BER	Rate (Mbps)	Spec. Eff. (bits/s/Hz)	Channel	Coding	FoM $\alpha = 0.2$	FoM $\alpha = 0.5$
IEEE	802.11a SISO-OFDM	64QAM	19	3×10^{-3}	54	2.7	50 ns known channel	¾ rate	12	6
vanZelst	4 × 4 MIMO SDM-OFDM	BPSK	3	10^{-4}	24	1.2	50 ns known channel	½ rate	11	10
vanZelst	3×3 MIMO SDM-OFDM	64QAM	26	10^{-1}	162	8.1	100 ns known channel	¾ rate	14	6
Ogawa [69]	4 × 4 MIMO SDM-OFDM	QPSK	10	10^{-2}	96	4.8	Known Multipath Rayleigh	None	20	17
Boubaker	4 × 4 VBLAST OFDM	16QAM	10	4×10^{-2}	192	9.6	50 ns known channel	None	29	26
Stuber	4 × 4 STBC-OFDM	16QAM	10	10^{-7}	36	2.7	Known 3 tap SUI-4 model	¾ rate STBC	42	39
Shao	2×3 MIMO SFBC-OFDM	64QAM	19	5×10^{-5}	96	4.8	50 ns known channel	LCF precoding	44	38
Divakaran	4 × 4 MIMO STC-OFDM	64QAM	19	3×10^{-4}	144	7.2	50 ns with Channel estimation	None	55	48

Table 6.2 Coding and Interleaving Gains for MIMO-STC-OFDM system

Coded Rate Mbps	Data Rate Mbps	Spectral Efficiency (bps/Hz)	Coding and Interleaving Gains (G_C, G_I)	SNR (Eb/No) dB			
				10 dB	15 dB	19 dB	22 dB
N/A	144	9.6	N/A (0,0)	$2x10^{-2}$	$2x10^{-3}$	$3x10^{-4}$	$4x10^{-5}$
144	108	7.2	(5,0)	$2x10^{-3}$	$2x10^{-4}$	$3x10^{-5}$	$4x10^{-6}$
			(6,0)	$1x10^{-3}$	10^{-4}	10^{-5}	
			(7,0)	$8x10^{-4}$	$5x10^{-4}$	$8x10^{-6}$	
			(8,0)	$3x10^{-4}$	$2x10^{-5}$	$4x10^{-6}$	
144	108	7.2	(5,3)	$3x10^{-4}$	$2x10^{-5}$	$4x10^{-6}$	
			(5,4)	$2x10^{-4}$	10^{-5}		
			(8,3)	$8x10^{-5}$	$8x10^{-6}$		
			(8,4)*	$4x10^{-5}$	$4x10^{-6}$		

6.6 Conclusion

A novel MIMO STC-OFDM technique has been presented that achieves both high spectral efficiency and high performance over frequency selective channels. This is accomplished by a combination, or layering, of MIMO OFDM, group coded transmit signals and antennas, array processing at the receiver for interference suppression on a per carrier basis, and a new decoding scheme which uses components that are *K*/2 FFT frequencies apart and least-squares estimation to arrive at the decision statistics. Simultaneously, the scheme is a low complexity scheme. At 22 dB, this new scheme achieves a BER of 4 x 10^{-5}, without coding or interleaving. The data rate achieved, over a bandwidth of 20 MHz, is 144 Mbps with a corresponding spectral efficiency of 9.6 bits/s/Hz. If channel coding and interleaving gains of 8 and 4 dB respectively, are assumed, the proposed technique can achieve a BER of $4x10^{-5}$ at 10 dB and a BER of

10^{-5} at about 13 dB. Correspondingly, the data rate becomes 108 Mbps with a spectral efficiency of 7.2 bits/s/Hz. Future work could involve studying and minimizing the overhead and extension to other configurations, e.g., 4x3, 4x5, and 6x4.

CHAPTER 7

CHANNEL ESTIMATION FOR THE NEW MIMO-STC-OFDM SYSTEM

7.1 Introduction

This chapter presents an efficient channel estimation technique for the novel MIMO STC-OFDM system, a WLAN signaling scheme with high spectral efficiency and high performance over frequency selective channels. The new system employs a combination, or layering [36], of MIMO OFDM [12]-[16], group coded transmit signals and antennas [37], array processing at the receiver for interference suppression on a per carrier basis, frequency diversity which uses FFT components (for STC purposes) that are K/2 apart, and a new LS decoding scheme [33], [35] that uses least-squares upon the these components. In term of MIMO classification, it is a 4×4 system, i.e., it has four transmit and four receive antennas. For a 50 ns delay spread WLAN, the time domain formulation [34], [35] for the unknown channel coefficients leads to estimates that have an SNR on the order of 48 dB when just one block of 64 symbols per transmitter is used and while the receive signal SNR is 19 dB. (Actually, only 52 non-zero symbols, since there are twelve zero carriers; 11 at the guardbands, and one at zero frequency.) The final 4×2 equivalent channel matrix, for each of the two component systems, is shown to have a corresponding SNR of 37 dB. Most importantly, the impact on the system BER performance due to the channel estimation process (compared to the known channel case) is found to be negligible.

The training symbol blocks transmitted for channel estimation, preceding the actual data transmission, use high power QPSK symbols [44], ±7±7j, which are the outer corners of the 64QAM constellation. This leads to a 3 dB advantage over high power BPSK symbols with no additional cost. Employing this channel estimation technique on a 50 ns delay spread WLAN, the new MIMO STC-OFDM scheme [33], [35] achieves a BER of 3×10^{-4} at 19 Db signal SNR, without the need for any channel coding or interleaving. The corresponding data rate over a bandwidth of 20 MHz, is 144 Mbps with an associated spectral efficiency of 7.2 bits/s/Hz. If a combined 3/4-rate channel coding and interleaving [1] gain of 10 dB is assumed, the proposed technique could achieve a BER of 3×10^{-4} at 9 dB signal SNR. Then, the data rate would become 108 Mbps with a spectral efficiency of 5.4 bits/s/Hz. Before frequency selective channels, channel equalization scheme for Tarokh's [37] MIMO system using grouped antennas and array processing in flat fading channels will be discussed.

7.2 Channel Estimation for Grouped Antennas and Array Processed MIMO System in Flat Fading Channels

In 6.2, a 4×4 MIMO system has been studied with group coded transmit antennas and array processing at the receiver. The four transmit antennas are divided into two groups of two antennas each, and each of these groups uses the Alamouti STC code [39]. At the receiver, array processing was used to separate signals from different groups, i.e. the transmitted signals from one antenna group were decoded/detected separately while suppressing signals from all other groups. In the case of flat fading channels, the received signal is given by

$$\underline{r} = H\,\underline{s} + \underline{n} \tag{7.1}$$

Where the vector $\underline{s}$ denotes the transmitted signals, $\underline{r}$ the received signals, and $\underline{n}$ the additive white Gaussian noise. The $M \times N$ matrix $H = [\, h_{ij} \,]$, represents the multiple flat-fading channels where M is number of receive antennas and N is number of transmit antennas. The channel matrix H is partitioned into two sub-matrices, namely L_1 consisting of channels associated with group 2 and L_2 with channels for group 1. The null space of the transpose of the second group's channel matrix is used to extract first group's signals (from the received signals). Conversely, the null space of the first group's channel matrix is used to extract second group's signals. Q_1 is the null matrix of L_2^t. Multiplying both sides of (5.1) by its transpose and noting that $Q_1^T L_1 = 0$.

$$Q_1^T\,\underline{r} = Q_1^T H\,\underline{s} + Q_1^T\,\underline{n} = Q_1^T H_1\,\underline{s}_1 + Q_1^T\,\underline{n} \tag{7.2}$$

where $\underline{s}_1$ represents the vector of all group 1 signals and H_1 represents channel matrix for group 1. Setting

$$\tilde{\underline{r}}_1 = Q_1^T\,\underline{r}\,; \quad H_{1t} = Q_1^T H_1\,; \quad \tilde{\underline{n}} = Q_1^T\,\underline{n}$$

The array processed input to the group 1 decoder is given by

$$\tilde{\underline{r}}_1 = H_{1t}\,\underline{s}_1 + \tilde{\underline{n}} \tag{7.3}$$

Here all the signals from group 2 are suppressed. This process is repeated for group 2 where signals from group 1 will be suppressed. For decoding, channel estimation is necessary to cancel the effect of array processed matrices H_{1t} and H_{2t}. A channel estimation scheme is illustrated in Figure 5.1.

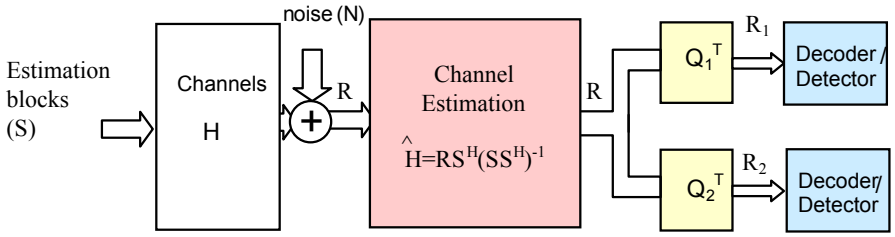

Figure 7.1 Channel Estimation for Flat Fading Channels

The channel estimation is done by transmitting a estimation block of data *S* of size *4* ×*D* preceding the transmission of the data block. The estimation blocks use high power QPSK symbols {7+7j, 7-7j, -7+7j, -7-7j}. These symbols provide an Eb/No advantage of approximately 17 dB over the normal QPSK symbols. The received signal after channel mitigation is given by

$$R = HS + N \tag{7.4}$$

The channel matrix estimation is done in the frequency domain, and is given by [34], [35]

$$\hat{H} = R\, S^H (S\, S^H)^{-1} \tag{7.5}$$

For the *4* × *4* system the minimum size of estimation block *S* is *4* × *4*. *S* matrices are designed to have a conditional number of 1 to enhance the estimation process.

The SNR of the estimated flat channels for channel matrix *H*, array processed matrices H_{1t} and H_{2t} and BER results for the 4 × 4 64-QAM system (Eb/No = 19 dB) are given in Figure 5.2 for various values of *D*. The SNR is calculates as given below $\underline{e} = \hat{\underline{h}} - \underline{h} \Rightarrow SNR_h = E\left(\|h\|^2\right) \Big/ E\left(\|e\|^2\right)$. For example, for D = 16; SNR for estimated channels {*H*, H_{1t}, H_{2t}} were {42.4 dB, 35.8 dB, 35 dB}. Using these estimated channels a

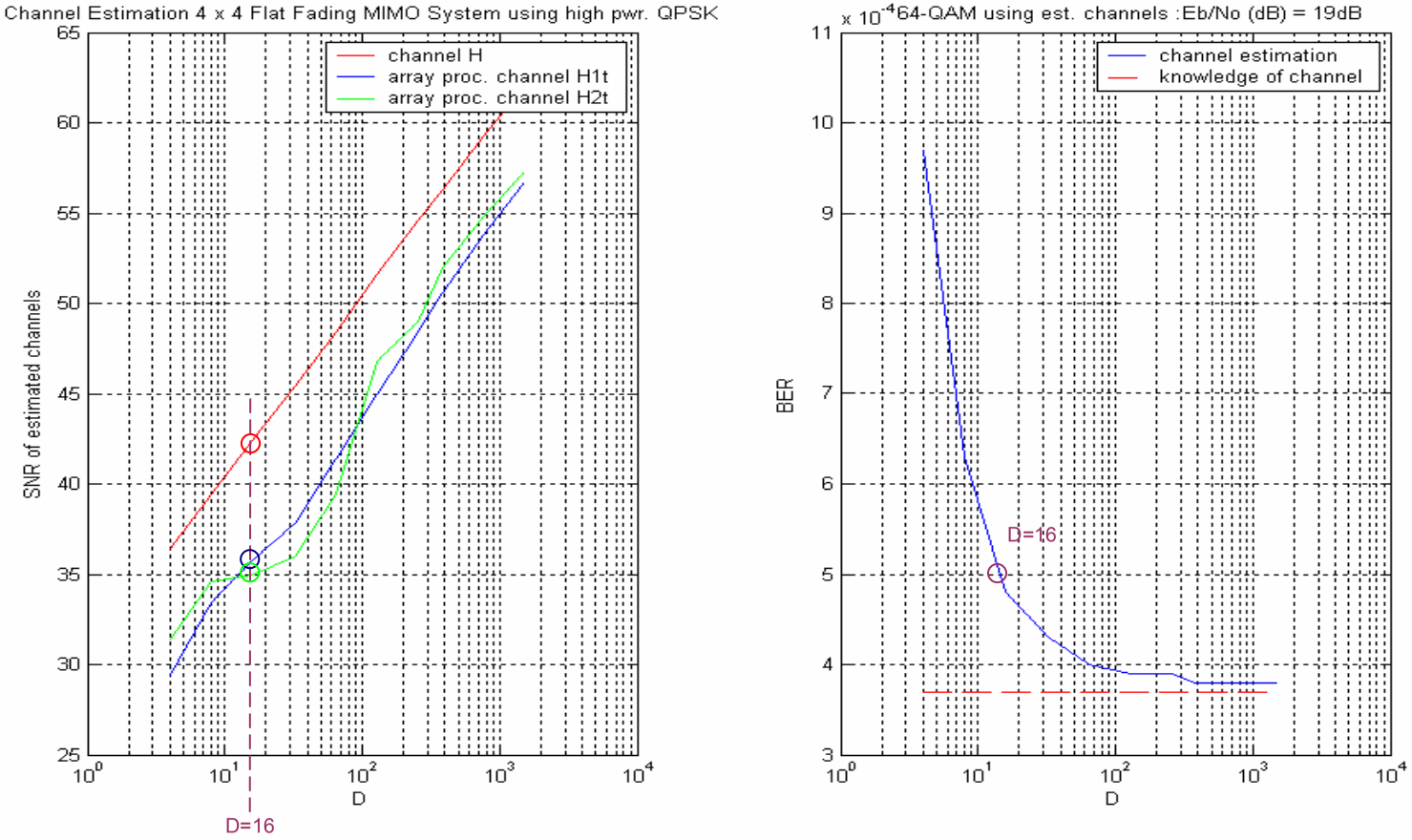

Figure 7.2 SNR of Estimated Flat Channels and Associated BER for Varying Values of D in a 4 × 4 MIMO-STC-OFDM System

(Eb/No = 19dB)

64-QAM 4 × 4 system has a BER of 5×10^{-4}. If the minimum $D = 4$ is used, a BER of 9.6×10^{-4} is obtained. For perfect channel information, the BER achievable is 3.7×10^{-4}, however a close performance of 4×10^{-4} can be achieved with $D = 60$.

7.3 Frequency Domain Estimation for the New MIMO-STC-OFDM system in Multipath Fading Channels

In the system the post FFT received signal on a per sub-carrier basis (k) is

$$\underline{r}^k = H^k \underline{s}^k + \underline{n}^k \tag{7.6}$$

Where $\underline{s}^k$ is the per carrier input to the IFFT block at transmitter and $\underline{n}^k$ is the per carrier FFT of noise and H^k is the per sub-carrier FFT of the frequency selective channel. The frequency domain channel estimation can also be done on a per sub-carrier basis by using estimation frames S preceding the data. The process is illustrated in Figure 7.3. D estimation frames of size $N \times K$ where K is the number of sub-carriers. For a 4×4 - 64 sub-carrier system D estimation frames of size 4×64 will be used. The estimation frames also use high power symbols and the columns representing sub-carrier k are collected over all D frames, they form a matrix S^k of conditional number 1. The received signals can also be collected into a similar matrix R^k, and channel estimation carried out on a per sub-carrier basis.

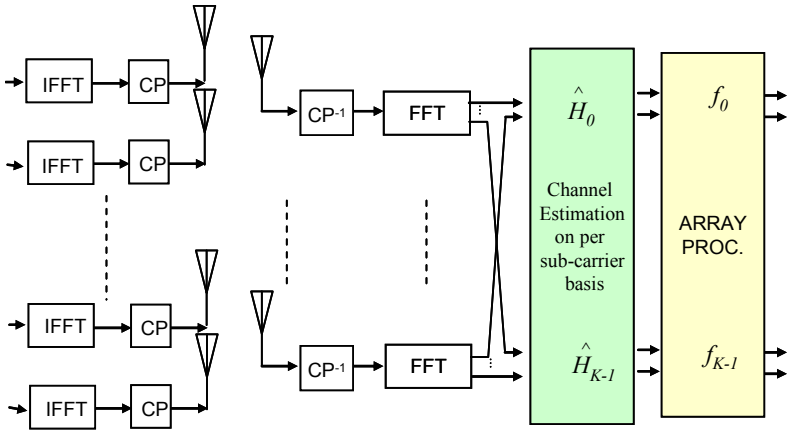

Figure 7.3 Frequency Domain Channel Estimation for the New MIMO-STC-OFDM System

$$R^k = H^k S^k + N^k \quad \Rightarrow \quad \hat{H}_k = R^k (S^k)^H [S^k (S^k)^H]^{-1} \tag{7.7}$$

The estimated channel SNR using high power QPSK symbols in the 4 x 4 system with 50 ns delay spread Naftali channels [62], [63] for varying values of *D* are given below in Figure 7.4. The channel SNR for each sub-carrier is constant and hence the average channel SNR over all carrier is plotted below in the figure. The SNR of the channel estimation for a 50ns delay spread Naftali channel in the 4 × 4 system using 4 estimation frames (size 4 × 64) of high power QPSK symbols was found to be 33.4 dB, for 8 frames it was 36.4 dB and for16 frames it was 39.4 dB. This represents a drop of 3 dB in performance as compared to the flat fading channel case.

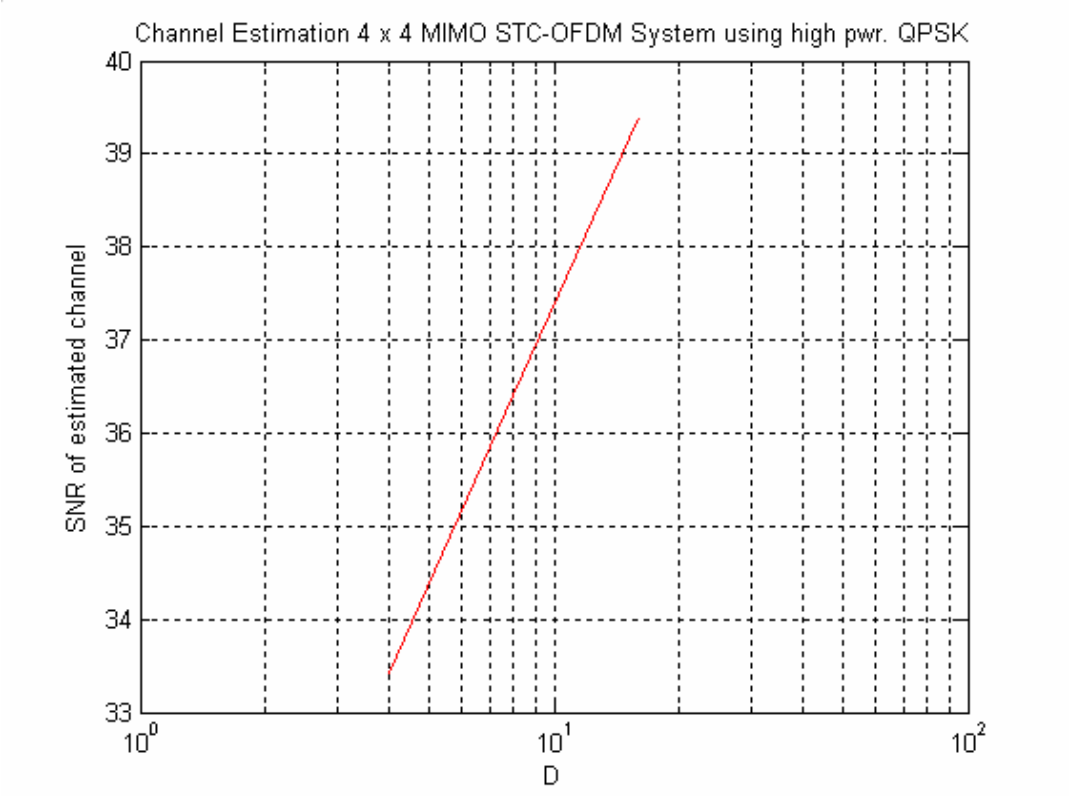

Figure 7.4 SNR of Estimated Flat Channels for Varying Values of D in a 4 × 4 MIMO-STC-OFDM System (Eb/No = 19dB)

7.4 Time Domain Channel Estimation for the New MIMO-STC-OFDM System in Multipath Fading Channels

Consider the $N \times M$ OFDM system as illustrated in Figure 7.5. The input to the IFFT block for the j-th transmitter $\underline{a}_j$, j=1,2,3,..N. The estimation blocks use high power QPSK symbols ± 7 ± 7j. The output of the corresponding IFFT operation is $\underline{s}_j$ =ifft ($\underline{a}_j$) = [$s_j(1)$ $s_j(2)$ … $s_j(K)$]T where K is the number of sub-carrier frequencies. Cyclic prefix is then prepended to these signals before transmission. The $M \times N$ channel impulse responses, each of length L, are denoted as $\underline{h}_{i,j}$, i=1,2, ..M ; j=1,2,3,..N. Note that $\underline{h}_{i,j}$ is a

column vector of length L. The received signal at the i-th receive antenna after removal of cyclic prefix is given by

$$r_i(k) = \sum_{j=1}^{N} (h_{i,j}(k) * s_j(k)) + n_i(k) = \sum_{j=1}^{N} r_{i,j}(k) + n_i(k) \tag{7.8}$$

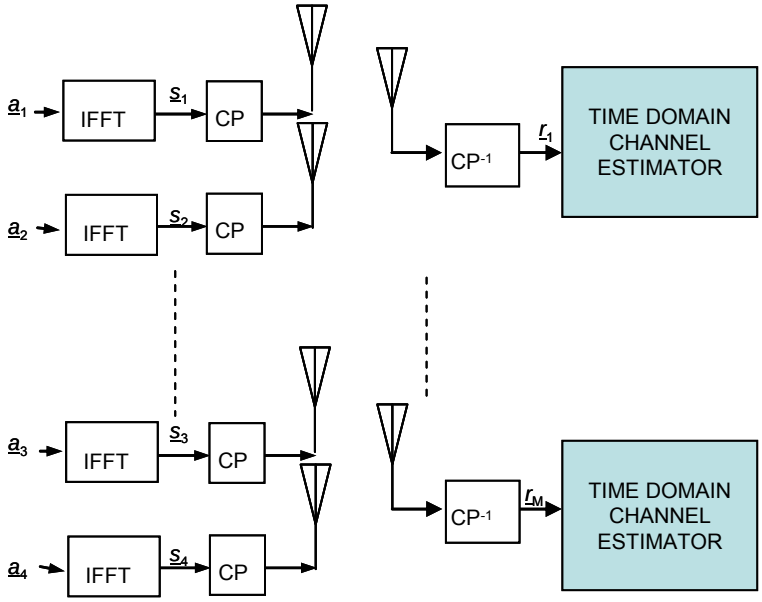

Figure 7.5 Time Domain Channel Estimation for the New MIMO-STC-OFDM System

where n_i is the noise. The channels associated with the i-th receiver can be collected in a vector of size $N \times L$

$$\underline{h}_i = \left[\underline{h}_{i,1}^{\ T} \quad \underline{h}_{i,2}^{\ T} \quad \cdots \quad \underline{h}_{i,N}^{\ T} \right]^T \tag{7.9}$$

The time domain convolution can be expressed as a matrix vector product. The known OFDM symbols can be collected in a circular convolution (rectangular) matrix as shown below

$$S_j = \begin{bmatrix} s_j(1) & s_j(K) & \cdots & s_j(K-L+2) \\ s_j(2) & s_j(1) & \cdots & s_j(K-L+3) \\ \vdots & \vdots & \ddots & \vdots \\ s_j(K) & s_j(K-1) & \cdots & s_j(K-L+1) \end{bmatrix}_{K\times L} \tag{7.10}$$

Then the convolution expression for the received signal can be written as

$$\begin{aligned} \underline{r}_i &= \left[S_1 \;\middle|\; S_2 \;\middle|\; \cdots \;\middle|\; S_N \right] \underline{h}_i + \underline{n}_i \\ &= S_{K\times(N\times L)}\,\underline{h}_i + \underline{n}_i \end{aligned} \tag{7.11}$$

The matrix $\boldsymbol{S}_{K\times(N\times L)}$, applicable to a single frame of channel estimation phase symbols, is shown in equation (7.12).

$$S_{K\times(N\times L)} = \left[\begin{array}{cccc|c|cccc} s_1(1) & s_1(K) & .. & s_1(K-L+2) & .. & s_N(1) & s_N(K) & .. & s_N(K-L+2) \\ s_1(2) & s_1(1) & .. & s_1(K-L+3) & .. & s_N(2) & s_N(1) & .. & s_N(K-L+3) \\ \vdots & \vdots & \ddots & \vdots & .. & \vdots & \vdots & \ddots & \vdots \\ s_1(K) & s_1(K-1) & .. & s_1(K-L+1) & .. & s_N(K) & s_N(K-1) & .. & s_N(K-L+1) \end{array}\right] \tag{7.12}$$

If more than one frame is used, $S_{K\times(N\times L)}$ matrices for each frame are stacked one on top of the other to create a matrix $S_{(B\times K)\times(N\times L)}$ where B is the number of frames. This is shown in (7.13) after two pages. Then the channel impulse response for the i-th receiver can be estimated using the least squares criterion, as follows

$$\hat{\underline{h}}_i = (S^H S)^{-1} S^H \underline{r}_i \tag{7.14}$$

The components of the channel impulse response can be separated into individual four channels associated with the i-th receiver. The process is repeated for each receiver, to estimate all sixteen channel in the 4 × 4 system and thereupon, FFT of the individual channel impulse responses will be used for array processing, equalization and decoding.

From (7.14), the estimated channel vector can clearly be written as

$$\underline{\hat{h}}_i = C\underline{r}_i \tag{7.15}$$

where $C = (S^H S)^{-1} S^H$ (7.16)

The matrix C of equations (7.15) and (7.16) is known and can therefore be pre-stored. The channel estimation process then involves the matrix-vector multiplication $C^*\underline{r}_i$. The matrix C has a size $(N\times L)\times K$. For a 50ns delay spread (5 tap channel) 4 × 4 MIMO WLAN (K=64), C would be a 20 × 64 matrix.

High power BPSK symbols were tried in the estimation process. However they suffered from a 3dB SNR loss. If it were possible to design a matrix S, whose columns are orthogonal, then S^HS will become a diagonal matrix [34], [35]. This may simplify the matrix-vector multiplication process in (7.15).

$$
S = \left[\begin{array}{cccc|cc|c}
s_1(1) & s_1(K) & \cdots & s_1(K-L+2) & s_N(1) & s_N(K) & \cdots \; s_N(K-L+2) \\
s_1(2) & s_1(1) & \cdots & s_1(K-L+3) & s_N(2) & s_N(1) & \cdots \; s_N(K-L+3) \\
\vdots & \vdots & \ddots & \vdots & \vdots & \vdots & \ddots \quad \vdots \\
s_1(K) & s_1(K-1) & \cdots & s_1(K-L+1) & s_N(K) & s_N(K-1) & \cdots \; s_N(K-L+1)
\end{array}\right]_{(B\times K)\times(N\times L)}
$$

Frame 1 | *Frame 2* | *Frame B*

(7.13)

7.5 Simulations based on the Time Domain Channel Estimation

The channel estimation can be done using B frames of known time domain OFDM symbols (IFFT of high power QPSK symbols) of size K before the actual transmission of data symbols. The SNR (SNR_h) of estimated channel parameters (H_k) and estimated array processed channel parameters (U_k) using varying number of frames is shown in Figure 7.6 (for signal Eb/No = 19 dB). The SNR is calculates as

$$\underline{e}_{i,j} = \underline{\hat{h}}_{i,j} - \underline{h}_{i,j} \quad \Rightarrow \quad SNR_h = E\left(\left\|h_{i,j}\right\|^2\right) \Big/ E\left(\left\|e_{i,j}\right\|^2\right)$$

For example, for one frame (K=64) and 5 tap channel, the SNR of the estimated channel parameters is 49 dB and for two frames it is 52 dB. The SNR of estimated channel parameters for the time domain translates in the frequency domain for a per sub-carrier frequency domain channel matrix, as FFT of the carrier frequency domain channel matrix, as FFT of the estimated time domain channels is a orthogonal transformation. The figure also shows the SNR of estimated array processed channels in the frequency domain, taking into account the inherent frequency diversity of the system by using block based STC-OFDM. For example for one frame the SNR of estimated array processed channels is 48 dB.

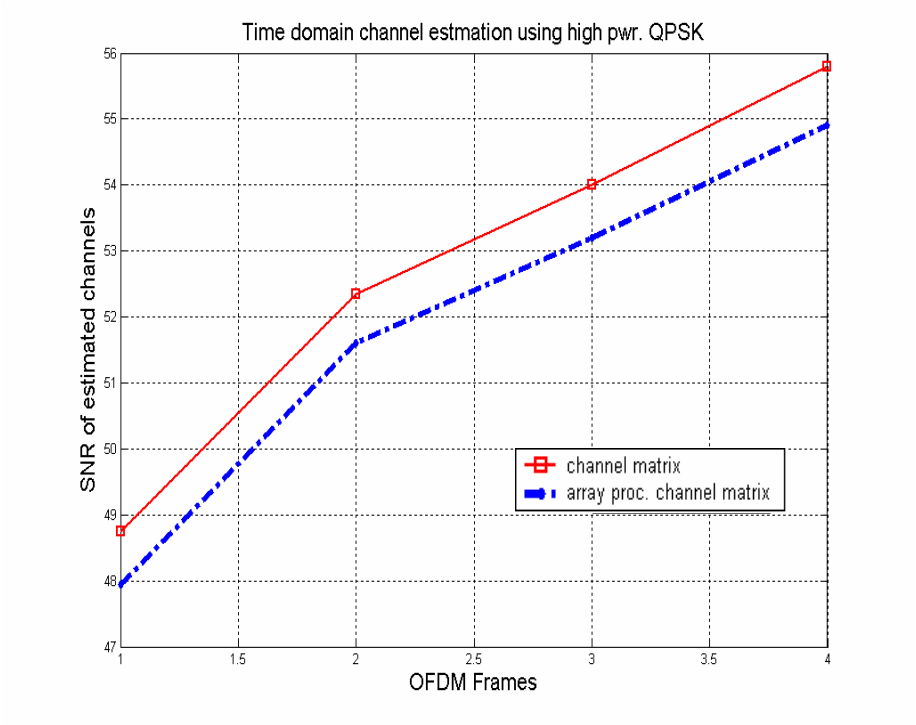

Figure 7.6 SNR of Time Domain Estimated Channel Parameters at 19 dB Signal SNR

Simulation results on a 4×4 system using the time domain estimation scheme and Alamouti STC codes with 2 groups of 2 transmit antennas each is shown in Figure 7.7. System parameters are as follows: B=1, K=64, 64-QAM symbol constellation, and 50ns delay spread Naftali channel [62], [63] (5 tap) model. The spectral efficiency is 9.6 bits/s/Hz (assuming that only 48 carriers are used for data), which is more than two times that of an 802.11a SISO OFDM system [4], [8]. The data rate becomes 144 Mbps. The bandwidth used is 20 MHz with K=64 sub-carrier frequencies. These input parameters generally conform to the 802.11a standard [4], [8]. The figure shows the BER curves with channel estimation and with perfect knowledge of the channel, showing that highly efficient results are obtained using a single frame.

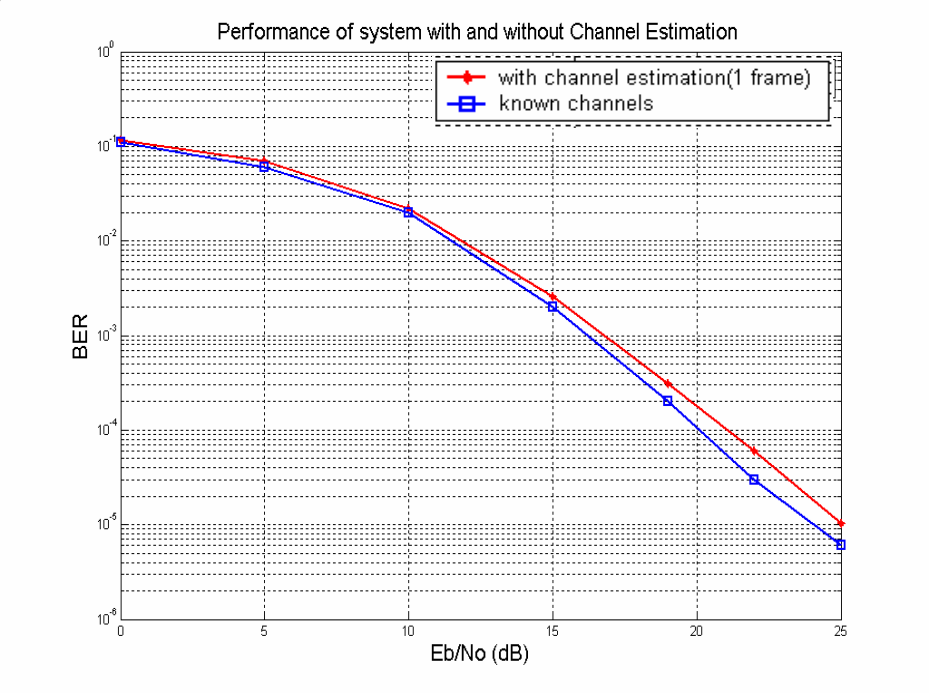

Figure 7.7 System Performance with Known Channels and Time Domain Channel Estimation

7.6 Conclusions

An efficient time domain formulation for channel estimation has been presented, for the new high performance MIMO STC-OFDM system, which uses high power QPSK symbols. Four matrix-vector multiplications enable high accuracy estimation of all sixteen MIMO channels. For a 50 ns delay spread WLAN, at 22 dB signal SNR this new scheme, together with channel estimation incorporation, achieves a BER of 4×10^{-5} without coding or interleaving. The corresponding data rate over a bandwidth of 20 MHz, is 144 Mbps with a corresponding spectral efficiency of 7.2 bits/s/Hz. Further work could involve improvising on the frequency domain channel estimation and optimizing the time domain estimation block.

CHAPTER 8

CONCLUSIONS AND FUTURE WORK

In this dissertation, two different technologies are presented for the next generation of high speed WLANs, OWSS and MIMO-STC-OFDM. OWSS, or Orthogonal Wavelet Division Multiplexed - Spread Spectrum was first introduced as a new class of pulses and a corresponding signaling system which can be a candidate signaling scheme for the next generation high speed WLANs. OWSS offers multiplexing capability both at the PHY and MAC layers. However, multiplexing at the MAC layer is more preferable, as it would enable full rate shared access of the bandwidth (in this case 108 Mbps) to bursty users. Towards this end, it was proposed that OWSS will use a CSMA/CA based MAC protocol similar to the IEEE 802.11a standard to access the medium. A frame format for OWSS data packets in the MAC layer and MAC attributes of OWSS in terms of DCF parameters was also proposed. Using a simple theoretical model for performance analysis, the MAC layer of OWSS showed excellent performance results, a saturation throughput of 66% and an average packet delay of 5 ms using RTS-CTS – for a moderate number of stations (say, less than 50). At the PHY layer, a critical attribute of OWSS was looked at, its spectral characteristics. OWSS can avoid substantial overhead penalties through the elimination of the prefix, the guard zero-carriers, and channel. coding, while still providing a desired BER performance at practical SNRs. It was shown that the theoretical baseband spectrum is perfectly flat, and the passband

spectrum offers a 30-40% bandwidth advantage over 802.11a OFDM for 54 Mbps operation. OWSS readily extends to higher bit rates, such as 108 Mbps, in a bandwidth efficient manner. Spectrum masks for 54 Mbps and 100 Mbps OWSS operation were also proposed.

Unlike the pulses used in OFDM, CDMA, and TDMA, OWSS pulses are based on a new family of pulses which have both a wide time support and a wide frequency support. As a consequence of the wide frequency support, effective equalization in a multipath environment can be achieved using an FE–DFE structure in the receiver together with the LMS adaptation algorithm. The fundamental limits to its system performance is investigated out by formulating the system as a multi-rate signal processing system, using hierarchical matrices, and thereupon minimizing the total mean-square error (TMSE). The TMSE governs the BER performance of the system, and is defined as the sum of the MSE of the unequalized residual error and the MSE due to the channel noise amplified by the forward equalizer. The problem is formulated at the chip level so as to truly discern the fundamental limits to the performance of the equalizer. This approach enables estimation of the optimum equalizer for mitigating the effect of the multipath channel, prior to correlation and detection blocks embedded in the FE–DFE loop, and thereby the system performance. Simulation results demonstrate its effectiveness. For a 108 Mbps system with a 50 ns delay spread channel, a very low BER of 10^{-5} and high spectral efficiency up to 5.2 bits/s/Hz can be achieved at a bit SNR of 19 dB.

Moving away from OWSS, a new MIMO-STC-OFDM system was then introduced that achieves both high spectral efficiency and high performance over frequency selective channels. This is accomplished by a combination, or layering, of MIMO OFDM, group coded transmit signals and antennas, array processing at the receiver for interference suppression on a per carrier basis, and a new decoding scheme which uses components that are K/2 FFT frequencies apart and least-squares estimation to arrive at the decision statistics. Simultaneously, the scheme is a low complexity scheme. At 22 dB, this new scheme achieves a BER of 4×10^{-5}, without coding or interleaving. The data rate achieved, over a bandwidth of 20 MHz, is 144 Mbps with a corresponding spectral efficiency of 9.6 bits/s/Hz. If coding and interleaving gains of 8 and 4 dB respectively, are assumed the proposed technique can achieve a BER of 4×10^{-5} at 10 dB and a BER of 10^{-5} at about 13 dB. Correspondingly, the data rate will become 108 Mbps with a spectral efficiency of 7.2 bits/s/Hz.

Finally the frequency selective channel for the new 4×4 system was modeled. Frequency domain equalization using high power QPSK symbols provided excellent results for flat fading channels but did not port too well to the frequency selective channels. So an efficient time domain formulation for channel estimation was presented, for the new high performance MIMO STC-OFDM system, which uses high power QPSK symbols. Four matrix-vector multiplications and a single estimation data frame enabled high accuracy estimation of all sixteen MIMO channels.

To summarize we again list the specific contributions of this dissertation below. Following this, possible extensions of the work done are discussed.

(1) OWSS and MIMO-STC-OFDM are both presented as viable candidates for the next generation of high speed WLANs. OWSS is a new modulation technique capable of high data rates without using multiple antennas at the transmitter and receiver. MIMO-STC-OFDM on the other hand, achieves next generation data rates by combining transmit and receive diversity techniques with legacy OFDM systems.

(2) A CSMA/CA based MAC protocol is proposed for OWSS to access the medium. A frame format for OWSS data packets and MAC attributes of OWSS are also proposed. Performance of OWSS at the MAC layer in terms of saturation throughput and average delay was analyzed using Bianchi's model.

(3) The spectrum efficiency of OWSS was analyzed vis-a-vis OFDM. The OWSS passband spectrum is found to have 30-40% bandwidth advantage over OFDM for 54 Mbps operation. OWSS also readily extends to higher bit rates, such as 108 Mbps, in a bandwidth efficient manner.

(4) A novel pre-distortion scheme was developed to compensate for the passband spectral regrowth due to PA non-linearity. At 6 dB backoff in 108 Mbps OWSS, this scheme yields an improvement of 10 dB in spectral regrowth distortion levels.

(5) A Forward Equalizer - Decision Feedback Equalizer (FE-DFE) structure was originally proposed for the OWSS receiver. Towards this end, a novel multi-level matrix formulation has been conceptualized to model the entire OWSS transreceiver and establish its fundamental theoretical performance (BER) in random multipath fading

channels. This formulation can also be used for channel estimation, i.e. to estimate the optimum channel equalizer (weights of the FE and DFE) for these channels.

(5) A new MIMO-STC-OFDM system has been developed that achieves both high spectral efficiency and high performance over frequency selective channels. This new system was achieved combining MIMO-OFDM, group coding antennas using STC, array processing at the receiver (for interference suppression) and new LS decoding technique.

(6) A highly effective channel equalization technique in the time domain has also been developed for the new MIMO-STC-OFDM system. The multipath channel model for the system was also conceptualized.

OWSS achieves high data rates without the use of MIMO technology and if combined with MIMO technology is capable of data rates in excess of 200 Mbps within current bandwidth limitations. The potent mixture of MIMO, OWSS and STC could make these data rates possible with high performance and bandwidth efficiency. Future work in OWSS could include a MIMO-OWSS system and reducing the complexity of the OWSS receiver. Researchers could also look into other PHY issues related OWSS namely effect of offsets, effects of clipping to reduce PAPR etc.

MIMO-STC-OFDM is a new system based on current trends of R&D for 4G WLANs. The 4 × 4 MIMO-STC-OFDM system is capable both of high performance and high spectral efficiency at a data rate of 108 Mbps. Future work could involve extending the 4 × 4 systems to larger systems such as 6 × 6, capable of even higher data rates. With the current system, researchers could look into improvising on the frequency domain

channel estimation and optimizing the time domain estimation frames so as to reduce overhead and complexity. The susceptibility of MIMO-STC-OFDM to general OFDM impairments like frequency offset should also be explored.

REFERENCES

[1] T.S. Rappaport, *Wireless Communications, Principles and Practice*, 2nd ed., Prentice-Hall Inc., 2002.

[2] R. Prasad and L. Munoz, *WLANs and WPANs Towards 4G Wireless*, Artech House Publishers, 2003.

[3] M. C. Chuah and Q. Zhang, *Design and Performance of 3G Wireless Networks and Wireless LANs*, Springer, 2005.

[4] *Local and metropolitan area networks - specific requirements. Part 11: wireless LAN Medium Access Control (MAC) and Physical Layer (PHY) specifications: high-speed physical layer in the 5 GHz band*, The Institute of Electrical and Electronics Engineering, Inc. Std., IEEE 802.11a, Sept. 1999.

[5] *IEEE standard for information technology- telecommunications and information exchange between systems- local and metropolitan area networks- specific requirements Part II: wireless LAN medium access control (MAC) and physical layer (PHY) specifications*, IEEE Std 802.11g-2003 (Amendment to IEEE Std 802.11, 1999 Edn. (Reaff 2003) as amended by IEEE Stds. 802.11a-1999, 802.11b-1999, 802.11b-1999/Cor 1-2001, and 802.11d-2001) Std., 2003.

[6] R. Prasad and R. Van Nee, *OFDM for Wireless Multimedia Communications*, Artech House Publishers, 2000.

[7] R. Prasad, *OFDM for Wireless Communication Systems*. Artech House Publishers, 2004.

[8] J. Heiskala, *OFDM Wireless LANs: A Theoretical and Practical Guide*, SAMS Publishing, 2002.

[9] E. Biglieri, R. Calderbank, A. Constantinides, A. Goldsmith, A. Paulraj and H. V. Poor, *MIMO Wireless Communications*, Cambridge University Press, 2007.

[10] A. J. Paulraj, D. Gore, R. U. Nabar, and H. Bolcskei, "An Overview of MIMO Communications - A Key to Gigabit Wireless", *Proceedings of IEEE*, 2004.

[11] G.J.Foschini and M.J. Gans, "On Limits of Wireless Communications in a Fading Environment when Using Multiple Antennas", *Wireless Personal Communications*, vol.6, pp.311-335, 1998.

[12] I. E. Telatar, "Capacity of multi-antenna Gaussian channels", ATT-Bell Labs Murray Hill, Tech. Memo, 1995.

[13] A. van Zelst, T. C. W. Schenk, "Implementation of a MIMO OFDM Based WLAN system", *IEEE. Trans. Sig. Proc.*, vol. 52, no. 2, February 2004.

[14] Z-Y. Ding, C-Y. Chen and T-D. Chiueh, "Design of a MIMO OFDM baseband receiver for next-generation wireless LAN," *Proc. Int. Symp. on Circuits and Systems*, pp, 6551-5654, 2006.

[15] H. Sampath, S. Talwar, J. Tellado, V. Erceg and A Paulraj, "A fourth-generation MIMO-OFDM broadband wireless system: design, performance, and field trial results", *IEEE Communications Magazine*, September 2002.

[16] G.L. Stuber, J.R. Barry, S.W. McLaughlin, L.Ye, M.A. Ingram and T.G. Pratt, "Broadband MIMO-OFDM wireless communications", *Proceedings of the IEEE*, February 2004.

[17] Y. Xiao, "IEEE 802.11n: enhancements for higher throughput in wireless LANs", *IEEE Wireless Communications*, December 2005.

[18] R. Van Nee , V. K. Jones, G. Awater, A. Van Zelst, J. Gardner and G. Steele," The 802.11n MIMO-OFDM Standard for Wireless LAN and Beyond," *Wireless Personal Communications,* Springer, May 2006.

[19] V. K. Jain, "OWSS Multiple-access system for 100 Mb/s wireless LANs," *Proc. IEEE International Conference on Communications* (*ICC'2001*), pp. 1471-1475.

[20] V. K. Jain, "Hybrid Wavelet/Spread-spectrum System for Broadband Wireless LANs," *Proc. Int'l. Symp. Circuits and Sys*., May 2001, pp. IV-554 to IV-557.

[21] V. K. Jain and B. A. Myers, "OWSS: A new signaling system for 100-150 Mb/s WLANs," *IEEE Wireless Commununications*, vol. 10, pp. 16-24, Aug. 2003.

[22] V. K. Jain and B. A. Myers, Communication System Using Orthogonal Wavelet Division Multiplexing (OWDM) and OWDM-Spread Spectrum (OWSS) Signaling, *U.S. Patent No. 7058004,* U.S. Patent and Trademark Office.

[23] M. Vetterli and J. Kovacevic, *Wavelets and Subband Coding*, Prentice-Hall, 1995.

[24] R. V. Dalal, "Orthogonal Wavelet Division Multiplexing (OWDM) for Broadband Wireless Communications," *M.S. thesis*, Univ. of South Florida, 1999.

[25] R. L. Peterson, R. E. Ziemer and D. E. Borth, *Introduction to Spread Spectrum Communications*, Prentice Hall, 1995.

[26] D. Divakaran, V.K. Jain and B. Myers, "Spectral characteristics of OWSS signal", *IEEE Communication Letters*, Vol.9 No. 4, pp 325-327, April 2005.

[27] V. K. Jain, D. Divakaran and B.A. Myers, "Performance limits of OWSS: A spectrally efficient WLAN system," Digital Signal Processing, Vol. 9 No. 4, pp. 347-366, July 2005.

[28] D. Divakaran, V. K. Jain, and B. A. Myers, "108 Mb/s OWSS WLANs: CSMA/CA throughput and delay analysis," *Proc. ASILOMAR Conference on Signals, Systems and Computers (ASILOMAR'2003)*, pp. 522-526.

[29] J. Dholakia, V.K. Jain, B.Myers, "Adaptive equalization for 100 Mbps OWSS wireless LANs", *Proc. IEEE GLOBECOM 2001*, pp. 162–166.

[30] J. Dholakia, "Multirate Adaptive equalization for 100 Mbps OWSS wireless LANs", *M.S. thesis*, Univ. of South Florida, 2001.

[31] V. K. Jain and D. Divakaran, Transforming OWSS into a 4G Wireless Technique, *Final Report to Conexant Systems*, March 2004.

[32] V. K. Jain and D. Divakaran, Ultra High Speed OWSS Wireless Networks, *Final Report to Globespan Virata Systems : Part II*, March 2003.

[33] D. Divakaran and V. K. Jain, "A novel MIMO STC-OFDM technique with high spectral efficiency and high performance", Proc. IEEE Radio and Wireless Symposium 2008, pp. 299-302, January 2008.

[34] V. K. Jain, and D. Divakaran, "Channel estimation for a new high performance MIMO STC-OFDM WLAN system", *Proc. Int. Symp. on Circuits and Systems* (*ISCAS 2005*), pp. 4473-4476, May 2005.

[35] V. K. Jain and D. Divakaran, Advanced Issues for 4G OFDM Wireless LANS, *Final Report to Conexant Systems*, March 2005.

[36] G. J. Foschini, "Layered space-time architecture for wireless communication in a fading environment when using multiple antennas", *Technical Journal*, Bell Labs, Autumn 1996.

[37] V. Tarokh, A. Naguib, N. Sheshadri, A.R. Calderbank, "Combined Array Processing and Space Time Coding", *IEEE. Trans. Information Theory*, vol. 45, no. 4, May 1999.

[38] V. Tarokh, H. Jafarkhani and A.R. Calderbank, "Space-time block coding for wireless communications: performance results," *IEEE Jour. Sel. Areas Comm*., vol. 7, no. 3, March 1999.

[39] S. Alamouti, " A simple transmit diversity technique for wireless communication," *IEEE Jour. Sel. Areas Comm*., vol. 16, no. 8, October 1998.

[40] E. Ziouva and T. Antonakopoulos, "CSMA/CA performance under high traffic conditions: throughput and delay analysis", Computer Communications, Elsevier, February 2002.

[41] G. Bianchi, "IEEE 802.11 saturation throughput analysis", *IEEE Communication Letters*, Vol. 2, pp. 318 -320, Dec 1998.

[42] G. Bianchi, "Performance analysis of the IEEE 802.11 distributed coordination function", *IEEE Jour. Sel. Areas Comm*., vol. 18, pp. 535-547, March 2000.

[43] R. Prasad, *CDMA for Wireless Personal Communications*, Artech House Publishers, 1996.

[44] E. A. Lee and D. G. Messerschmitt, *Digital Communications*, 2nd edition, Kluwer Academic Publishers, 1988.

[45] A. V. Oppenheim and R. W. Shafer, *Discrete-Time Signal Processing*, Prentice Hall, 1989.

[46] V. K. Jain, "Unified approach to the Design of Quadrature- Mirror Filters", *Proc. IEEE Int. Conf. On Acoustics Speech and Signal Processing*, pp. 2085-2088, May 1997.

[47] V. K. Jain, and R. E. Crochiere, "Quadrature-mirror filter design in time domain," *IEEE Trans. on Acoustics Speech and Signal Proc*., Vol. ASSP-32, pp. 353-361, April 1984.

[48] H. D. Li, and V. K. Jain, "An approach to the design of discrete-time wavelets", *Proc. SPIE Conf AeroSense '96*, Vol. 2750, pp. 169-179, April 1996.

[49] L. Andrew, V. T. Franques, and V. K. Jain, "Eigen design of quadrature mirror filters", *IEEE Trans. on Circuits and systems II: Analog and Digital Signal Processing,* pp. 754-757, Sept. 1997.

[50] R. Ganesh, and K. Pahalvan, "Statistical modeling and computer simulation of indoor radio cahannel," *IEE Proceedings-I*, Vol. 138, pp. 153-161, June 1991.

[51] R. Crochiere and L. R. Rabiner, *Multirate Digital Signal Processing*, Prentice Hall, 1983.

[52] E. G. Larsson and P. Stoica, *Space-Time Block Coding for Wireless Communications*, Cambridge University Press, 2003.

[53] G. B. Giannakis, Z. Liu, X. Ma and S. Zhou, *Space-time Coding for Broadband Wireless Communications*, Wiley Inter-Science, 2007.

[54] H. Sampath, P. Stoica and A. Paulraj, "Generalized linear precoder and decoder design for MIMO channels using the weighted MMSE criterion", *IEEE Trans. On Communications*, December 2001.

[55] C. Windpassinger, R. F. H. Fischer, T. Vencel and J.B. Huber, "Precoding in multiantenna and multiuser communications", *IEEE Trans. On Wireless Communications*, July 2004.

[56] X. Li, H. Huang, G. J . Foschini, R. A. Valenzula, "Effects of iterative detection and decoding on the performance of BLAST," *Proc. GLOBECOM 2000.*

[57] N. Boubaker, K. B. Letaief, R. D. Murch, "A low complexity multicarrier BLAST architecture for realizing high data rates over dispersive fading channels," *Proc. IEEE VTC 2001.*

[58] P.W. Wolniansky, G.J. Foschini, G.D. Golden and R. A. Valenzuala, "V-BLAST: an architecture for realizing very high data rates overthe rich-scattering wireless channel", *Proc. URSI Intl. Symp. On Signals, Systems and Electronics ISSSE 1998*.

[59] W. Stallings, *Data & Computer Communications*, 6th edition, Prentice Hall, 2000.

[60] S. Abraham, A. Meylan and S. Nanda, "802.11n MAC design and system performance", *Proc. Intl. Conf. on Communications ICC 2005*.

[61] V. K. Jain, "Very high SFDR interpolation filters for software defined radio," in *Proc. IEEE International Workshop on Signal Processing Systems*, 2000, pp. 397-407.

[62] K. Halford, M.Webster, Multipath measurements in wireless LANs, *Application Note AN9895.1*, Intersil Corp., October 2001.

[63] S. M. Nabritt, "Performance of IEEE WLAN in a multipath environment," *Proc. Of Communications Design Conference* 2003 .

[64] S. Thoen, L. Van der Perre, M. Engels, H. De Man, "Adaptive loading for OFDM/SDMA-based wireless networks" , *IEEE Trans. Commun. 2002.*

[65] C. Li, S. Roy, "Subspace-based blind channel estimation for OFDM by exploiting virtual carriers", *IEEE Trans. Wireless Commun. 2003*.

[66] L. Shao, S. Sandhu, S. Roy and M. Ho, "High rate space frequency block codes for next generation 802.11 WLANs," *Proc. ICC, 2004*.

[67] Luca Rugini, Member, IEEE, and Paolo Banelli, "BER of OFDM Systems Impaired by Carrier Frequency Offset in Multipath Fading Channels," *IEEE Trans. on Comm.*, pp. 2279-2288, Sept. 2005.

[68] G. E. Shilov, *Linear Algebra*, Dover Publications, 1977.

[69] Y. Ogawa, K. Nishio, T. Nishimura and T. Ohgane, "A MIMO-OFDM system for high-speed transmission," *Proc. of IEEE VTC 2003*.

[70] D. Divakaran and W. Moreno, "Compensation of PA nonlinearity in 108 Mbps OWSS WLANs", submitted to the *IEEE Topical Conference on Power Amplifiers for Wireless Communications*, January 2009.

[71] G. T. Zhou and J. S. Kenney, "Predicting spectral regrowth of non-linear power amplifiers," *IEEE Trans. on Comm.*, vol. 50, issue 5, pp 718-722, May 2002.

[72] C. Rapp, "Effects of HPA-Nonlinearity on a 4-DPSK/OFDM Signal for a Digital Sound Broadcasting System," *Proc. of the second European Conference on Satellite Communications*, Belgium, pp. 179-184, October, 1991.

[73] R. Marsalek, P. Jardin and G. Baudoin, "From post-distortion to pre-distortion for power amplifiers linearization," *IEEE Communication Letter*s, vol. 7, issue 7, pp 308-310, July 2003.

APPENDICES

Appendix A An Example Based on the Multi Level Matrix Formulation

For a single stage (M = 2) OWDM synthesizer, the OWDM pulses generated using a 4 tap Daubecheis filter is given by φ_0=[-0.3415 0.5915 -0.1585 -0.0915] and φ_1= [-0.0915 0.1585 0.5915 0.3415]. The above OWDM pulses are spread in the wavelet domain by using Hadamard codes given by [1 1] and [1 -1]. The single stage OWSS pulses thus generated, are [-0.433 0.75 0.433 0.25] and [-0.25 0.433 -0.75 -0.433]. For this example, the first pulse, ψ=[-0.4330 0.7500 0.4330 0.2500] will be used. The channel is a real 3 tap channel (L = 3), given by c = [1 -0.8 1]. For simplicity of presentation, only 4 BPSK symbols (D = 4, ζ^2 = 1) will be used to estimate the equalizer, with N_w = 2 and N_b = 2. The effect of noise will also be neglected. The OWSS filter matrix H_1 and multipath channel matrix C, from (5.3), are given by

$$H_1 = \begin{bmatrix} -0.433 & 0 & 0 & 0 & 0 & 0 & 0 & 0 \\ 0.75 & -0.433 & 0 & 0 & 0 & 0 & 0 & 0 \\ 0.433 & 0.75 & -0.433 & 0 & 0 & 0 & 0 & 0 \\ 0.25 & 0.433 & 0.75 & -0.433 & 0 & 0 & 0 & 0 \\ 0 & 0.25 & 0.433 & 0.75 & -0.433 & 0 & 0 & 0 \\ 0 & 0 & 0.25 & 0.433 & 0.75 & -0.433 & 0 & 0 \\ 0 & 0 & 0 & 0.25 & 0.433 & 0.75 & -0.433 & 0 \\ 0 & 0 & 0 & 0 & 0.25 & 0.433 & 0.75 & -0.433 \end{bmatrix}$$

$$C = \begin{bmatrix} 1 & 0 & 0 & 0 & 0 & 0 & 0 & 0 \\ -0.8 & 1 & 0 & 0 & 0 & 0 & 0 & 0 \\ 1 & -0.8 & 1 & 0 & 0 & 0 & 0 & 0 \\ 0 & 1 & -0.8 & 1 & 0 & 0 & 0 & 0 \\ 0 & 0 & 1 & -0.8 & 1 & 0 & 0 & 0 \\ 0 & 0 & 0 & 1 & -0.8 & 1 & 0 & 0 \\ 0 & 0 & 0 & 0 & 1 & -0.8 & 1 & 0 \\ 0 & 0 & 0 & 0 & 0 & 1 & 0.8 & 1 \end{bmatrix}$$

Appendix A (Continued)

The correlator matrix, from (5.5), is given by

$$H_2 = \begin{bmatrix} 0.1875 & -0.3248 & -0.1875 & -0.1083 & 0 & 0 & 0 & 0 \\ -0.3248 & 0.5625 & 0.3248 & 0.1875 & 0 & 0 & 0 & 0 \\ -0.1875 & 0.3248 & 0.3750 & -0.2165 & -0.1875 & -0.1083 & 0 & 0 \\ -0.1083 & 0.1875 & -0.2165 & 0.6250 & 0.3248 & 0.1875 & 0 & 0 \\ 0 & 0 & -0.1875 & 0.3248 & 0.3750 & -0.2165 & -0.1875 & -0.1083 \\ 0 & 0 & -0.1083 & 0.1875 & -0.2165 & 0.6250 & 0.3248 & 0.1875 \\ 0 & 0 & 0 & 0 & -0.1875 & 0.3248 & 0.3750 & -0.2165 \\ 0 & 0 & 0 & 0 & -0.1083 & 0.1875 & -0.2165 & 0.6250 \end{bmatrix}$$

Neglecting the edge effects, the repetitive component blocks, from (5.18), are given by

$$K_1 = \begin{bmatrix} 0.3750 & -0.2165 \\ -0.2165 & 0.6250 \end{bmatrix}; \quad K_2 = \begin{bmatrix} 0.3750 & -0.2165 \\ -0.2165 & 0.6250 \end{bmatrix}$$

$$J_{1,1} = \begin{bmatrix} -0.1875 & -0.1083 \\ 0.3248 & 0.1875 \end{bmatrix}; \quad J_{1,2} = \begin{bmatrix} 0 & 0 \\ 0 & 0 \end{bmatrix}; \quad J_{2,1} = \begin{bmatrix} -0.1875 & -0.1083 \\ 0.3248 & 0.1875 \end{bmatrix}$$

Using (5.21), matrix F_1 can be calculated

$$F_1 = \begin{bmatrix} 1.5000 & -0.8660 & -0.5625 & -0.3248 & 0 & 0 & 0 & 0 \\ -0.8660 & 2.5000 & 0.9743 & 0.5625 & 0 & 0 & 0 & 0 \\ -0.5625 & 0.9743 & 1.1250 & -0.6495 & -0.3750 & -0.2165 & 0 & 0 \\ -0.3248 & 0.5625 & -0.6495 & 1.8750 & 0.6495 & 0.3750 & 0 & 0 \\ 0 & 0 & -0.3750 & 0.6495 & 0.7500 & -0.4330 & -0.1875 & -0.1083 \\ 0 & 0 & -0.2165 & 0.3750 & -0.4330 & 1.2500 & 0.3248 & 0.1875 \\ 0 & 0 & 0 & 0 & -0.1875 & 0.3248 & 0.3750 & -0.2165 \\ 0 & 0 & 0 & 0 & -0.1083 & 0.1875 & -0.2165 & 0.6250 \end{bmatrix}$$

Appendix A (Continued)

F_2 and F_3 are submatrices of F_1

$$F_2 = \begin{bmatrix} 0 & 0 \\ 0 & 0 \\ -0.3750 & -0.2165 \\ 0.6495 & 0.3750 \\ 0.7500 & -0.4330 \\ -0.4330 & 1.2500 \\ -0.1875 & 0.3248 \\ -0.1083 & 0.1875 \end{bmatrix}; \quad F_3 = \begin{bmatrix} 0.7500 & -0.4330 \\ -0.4330 & 1.2500 \end{bmatrix}$$

The matrices Q_1, Q_2, Q_3 and Q_4, given in equations (5.19), (5.20), (5.22) and (5.23) can now be calculated

$$Q_1 = \begin{bmatrix} 3.75 & 0.3248 \end{bmatrix}; \quad Q_2 = \begin{bmatrix} 5.7987 & -2.1343 \\ -2.1343 & 1.7119 \end{bmatrix};$$

$$Q_3 = \begin{bmatrix} 0.7160 & 0.5866 \\ -0.4584 & -0.3729 \end{bmatrix}; Q_4 = \begin{bmatrix} 0.7500 & -0.4330 \\ -0.4330 & 1.2500 \end{bmatrix}$$

Using the above matrices, the optimum FE and DFE are estimated to be

$\underline{w}$ = [1.1302 0.8508] and $\underline{b}$ = [0.8983 0.5877]

Using the above equalizer, the normalized MSE of the unequalized error is found to be 0.010174. Note that the decision boundary for correct detection of a BPSK symbol is a unit distance away from either BPSK symbol, −1 or 1. An MSE of 0.010174 represents a standard deviation of approximately 0.1, around the transmitted symbols 1 and −1. If 8 BPSK symbols are used to estimate the equalizer, the FE and DFE are found to be w = [1.1053 0.7902] and b = [0.90298 0.62995] and the normalized MSE improves to 0.0068931. Finally if 100 BPSK symbols are used, the FE and DFE are

Appendix A (Continued)

estimated to be w = [1.0894 0.55148] and b = [1.112 0.76697] and the normalized MSE is further reduced to 0.0044986.

For illustration purposes, a N_w = 2-tap FE is used. For a longer 5-tap FE and 100 symbols for estimation, the optimum equalizer turns out to be $\underline{w}$ = [1.1394, 0.57591, −0.31036, 0.037525, 0.12544] and $\underline{b}$ = [0.80517, 0.3338], with a corresponding MSE = 6.7 × 10−5. The feedback equalizer was still maintained at a length N_b = 2. This success, even for a difficult channel, may be attributed to the wide frequency support of the OWSS pulses. As a reminder, in this simple example, the effect of AWGN was ignored.

ABOUT THE AUTHOR

Dinesh Divakaran received his B.E. degree in Electronics Engineering from University of Mumbai, in 1999, and his M.S. degree in Electrical Engineering from University of South Florida (USF) in 2002. Currently, he is a PhD candidate working toward his doctorate degree in Electrical Engineering at USF. During his graduate studies at USF, he has worked as a Research Assistant, Teaching Assistant and Adjunct Instructor in Electrical Engineering department. As a Adjunct Instructor he has taught various undergraduate courses in electrical engineering. His research interests are in signal processing techniques for wireless communication systems.